The Dissertation Committee for Rachel Michelle Wright Certifies that this is the approved version of the following dissertation:

Intraspecific Variation in Corals' Responses to Environmental Stressors

Committee:

Mikhail V. Matz, Supervisor

Hans Hofmann

Nancy Moran

Dan Bolnick

Marvin Whiteley

Intraspecific Variation in Corals' Responses to Environmental Stressors

by

Rachel Michelle Wright, B.S.Bio.

Dissertation

Presented to the Faculty of the Graduate School of

The University of Texas at Austin

in Partial Fulfillment

of the Requirements

for the Degree of

Doctor of Philosophy

The University of Texas at Austin

May 2017

Dedication

I dedicate this dissertation to my siblings, who are cumulatively more me than I am.

Acknowledgements

Infinite thanks to that mass conglomerate I call “family” for providing sanctuary. Thanks to my parents, who never needed to understand me (or my positions on global climate change) to encourage me anyway. Thanks to my siblings, who have to deal with this mess for another 60 years but don’t seem that bummed about it. Thanks to my grandparents, who cheer me on at 9PM every day. “Thanks” isn’t nearly sufficient for what owe Burt, who taught me not to be afraid of the water at the bottom of the ocean during our first dive. My dissertation topic would probably have been very, very land-based had that fear persisted, so the corals thank Burt too. The years passed during this dissertation have brought about situations scarier than a dark abyss, but it’s cheatingly easy to stay focused with his unfailing support. Thanks also to his family, though they have been included in my aforementioned conglomerate for years.

Thanks are also owed to my friends for balancing my life. Thanks to Andrea, my ride-or-die since the Patriot Act of 2008. Muchos thanks to The Baffles, for providing the soundtrack to my graduate career. Herther, Chris, AB, and Danny: these years would have been lame without our hikes and mellow-harshing. Thanks to Rayna, the Swiss army knife of friends. This woman is equally helpful when you don’t know how to pay tabs when entertaining speakers or when you need accessorizing for David Bowie’s wake.

The entire Matz Lab has been as much friend as colleague, which has really made these years fly by. Misha immediately encouraged my independence, though "independent" is pretty euphemistic for much of my personality. Misha inspires scientific curiosity and excitement in every interaction. He's equally enthusiastic when we're talking about our own work, the maths of shoelace knot-slippage, or how this is all just a big simulation anyway. I've seen first-hand how his mentorship has produced confident scientists. Thanks to all of my former and current Matz lab colleagues: Dr. Sarah (Ted) Davies, Dr. Carly (Carl) Kenkel, Dr. Chintan (ChinChin) Modi, Marie (Mur) Strader, Groves (Dixie) Dixon, and Sarah (Bart) Barfield. Some of you tried to kill me via electrocution and drowning, but mostly you saved me every day via empathy and gummies. Finally, thanks to Galina (the HB) Aglyamova for holding us all together. I'll never understand how such a tiny woman can have such a large appetite (for freezer space).

Many thanks to my committee members: Hans Hofmann, Dan Bolnick, Marvin Whiteley, and Nancy Moran. This dissertation involves gene expression analysis, quantitative genetics, marine microbiology, and symbiosis studies. I could not have undertaken such a multidisciplinary dissertation without their guidance and support.

This dissertation could not have been completed, or even conceived, without the advice, mentorship, and facilitation of Dr. Line Bay at the Australian Institute for Marine Science (AIMS). Dr. David Bourne offered advice on designing the experiments in Chapter 2 and supplied microbes for the bacterial challenges. Hanaka Mara completed many of the physiological assays in Chapter 3.

Scientists at Mote Tropical Marine Laboratory in Summerland Key were not directly involved in any of the research outlined in this dissertation, but I still thank Erich Bartels, Dr. David Vaughan, and Chris Page for their enthusiastic assistance in all the experiments I could conceive to study coral stress and for their general friendly attitudes that made even the most tedious, mucus-y fieldwork seem important and fun. Likewise, Emma Hickerson and the crew of the NOAA M/V Mantis have my gratitude for including me and the rest of the Matz lab in endeavors to learn about coral biology while protecting the beautiful Texas Flower Garden Banks.

Funding for this dissertation was provided by the National Science Foundation (DEB-1054766) to MV Matz, P.E.O Women's International, and the American Association of University Women.

Intraspecific Variation in Corals' Responses to Environmental Stressors

Rachel Michelle Wright, Ph.D.

The University of Texas at Austin, 2017

Supervisor: Mikhail V. Matz

Climate change threatens reef-building corals in various ways. Increasing temperatures disrupt coral–algal symbioses, acidification impacts calcification, and increasingly prevalent diseases cause tissue loss and mortality. This dissertation investigated coral responses to all of these stressors. First, I measured gene expression in response to natural disease in *Acropora hyacinthus*. I compared expression profiles of eight healthy colonies against eight colonies exhibiting symptoms commonly associated with white syndromes. Both visibly affected and apparently healthy tissues were collected from diseased colonies. Differences between healthy and diseased tissues indicated activation of innate immunity and tissue repair pathways accompanied by reduced calcification and metabolism of stored lipids. Expression profiles of unaffected tissues from diseased colonies were not significantly different from fully healthy samples, indicating weak systemic effects of white syndromes on *A. hyacinthus*. Next, I challenged eight *A. millepora* genotypes with a putative bacterial pathogen to assess intraspecific variation in disease susceptibility. Genotypes varied from zero to >90% mortality, with bacterial challenge increasing mortality rates 4–6 fold and shifting the microbiome in favor of stress-associated taxa. Immune and transcriptomic responses to the challenge were more prominent in high-mortality individuals, whereas low-mortality corals maintained expression signatures of a healthier condition. This study supports that

intraspecific variation in disease susceptibility does exist; therefore, selection could promote disease resistance. My final dissertation project investigated the capacity for *A. millepora* to adapt to multiple environmental stressors: rising temperatures, ocean acidification, and infectious diseases. I measured growth rates, coral color (a proxy for algal symbiont density), survival, and a number of physiological estimates of coral and algal health in response to these three stressors and a combined treatment. Whereas treatments resulted in the predicted responses, I found no synergistic activity between stressors. A genetic variance–covariance matrix demonstrated within-trait variance and positive genetic covariances. Estimates for changes in trait means using the multivariate breeder's equation showed that co-variances between these traits reinforce, rather than constrain, adaptation to environmental threats. These findings emphasize the importance of acknowledging adaptive capacity when predicting reef cover under future climate scenarios.

Table of Contents

List of Tables

List of Figures

Introduction

Study System Biology

Reef-building scleractinian corals are cnidarians that, while capable of heterotrophic feeding (Houlbreque & Ferrier-Pages, 2009), rely on photosynthetic byproducts of intracellular algal symbionts (genus *Symbiodinium*) to meet nutritional demands (Muscatine & Porter, 1977). The coral species in this dissertation are hermaphrodites: individual polyps that compose a clonal colony release gamete bundles that contain both egg and sperm once per year. Pelagic larvae produced by these annual broadcast spawning events establish symbioses with *Symbiodinium*, settle on reef substrate, and transition to the sedentary adult stage (Baird, Guest, & Willis, 2009). As reef-building adult colonies, scleractinian corals build aragonite skeletons using calcium and dissolved inorganic carbon (Allemand et al., 2004). Adult corals host a variety of microorganisms other than *Symbiodinium*. Bacteria, archaea, and viruses found within coral cells and in secreted coral mucus may promote host health via nutrient production or defense against invading pathogens (Benavides, Bednarz, & Ferrier-Pagès, 2017; Rosenberg, Koren, Reshef, Efrony, & Zilber-Rosenberg, 2007). Relationships between the coral host and coral-associated microbiota are affected by biotic and abiotic stressors (Tracy D Ainsworth et al., 2015; Casey, Connolly, & Ainsworth, 2015; M. J. Sweet & Bulling, 2017; Thurber et al., 2009), just as coral–*Symbiodinium* relationships break down under thermal stress in an event known as coral "bleaching."

Problem Statement and Research Overview

Coral diseases cause global coral mortality (Precht, Gintert, Robbart, Fura, & van Woesik, 2016; Sussman, Willis, Victor, & Bourne, 2008), but remain poorly understood (Pollock, Morris, Willis, & Bourne, 2011). Therefore, the first objectives of this

dissertation work were to elucidate the cellular responses to and physiological consequences of coral disease. However, corals are not exposed to abiotic stress alone. Global climate change is warming and acidifying waters inhabited by reef-building corals (Hoegh-Guldberg et al., 2007). Corals must maintain algal health, biomineralization rates, and immune defenses to persist in ever-worsening environments that simultaneously stress coral–algal symbioses (Brown, 1997), alter calcification chemistry (Andersson & Gledhill, 2011), and increase pathogen abundance and/or virulence (A. W. Miller & Richardson, 2015). This dissertation addresses the capacity for corals to adapt to simultaneous environmental stressors by measuring intraspecific differences in coral stress tolerances and fitness parameters.

Chapter 1[1]: Gene expression associated with white syndromes in a reef building coral, *Acropora hyacinthus*.

ABSTRACT

Corals are capable of launching diverse immune defenses at the site of direct contact with pathogens, but the molecular mechanisms of this activity and the colony-wide effects of such stressors remain poorly understood. Here I compared gene expression profiles in eight healthy *Acropora hyacinthus* colonies against eight colonies exhibiting tissue loss commonly associated with white syndromes, all collected from a natural reef environment near Palau. Two types of tissues were sampled from diseased corals: visibly affected and apparently healthy. Tag-based RNA-Seq followed by weighted gene co-expression network analysis identified groups of co-regulated differentially expressed genes between all health states (disease lesion, apparently healthy tissues of diseased colonies, and fully healthy). Differences between healthy and diseased tissues indicate activation of several innate immunity and tissue repair pathways accompanied by reduced calcification and the switch towards metabolic reliance on stored lipids. Unaffected parts of diseased colonies, although displaying a trend towards these changes, were not significantly different from fully healthy samples. Still, network analysis identified a group of genes, suggestive of altered immunity state, that were specifically up-regulated in unaffected parts of diseased colonies. Similarity of fully healthy samples to apparently healthy parts of diseased colonies indicates that systemic effects of white syndromes on *A. hyacinthus* are weak, which implies that the coral colony is largely able to sustain its physiological performance despite disease. The genes specifically up-regulated in unaffected parts of diseased colonies, instead of being the

[1] This chapter is published: Wright, R.M., Aglyamova G.A., Meyer, E., Matz, M.V. (2015). Gene expression signatures associated with white syndromes in a reef building coral, *Acropora hyacinthus*. *BMC Genomics*. 16:371.

consequence of disease, might be related to the originally higher susceptibility of these colonies to naturally occurring white syndromes.

INTRODUCTION

Increasing rates of disease have contributed greatly to global coral population declines over the last few decades (Hoegh-Gulberg, 1999; Porter et al., 2001). The broadly defined "white syndromes" in Indo-Pacific regions, characterized in the field by tissue loss resulting in exposure of the coral skeleton, have been attributed to *Vibrio spp*. (Sussman et al., 2008), a genus of bacteria involved in several coral diseases (Ben-Haim, 2003; Cervino et al., 2008; Kushmaro, Banin, Loya, Stackebrandt, & Rosenberg, 2001; Ushijima et al., 2014; Vezzulli et al., 2010). Other reports find no evidence of pathogenic bacteria in diseased corals (George Roff et al., 2011) and instead blame stress-triggered programmed cell death for the manifestation of symptoms (T. D. Ainsworth, Kvennefors, Blackall, Fine, & Hoegh-Guldberg, 2007). These conflicting conclusions, drawn mostly from culturing assays and histological observations, are further confounded by insufficient knowledge of the cnidarian immune response.

Corals, like all invertebrates, rely entirely on innate immunity for protection from invading pathogens. Features of innate immunity in corals include physical barriers (B. Brown & Bythell, 2005), molecular pattern recognition (D. J. Miller et al., 2007), secretion of antimicrobial macromolecules (Vidal-Dupiol, Ladrière, Destoumieux-Garzón, et al., 2011), and cellular responses (*e.g.,* phagocytosis) (Mydlarz & Harvell, 2007; Mydlarz, Holthouse, Peters, & Harvell, 2008; Olano & Bigger, 2000). Recent efforts to characterize those features of immunity using various cnidarian genome and transcriptome sequence databases have identified putative components of coral stress management and immune response pathways by homology with better-studied organisms. The *Acropora digitifera* genome project revealed striking differences in innate immunity complexity in corals compared to a closely related cnidarian, *Nematostella vectensis* (Shinzato et al., 2011). Whereas the *N. vectensis* genome encodes

only a single Toll/Toll-like receptor (TLR), the *A. digitifera* genome included at least four TLRs, along with other related immune signaling molecules. Miller et al. reported the presence of TLR signaling components, including adaptor proteins that link that cascade with other signaling events, in the expressed sequence tag library of another acroporid coral, *A. millepora* (Miller et al., 2007). Together these elements suggest an ability of corals to respond to pathogen-associated molecular patterns (PAMPs) via TLR recognition and integrate that signal to cellular responses such as inflammation and apoptosis. Toll/TLR signaling can activate NF-κB transcription factor that, upon nuclear localization, up-regulates transcription of immune response genes. In corals, the identities of those response genes and the roles they play remain unclear. Some suggested immune response genes include lectins, complement c3 and apextrin, proteins involved in non-self recognition, aggregation and cell lysis respectively (Puill-Stephan, Seneca, Miller, van Oppen, & Willis, 2012). Metabolism and calcification genes demonstrated differential expression in addition to immunity genes in *A. millepora* challenged with bacterial and viral immunogens, providing a more comprehensive picture of cellular events during an acute infection (Weiss et al., 2013). Global RNA-sequencing of *A. cervicornis* displaying signs of White Band Disease (WBD) revealed that disease significantly affected the expression of genes involved in immune processes and apoptosis (Libro, Kaluziak, & Vollmer, 2013). The up-regulation of phagocytic cell surface receptors and reactive oxygen species (ROS) producing enzymes suggested that the phagocytosis and degradation of damaged cells drives the WBD response in corals.

These coral sequencing projects and experimental immune challenges have provided conclusive evidence that corals are capable of launching defensive responses upon direct contact with pathogens. A coral's ability to communicate the recognition of that pathogen along the colony, however, is less understood. Coral polyps utilize a

gastrovascular system lined with flagellated gastrodermal cells to transport organic products and zooxanthellae within the colony (Gladfelter, 1983). These channels are used to allocate energetic resources to areas that need them most, such as fast-growing branch tips (Fang, Chen, & Chen, 1989; Pearse & Muscatine, 1971; Taylor, 1977) and wounded regions (Oren, Rinkevich, & Loya, 1997). Radiolabeled carbon accumulation experiments have shown that corals preferentially direct energetic resources towards physically damaged regions (Oren et al., 1997) but away from disease-induced lesions (Roff, Hoegh-Guldberg, & Fine, 2006). These findings suggest that healthy coral tissues might possess means to detect and respond to an advancing disease lesion, but it is still unclear what the physiological consequences of this action might be.

Here I examine the gene expression profiles of *A. hyacinthus* displaying white syndromes (Figure 1.1) to determine the molecular consequences of the diseased condition. White syndromes advance along a colony in a way such that a distinct lesion forms between affected and unaffected tissues. Tissues ahead of the lesion are presumably healthy, while tissues at the lesion boundary are actively sloughing cells in response to infection. I compared gene expression profiles among three health states: affected tissues (diseased, "D"), apparently healthy tissues from diseased colonies ("ahead of the lesion", "AL"), and tissues from completely unaffected colonies (healthy, "H"). Comparing healthy regions of diseased colonies to completely disease-free individuals provided an opportunity to look for expression patterns that might indicate a colony-wide systemic effect of infection and/or disease susceptibility. I used tag-based RNA-Seq (Meyer, Aglyamova, & Matz, 2011) followed by weighted gene correlation network analysis (Langfelder & Horvath, 2008) to achieve systems-level insight into molecular responses to chronic disease in corals.

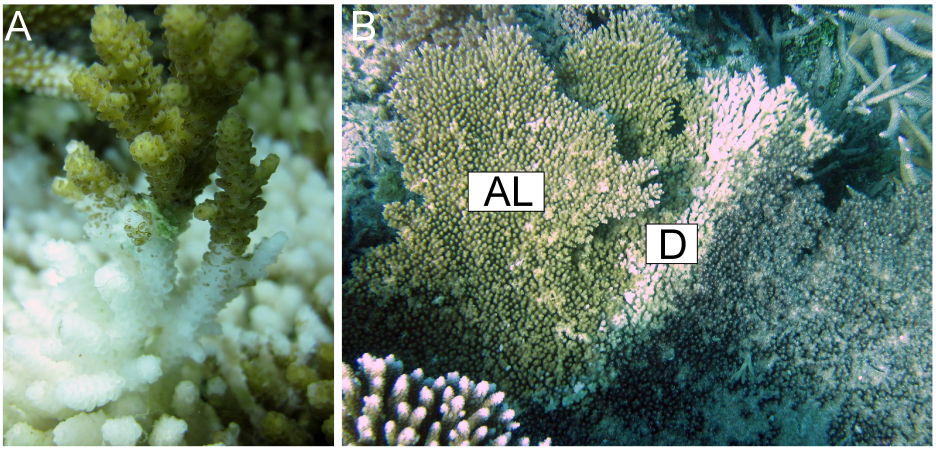

Figure 1.1: White syndrome in *A. hyacinthus* sampled in this study. (A) Close-up of the lesion area. (B) Position of sampled locations in diseased colonies: "D" – diseased, "AL" – ahead of the lesion. Tissues were also sampled from completely healthy individuals ("H", not pictured). Photo credit: Carly Kenkel.

METHODS

Sampling

Coral fragments from 16 colonies of *A. hyacinthus* were sampled in the spring of 2011 along the eastern coast of Palau (7° 18.738' N, 134° 30.423' E) and immediately stored in RNAlater (Ambion). Eight of these colonies were visibly affected with white syndromes (Figure 1.1). Colonies exhibiting diffuse tissue loss along a lesion of apparently healthy tissue directly adjacent to exposed white skeleton in accordance with (Beeden, Willis, Raymundo, Page, & Weil, 2008) were sampled. Colonies displayed no obvious signs of predation. The remaining eight colonies were completely symptom-free (designated healthy, H). From the eight affected colonies, coral fragments were sampled from both the lesion interface between diseased and healthy tissues (diseased, D) and areas well ahead of the lesion (AL, Figure 1.1B). AL coral fragments were sampled from approximately midway between the lesion boundary and the edge of the colony. AL

tissues are unlikely to be in direct contact with pathogen since previous studies have demonstrated declines in pathogens only ~1 cm in advance of a white syndromes lesion (Sweet, Bythell, & Nugues, 2013).

Transcriptome Assembly and Annotation

The *A. hyacinthus* transcriptome has been generated from 5-day aposymbiotic larvae as described previously (Meyer et al., 2009). It was annotated based on two resources: the proteome of the starlet sea anemone *Nematostella vectensis* (Putnam et al., 2007) and in-depth annotations of the *Acropora digitifera* proteome (Dunlap et al., 2013). Based on manual verifications of a subset of *A. digitifera* annotations, they were pre-filtered to include only protein sequences longer than 60 amino acids with the annotation assigned based on the listed e-value = 1e-20 or better. The GO, KEGG ("Kyoto Encyclopedia of Genes and Genomes"), KOG ("euKaryotic orthologous groups"), and gene name annotations were transferred to an *A. hyacinthus* contig if the contig matched one or both of these two resources with e-value = 1e-4 or better in blastx (Altschul et al., 1997). The GO and KOG annotations assigned to genes that were denoted FOG ("fuzzy orthologous group", (Tatusov et al., 2003)) in the *N. vectensis* data were removed, since such genes encode proteins with common domains and cannot be functionally annotated based on homology alone. The annotated *A. hyacinthus* transcriptome has been released for unrestricted use prior to this publication, http://www.bio.utexas.edu/research/matz_lab/matzlab/Data.html.

Tag-based RNA-Seq

Libraries were prepared following (Meyer et al., 2011) and sequenced using Applied Biosystems SOLiD v.3 platform. Read trimming, quality filtering, mapping, and conversion to per-gene counts was performed as described previously (Meyer et al.,

2011) with one modification: reads mapping to the same starting coordinate in the reference and aligning with 100% identity along the full length of the shorter read were discarded as potential PCR duplicates. The current step-by-step library preparation protocol as well as bioinformatic pipeline are available at https://sourceforge.net/projects/tag-based-rnaseq/; note however that the current version of the tag-based RNA-seq method utilizes advanced procedure for PCR duplicates removal based on degenerate tags incorporated during cDNA synthesis, and assumes sequencing on the Illumina HiSeq instrument.

Identification of Differentially Expressed Genes (DEGs)

All statistical analyses were performed using R3.1.1 (R Core Team, 2014). DEGs were identified using a generalized linear model implemented by the R package DESeq2 (Love, Huber, & Anders, 2014). No outlying samples were detected by the arrayQualityMetrics package (Kauffmann, Gentleman, & Wolfgang Huber, 2009). DESeq2 performed automatic independent filtering to remove lowly abundant transcripts and maximize the rate of DEG discovery post multiple testing correction at an alpha of 0.1. P-values for significance of contrasts between all three health states were generated based on Wald statistics and were adjusted for multiple testing using the false discovery rate method (Benjamini & Hochberg, 1995). The contrasts resulted in tables including adjusted and unadjusted p-values and log2 fold changes that were used in downstream analyses.

Gene Coexpression Network Analysis

A weighted gene correlation network analysis (WGCNA, Langfelder & Horvath, 2008) was used to identify groups of co-regulated genes in an unsupervised way. Genes with an unadjusted p-value < 0.1 for any of the three contrasts as determined by the

generalized linear model testing for the effect of health state were input into WGCNA. A sample network was constructed to identify outlying samples with a standardized connectivity score of less than -2.5 (Horvath, 2011). A signed gene co-expression network was constructed with a soft threshold power of 24. Groups of co-regulated genes (modules) correlated with each other with the Pearson correlation coefficient 0.42 or better were merged. The eigengenes of the resulting modules (the first principal component of the expression matrix corresponding to the genes included in the module) were correlated with health states (H, AL, or D).

Assessing the Robustness of the Analysis

Low quality of the SOLiD sequencing resulted in low number of reads mapped, raising concerns about the reliability of the data. In tag-based RNA-seq, unlike standard RNA-seq, every count represents an observation of an independent transcript. Thus low counts could still provide sufficient quantitative information about transcript abundances. In addition, high level of biological replication (n = 8 per group) in this experiment should have compensated for the low counts within each replicate to a certain degree. To confirm that low counts did not result in inflated false discovery rate, I have simulated a series of count datasets based on the empirical per-gene total counts and coefficients of variation across samples as well as empirical sample size factors, which included no effect of experimental conditions. Analysis of these simulated datasets recovered nearly identical sample size factors and highly similar dispersion estimates as in real data (Figure A1). When these simulated datasets were analyzed with DESeq2 using the same models as real data, at most four genes passed the 10% Benjamini-Hochberg false discovery rate (FDR) cutoff for each contrast. Compared to 646 genes passing the FDR 10% cutoff for the disease-healthy comparison and 333 genes passing the same cutoff for

the disease-AL comparison in the real dataset this is much less than 10%, indicating that the real data analysis was conservative. The simulation-based p-value cutoff achieving the empirical 10% FDR (Figure A2) would have yielded 1.05–1.5X more DEGs for these comparisons than the Benjamini-Hochberg procedure. Notably, the Benjamini-Hochberg correction did not yield any DEGs for the healthy-AL comparison, and accordingly, the DEG discovery rate in this comparison was even slightly lower than the simulation-based false discovery rate (Figure A2C), indicating that for this comparison DESeq2 analysis did not provide sufficient power. To keep the analysis conservative, I chose to report DESeq2-based DEGs discovered using the Benjamini-Hochberg procedure. The procedure for inferring empirical FDR based on simulations described above has been implemented in the R package empiricalFDR.DESeq2, hosted within the Comprehensive R Archive Network (CRAN).

WGCNA analysis provides one additional confirmation that the observed gene expression differences are driven by biological factors rather than stochasticity. WGCNA constructs gene co-expression modules from their correlation pattern across samples without using the information about how the samples are distributed among experimental conditions. The fact that post hoc the module eigengenes correlate strongly with coral condition (Figure A3) indicates that the gene expression patterns in the data truly reflect the biological processes related to disease. To verify this, I shuffled the condition designations among samples and indeed observed that the correlations with co-expression modules disappeared (Figure A4).

Principal Coordinate Analysis

Principal coordinate analysis to visualize clustering of gene expression between health states was performed using the adegenet package (Jombart, 2008) using variance

stabilized data for all genes and subsequently with only candidate differentially expressed genes (unadjusted p-value < 0.05), based on Manhattan distances which correspond to the sum of absolute log-fold changes across all genes. Effects of the three health states ("D", "H", and "AL") were calculated using the multivariate analysis of variance function *adonis* of the R package vegan (Dixon, 2003). Tukey's tests between specific health states based on the values of the first principal coordinate were performed using function *TukeyHSD* in R.

RESULTS

Differential Gene Expression between Health States

Sequencing yielded an average of 6,367,219 reads per sample. An average of 19.5% of these remained after filtering and of these, an average 31.45% mapped to the transcriptome. A total of 44,701 isogroups (clusters of contigs representing the same gene, from here on referred to as "genes") were detected. Reads were converted to unique transcript counts by removing PCR duplicates, yielding an average of 156,650 counts per sample. A generalized linear model with contrasts between all three tissues detected differentially expressed genes between health states (Figure A5). The disease-healthy contrast yielded 646 DEGs passing a Benjamini-Hochberg FDR cutoff of 10%. The disease-AL contrast yielded 333 DEGs passing an FDR cutoff of 10%. No genes passed the 10% FDR cutoff for the healthy–AL contrast. Between all contrasts, a total of 757 genes passed the FDR cutoff of 10%.

Principal coordinate analysis of the variance-stabilized data for all genes revealed expression differences mainly between disease (D) and the other two health states (Figure 1.2A). PCoA using the 3827 isogroups with an unadjusted p-value of less than 0.05 for

any contrast revealed more differences between health states, but a significant overlap in expression of healthy and AL tissues remains (Figure 1.2B).

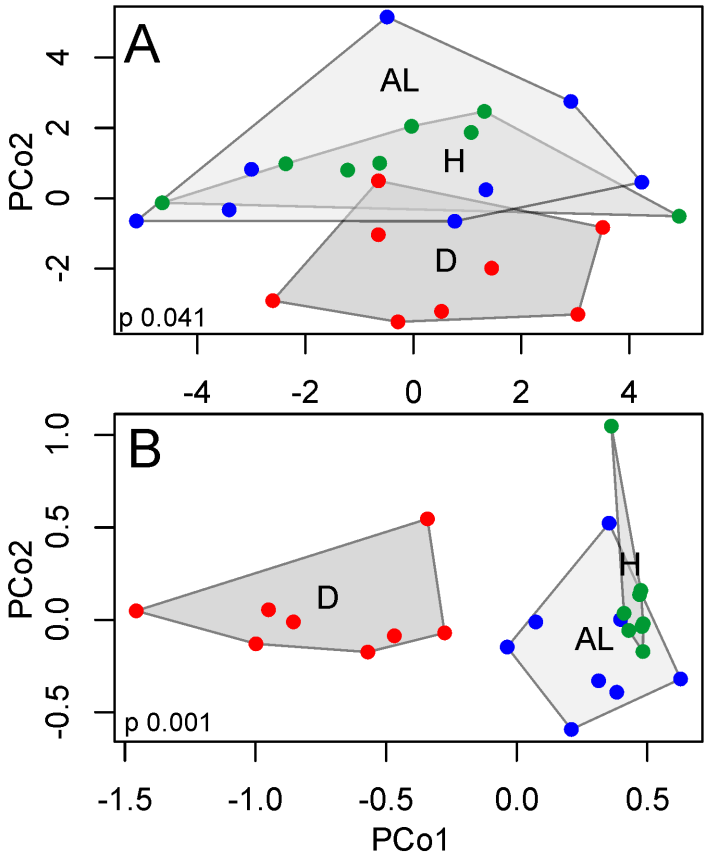

Figure 1.2: Principal coordinate analysis clusters samples by health state. Samples cluster by the presence of disease symptoms (D vs. AL and H) when all genes are included in the PCoA (A). Differences between health states become more evident when PCoA is performed on DEGs (unadjusted p-value < 0.05) only (B).

Gene Ontology (GO) Enrichment

Functional enrichments between all three contrasts allow a general examination of the molecular functions and biological processes being differentially regulated between health states. The enriched groups of both the disease–healthy and disease–AL contrasts

were largely identical (Figure 1.3 and Figure A6). Ribosomal proteins, oxidative stress responses, and translation factor activity were up-regulated in diseased tissues compared to both AL and healthy tissues. Likewise, receptor activity, regulation of biological quality, and extracellular matrix components (collagens) were down-regulated in diseased tissues compared to both healthier states. No GO terms were significantly enriched (FDR 10%) for the healthy-AL contrast.

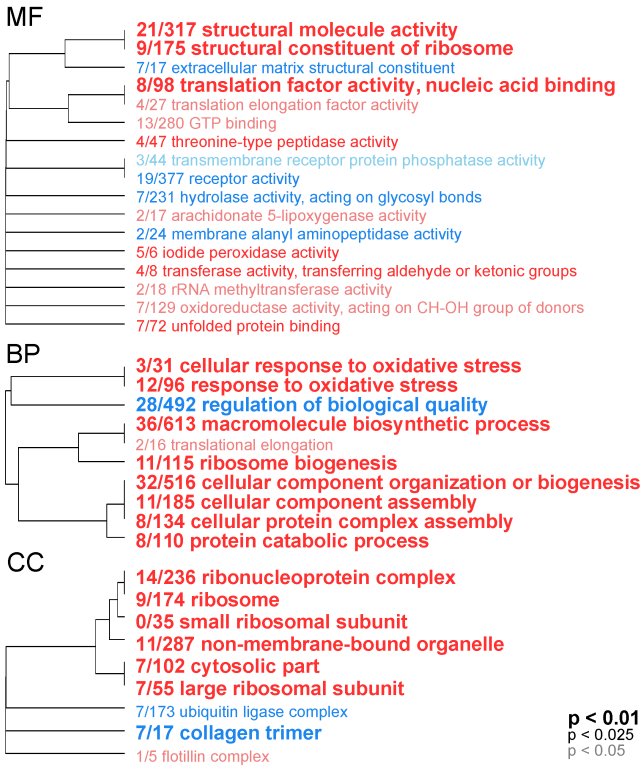

Figure 1.3: Gene ontology categories enriched by genes up-regulated (red) or down-regulated (blue) in diseased compared to fully healthy samples, summarized by molecular function (MF), biological process (BP), and cellular component (CC). The size of the font indicates the significance of the term as indicated by the inset key. The fraction preceding the GO term indicates the number of genes annotated with the term that pass an unadjusted p-value threshold of 0.05. The trees indicate sharing of genes among GO categories (the categories with no branch length between them are subsets of each other).

Gene Expression Analysis by Contrast

Gene expression heatmaps were constructed to show the relative expression patterns of the top most significant DEGs for each contrast (Figure 1.4A, A7, and A8).

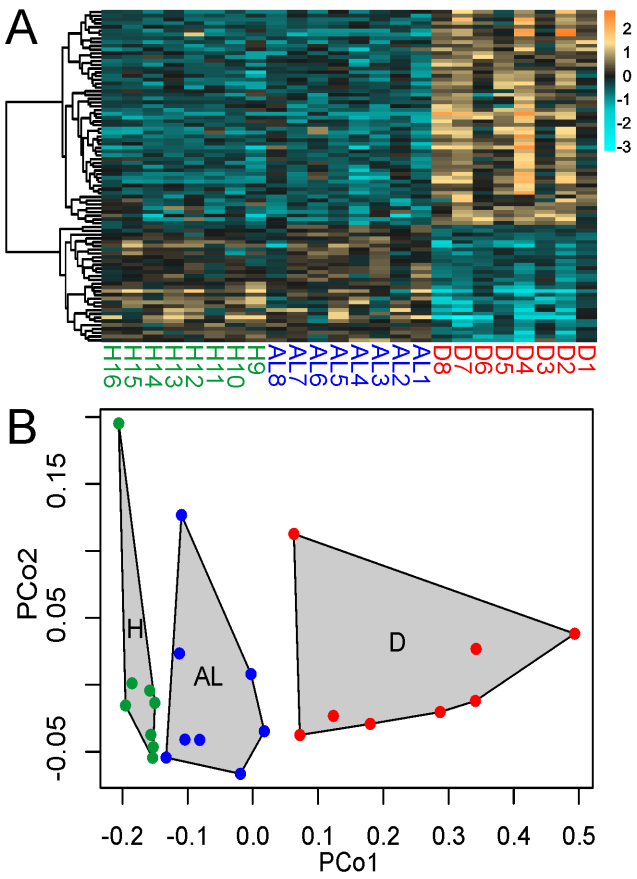

Figure 1.4: Expression of DEGs significant for disease-healthy contrast among health states. (A) Heatmap for top DEGs (FDR = 0.01). Rows are genes, columns are samples ordered as in the bottom panel: ahead-of-lesion (AL), healthy (H), and diseased (D). The color scale is in log2 (fold change relative to the gene's mean). The tree is a hierarchical clustering of genes based on Pearson's correlation of their expression across samples. (B) Principal coordinate analysis of all DEGs at 10% FDR for disease–healthy contrast.

Diseased vs. Healthy

Genes found to be up-regulated (Benjamini-Hochberg FDR < 0.01) in diseased tissues compared to healthy corals include key members of the oxidative stress response in corals (*e.g.*, catalases and peroxidases) and pentose phosphate metabolism (transketolase, transaldolase, and 6-phosphogluconate dehydrogenase). Both proteinases (astacin and cathepsin L) and protease inhibitors (alpha-macroglobulin and serine proteinase inhibitor Ku-type) were up-regulated in diseased tissues. Two of the genes annotated as C-type lectin, a carbohydrate-binding protein, and malate synthase, a key enzyme of the glyoxylate cycle, were also up-regulated in symptomatic tissues. Down-regulated genes (Benjamini-Hochberg FDR < 0.01) include those encoding extracellular matrix constituents (collagens, heparin sulfate proteoglycans) and carbonic anhydrase, a key enzyme in coral skeletal deposition. Red fluorescent protein was also down-regulated in diseased tissues, a hallmark of the coral stress response (Bay et al., 2009; DeSalvo et al., 2008; Rodriguez-Lanetty, Harii, & Hoegh-Guldberg, 2009; Roth & Deheyn, 2013; Smith-Keune & Dove, 2007).

AL vs. Diseased and Healthy

The expression differences between diseased and AL tissues within a colony paralleled the expression differences between diseased tissues and healthy corals. At the same significance threshold (Benjamini-Hochberg FDR < 0.01), almost the exact same top-candidate genes were identified. No differentially expressed genes passed the Benjamini-Hochberg 10% FDR when comparing the AL tissues and healthy corals.

To better quantify the behavior of disease-responsive genes in AL samples, the expression of genes passing a 10% FDR cutoff for the disease-healthy comparison was studied using principal coordinate analysis. Tukey's test based on the first principal coordinate values revealed highly significant differences between H and D as well as

between AL and D ($P < 0.001$ in both cases). Although AL samples appeared to be intermediate between H and D samples (Figure 1.4B), their scores along the first principal coordinate axis were not significantly different from healthy samples ($P = 0.11$).

Correlation Between Gene Network Modules and Health States

A total of 6737 DEGs with unadjusted p-value < 0.1 were input into WGCNA for network analysis. A sample network was constructed to identify outlying samples with a standardized connectivity score of less than -2.5. One sample (diseased individual "4") was identified as an outlier and removed from subsequent analysis (Figure A9). Twelve unique modules, assigned arbitrarily color labels, remained after merging highly correlated modules. Of these twelve modules, eight were highly correlated to a single coral individual and one (grey) is reserved to contain genes that do not fall into any co-expression module. The remaining three modules were highly correlated with the health states (Figure A3). Since I assembled these modules using a signed network, the sign of the correlation is equivalent to the direction of expression change with respect to the trait. For example, a module that is significantly negatively correlated to diseased corals contains genes that are down-regulated in that state.

The eigengene of the dark green module (1155 genes) was strongly correlated with diseased-healthy contrast (Pearson's R2 = 0.83, Pcor = 1e-6, Figure A3). The genes within this module are up-regulated in diseased tissues and down-regulated in healthy tissues, while tending to be down-regulated in AL samples. Conversely, the turquoise module (669 genes) was up-regulated in healthy tissues and down-regulated in diseased tissues (Pearson's $R^2 = -0.83$, $P_{cor} = 9e\text{-}7$, Figure A3). Expression of these two modules in AL samples demonstrated similar direction of change as in healthy tissues, although the change was not statistically significant. Notably, one module was identified (green, 661

genes) that was significantly up-regulated in AL (Pearson's $R^2 = 0.64$, $P_{cor} = 0.001$) and (to a lesser extent) down-regulated in diseased tissues (Pearson's $R^2 = -0.44$, $P_{cor} = 0.04$), while remaining unchanged in healthy tissues (Figure A3).

Within Module Gene Expression Analysis

Hierarchically clustered gene expression heatmaps were constructed to show the relative expression patterns of the genes within each module that best represent the module and show significant correlations to the health state, based on module membership and gene significance values (Figure 1.5 and Figure A10).

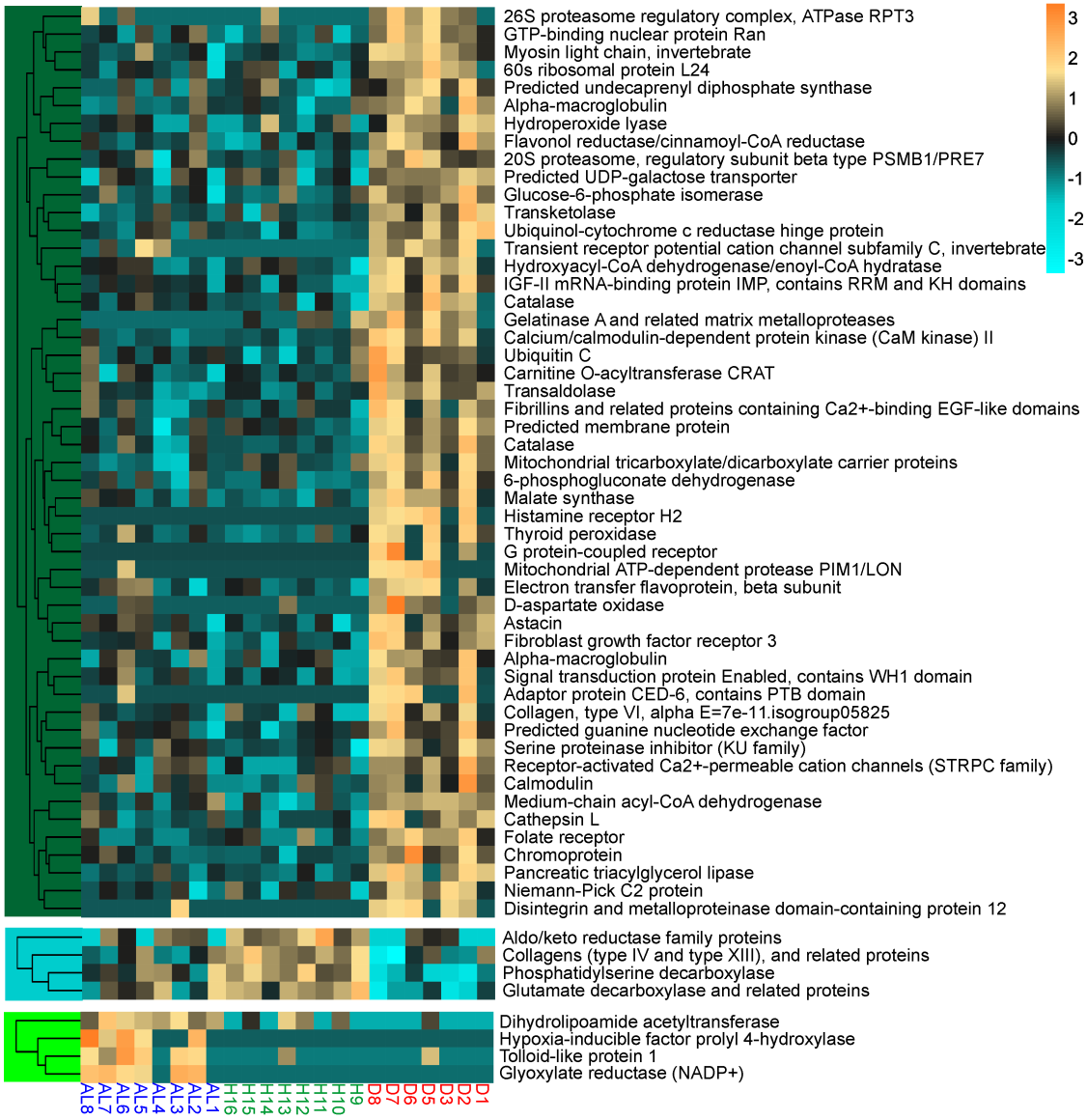

Figure 1.5: Gene expression heatmaps of annotated DEGs with a module membership and gene significance score greater than 0.6. Rows are genes, columns are samples ordered as in the bottom panel: ahead-of-lesion (AL), healthy (H), and diseased (D). The color scale is in $\log_2$ (fold change relative to the gene's mean). The trees are hierarchical clustering of genes based on Pearson's correlation of their expression across samples. The color block of the trees indicates the module to which these genes belong (dark green, turquoise, and green).

DISCUSSION

The major pattern of variation in gene expression was between asymptomatic (healthy and AL) and diseased (D) corals (Figure 1.2). There were no statistically significant differences in gene expression between healthy colonies (H) and asymptomatic parts of diseased colonies (AL), suggesting that these states are physiologically similar. The genes that are differentially regulated between diseased and healthy corals show a subtle trend towards disease-like gene expression in asymptomatic tissues of diseased colonies (Figure 1.4). This trend is, however, not statistically significant, indicating that white syndromes have little effect on the physiology of the unaffected portion of *A. hyacinthus* colony. Gene co-expression network analysis revealed groups of genes co-regulated with respect to each of the three states, including a group of genes specifically up-regulated in AL samples.

Diseased tissues up regulate immune response elements

Innate immunity provides immediate protection against non-self and responds to physical injury. Three general steps are involved in an innate immune response: detection, defense activation, and effector responses to neutralize the threat. Tissues sampled from the lesion of disease progression in corals exhibiting white syndromes have enhanced expression of genes involved in each of these three immune response phases. C-type lectins act as pattern recognition receptors to activate pathogen elimination through phagocytosis in invertebrates (Fujita, 2002). Cnidarian genomes encode c-type lectin genes with highly variable substrate regions, leading to hypotheses that these proteins recognize a large variety of pathogens (Kvennefors, Leggat, Hoegh-Guldberg, Degnan, & Barnes, 2008). In *A. millepora*, mannose-binding C-type lectins have been shown to respond immediately following an immune challenge (only 45 minutes after lipopolysaccharide injection in (Kvennefors et al., 2010), but show no significant

response at later time points (Brown, Bourne, & Rodriguez-Lanetty, 2013). The up-regulation of C-type lectins in tissues at the lesion may suggest that these tissues have very recently become infected. The second phase of an immune response prepares targets for elimination via antimicrobial peptide synthesis and immune cell activation. While this experiment did not discover any differentially regulated antimicrobial peptides, I do detect the activation of immune activating proteins C4, alpha-macroglobulin and CD109 in diseased tissues. The lectin pathway of immune activation is triggered by lectins binding a pathogen-associated molecule and results in the activation complement component factor C4 and C3 (Matsushita & Fujita, 1992). These complement factors, along with alpha-macroglobulin and CD109, tag pathogens and secreted proteases for elimination. In the final phase of an innate immune response, foreign organisms are engulfed and destroyed by phagocytic immune cells. Lysosomes within these phagocytic cells contain proteins capable of degrading engulfed material via the production of reactive oxygen species (ROS) or proteolytic enzymes, such as cathepsins. The up-regulation of cathepsin L in diseased tissue may be a consequence of such phagocytic activity. The up-regulation of immune-related transcripts in diseased corals is consistent with previous studies of both naturally occurring disease and experimental pathogen challenges (Closek et al., 2014; Libro et al., 2013; Weiss et al., 2013). Just like the rest of genes exhibiting H-D difference, these responses are confined to the symptomatic regions of the coral. One possible explanation of this fact is that the immunity-related gene expression changes are elicited by direct contact with a pathogen rather than a systemic signal throughout the colony.

Switch to lipid-based metabolism in diseased tissues

Transcripts involving lipid and carbohydrate metabolism (triacylglycerol lipase, phosphoenolpyruvate carboxykinase), including glyoxylate cycle metabolism (malate synthase), were up-regulated in diseased tissues compared to asymptomatic tissues. The differential regulation of these metabolic genes suggests that diseased corals may be utilizing stored energy reserves more than healthy corals. Fatty acids derived from stored lipids are oxidized by the beta-oxidation pathway and release acetyl-CoA to enter the citric acid cycle. Both carbons in one molecule of acetyl-CoA are consumed during the decarboxylation steps of the citric acid cycle and energy is released. The glyoxylate cycle is an alternative route through the citric acid cycle that allows organisms to thrive on two-carbon sources by catalyzing the conversion of acetyl-CoA to malate and succinate via a glyoxylate intermediate, bypassing the decarboxylation steps in the citric acid cycle (Kornberg & Krebs, 1957). These four carbon compounds contribute to the energetic requirements of the cell and serve as building blocks for cellular components, fulfilling all the same necessities of the citric acid cycle without the need to replenish oxaloacetate from the diet. One of the most significantly up-regulated transcripts in diseased coral tissues was malate synthase, one of the key enzymes of the glyoxylate cycle along with isocitrate lyase. Glyoxylate cycle enzymes are rare throughout the animal kingdom, but bioinformatic analyses suggest they exist in cnidarians (Kondrashov, Koonin, Morgunov, Finogenova, & Kondrashova, 2006). As additional support for a potential role of glyoxylate cycle metabolism in coral stress responses, glyoxylate cycle transcripts were up-regulated in A. palmata larvae subjected to thermal stress (Polato, Altman, & Baums, 2013). In higher plants, glyoxylate enzymes are active when the cell is switching from photosynthetic production of sugars to scavenging pathways from stored and structural lipids, as in starvation and/or senescence (Wanner, Keller, & Matile, 1991). In corals, this

metabolic shift might indicate a decline in shared energy reserves with zooxanthellae, presumably due to stress-induced symbiont loss.

Oxidative stress response genes are up-regulated in diseased tissues

Reactive oxygen species (ROS) are produced as a consequence of fatty acid oxidation. The up-regulation of antioxidants that protect the cell from these harmful byproducts corals could be a consequence of increased fatty acid metabolism. This explanation coincides well with the observed up-regulation of lipid metabolism and antioxidant (catalase, peroxidase) transcripts in diseased corals. The production of ROS is also a fundamental element of the innate immune response. While ROS are capable of neutralizing phagocytized pathogens, the harm they cause to the host must be countered if an organism is to withstand its own immune response. Catalases and peroxidases capable of hydrolyzing harmful peroxides provide a mechanism of such self-protection. The up-regulation of oxidative stress response genes is well characterized in corals experiencing thermal stress (M. DeSalvo, Sunagawa, Voolstra, & Medina, 2010), physical stress (Lõhelaid, Teder, Tõldsepp, Ekins, & Samel, 2014), and infectious disease (Libro et al., 2013).

Matrix metalloproteinases are up-regulated in diseased tissues

Stony corals are subject to many potential sources of physical injury such as predators (Rotjan & Lewis, 2008), boring organisms (Lee Shing Fang & Shen, 1988) and storms (J.C. Bythell, Bythell, & Gladfelter, 1993; John C Bythell, Hillis-Starr, & Rogers, 2000). The tissue regeneration mechanisms employed by corals that have sustained a physical injury are common to wound-healing processes across metazoans (Palmer, Traylor-Knowles, Willis, & Bythell, 2011). One of these steps involves restructuring of the extracellular matrix to encourage tissue regeneration. Matrix metalloproteinases

(MMPs) are a group of enzymes capable of such activities and have been shown to play a direct role in wound repair in Hydra (Bosch, 2007). In addition, MMPs act on pro-inflammatory cytokines to direct inflammation due to wounding and innate immune responses to pathogens (reviewed in (Parks, Wilson, & López-Boado, 2004)). The up-regulation of MMPs in response parasitic protists in a gorgonian coral suggests that these proteins are active in the immune response of cnidarians (Burge, Mouchka, Harvell, & Roberts, 2013). Astacin and gelatinase have matrix metalloproteinase activities and were up-regulated specifically in affected coral tissues. Additionally, a protease inhibitor alpha-macroglobulin was up-regulated, which is a vital component of the innate immune response that inactivates bacterial secreted proteases, thus compromising their virulence (Armstrong & Quigley, 1999).

Calcification genes are down-regulated in diseased tissues

Calcification rates in reef-building corals are sensitive to several environmental variables such as light, pH, and temperature (Clausen & Roth, 1975; Hoegh-Gulberg, 1999; Kleypas, 1999; Tentori & Allemand, 2006). While this experiment did not directly measure coral calcification, the identification of DEGs with functions in biomineralization suggests that disease negatively impacts coral skeletal deposition. Both general extracellular matrix structural components and coral-specific calcification functions were differentially regulated in diseased tissues compared to asymptomatic tissues. Coral biomineralization is directed by an extracellular skeletal organic matrix comprised of secreted glycosylated proteins (Goffredo et al., 2011). These proteins include collagens and negatively charged macromolecules (like chondroitin sulfate proteoglycans) that bind calcium ions to aid in crystal formation (Weiner & Addadi, 1991). Several collagens and a protein with high similarity to nematogalectin, a collagen

family protein that forms a major structural component in Hydra nematocyst tubules (Hwang et al., 2010), were down-regulated in diseased tissues. The down-regulation of these genes in diseased tissues suggests a weakening of the coral skeletal organic matrix and thus a diminished capacity for biomineral deposition. The potential impact of disease on coral skeletal growth is most clearly revealed by the down-regulation of carbonic anhydrase, an enzyme that plays a fundamental role in mediating bicarbonate supplies for calcification in scleractinian corals (Allemand et al., 2004; Furla, Galgani, Durand, & Allemand, 2000; Aurélie Moya et al., 2008).

AL-specific gene expression: a systemic response to disease or factors contributing to disease susceptibility?

Genes that are specifically regulated in apparently healthy tissues of diseased colonies could represent systemic (*i.e.*, colony-wide) response to disease. However, there is another possible interpretation: since expression of these genes is correlated with natural appearance of disease, it might signify disease susceptibility rather than disease effects. A recent study employing similar a sampling scheme to investigate transcriptomic effects of yellow band disease (YBD) in *Orcibella faveolata* (Closek et al., 2014) found that expression in asymptomatic regions of diseased colonies was intermediate between completely healthy corals and diseased tissue, which fits well with the systemic response interpretation. In this study the AL expression was most similar to the healthy state (Figure 1.2 and 1.4A), although genes differentially regulated between diseased and healthy states demonstrated a non-significant trend towards intermediate expression in AL samples (Figure 1.4B). The difference between the two studies could potentially be explained by unequal levels of colony integration between *Orbicella* and *Acropora* (Oren, Benayahu, Lubinevsky, & Loya, 2001) and references therein), which could affect the extent of the systemic signaling and/or spread of the pathogen throughout

the colony. The co-expression network analysis revealed a sizeable (661 genes) module that was up-regulated in the AL state compared to D and H states (Figure A3). Among the genes most strongly associated with this module were the genes coding for the immunity-related Tolloid-like protein and the hypoxia inducible factor prolyl 4-hydroylase (HIF-P4H, Figure 1.5). Up-regulation of HIF-P4H suggests that healthy tissues of diseased colonies might be experiencing hypoxic conditions (G. L. Wang & Semenza, 1993) (D'Angelo, Duplan, Boyer, Vigne, & Frelin, 2003). Notably, HIF-P4H has also been shown to modulate immune responses by modifying the kinase responsible for releasing NF-κB from its inhibitor (Cummins et al., 2006). Up-regulation of these genes in healthy parts of diseased colonies might therefore be a sign of altered immunity state potentially explaining higher disease susceptibility of the affected colonies in nature.

Conclusions

Our gene expression analysis identified several immune, repair, and metabolic molecular pathways expressed in coral regions affected with white syndromes. In contrast to *Orbicella faveolata*, *A. hyacinthus* does not show pronounced propagation of these responses to regions of the colony not visibly affected by disease, suggesting that the effect of chronic white syndromes on colony-wide *A. hyacinthus* physiology is small. Instead, asymptomatic regions of diseased colonies show gene expression signatures potentially related to higher disease susceptibility of the affected coral individuals. Further studies of natural disease-associated gene expression will contribute towards the development of diagnostic tools to predict and manage coral disease outbreaks.

Chapter 2[2]: Intraspecific differences in molecular stress responses and coral pathobiome contribute to mortality under bacterial challenge in *Acropora millepora*

ABSTRACT

Disease causes significant coral mortality worldwide; however, factors responsible for intraspecific variation in disease resistance remain unclear. I exposed fragments of eight *Acropora millepora* colonies (genotypes) to putatively pathogenic bacteria (*Vibrio spp.*). Genotypes varied from zero to >90% mortality, with bacterial challenge increasing average mortality rates 4–6 fold and shifting the microbiome in favor of stress-associated taxa. Constitutive immunity and subsequent immune and transcriptomic responses to the challenge were more prominent in high-mortality individuals, whereas low-mortality corals remained largely unaffected and maintained expression signatures of a healthier condition (*i.e.*, did not launch a large stress response). Our results suggest that symptoms appeared due to changes in the coral pathobiome (multiple bacterial species associated with disease) and general health deterioration after the biotic disturbance, rather than the direct activity of any specific pathogen. If diseases in nature arise because of weaknesses in holobiont physiology, instead of the virulence of any single etiological agent, environmental stressors compromising coral condition might play a larger role in disease outbreaks than is currently thought. To facilitate the diagnosis of compromised individuals, I developed and independently cross-validated a biomarker assay to predict mortality based on genes whose expression in asymptomatic individuals coincides with mortality rates.

[2] Chapter 2 is in press at *Scientific Reports*.

INTRODUCTION

Global declines in coral cover are compounded by a variety of diseases (Harvell et al., 1999; Weil & Rogers, 2011), many of which are ambiguously defined by macroscopic characterizations of lesions (Harvell et al., 1999; Pollock et al., 2011; Weil & Rogers, 2011). Several bacterial species from the genus *Vibrio* have been implicated as etiological agents of some coral diseases (Sussman et al., 2008; Ushijima et al., 2014; Ushijima, Smith, Aeby, & Callahan, 2012), but these bacteria may act merely as opportunistic pathogens exploiting compromised hosts (Lesser, Bythell, Gates, Johnstone, & Hoegh-Guldberg, 2007). The reported presence of pathogens on healthy colonies (Bourne & Munn, 2005) and diversity of bacterial species associated with diseased colonies (Closek et al., 2014; Roder, Arif, Daniels, Weil, & Voolstra, 2014) suggests that many instances of that coral disease cannot be attributed to a single pathogen. Instead, multiple bacteria appear to act opportunistically during coral disease events (Sunagawa et al., 2009). To describe these recurrent phenomena in coral disease biology, researchers have recently introduced the concept of the pathobiome (Sweet & Bulling, 2017). Instead of a single etiological agent, the pathobiome consists of all microbiota that contribute to disease and describes interactive effects between microbiome members and environmental conditions (Vayssier-Taussat, Albina, Citti, & Cosson, 2014).

Host immune health is considered to be a major determinant of disease transmission dynamics (Muller & van Woesik, 2012; Vollmer & Kline, 2008). Corals, like all invertebrates, rely entirely on innate immunity for protection from invading pathogens. Features of innate immunity in corals include molecular pattern recognition (Miller et al., 2007), secreted antimicrobial macromolecules (Vidal-Dupiol, Ladrière, Meistertzheim, et al., 2011), cellular responses (*e.g.*, phagocytosis) (Mydlarz & Harvell,

2007; Mydlarz, Jones, & Harvell, 2006), and physical barriers (*e.g.*, mucus) (Brown & Bythell, 2005; Teplitski & Ritchie, 2009). Melanin deposits serve as another physical barrier against invading pathogens (Petes, Harvell, Peters, Webb, & Mullen, 2003). The melanin synthesis cascade is activated when pathogen recognition triggers cleavage of prophenoloxidase (PPO) to phenoloxidase (PO). Reactive oxygen species (ROS) produced during melanin synthesis contribute to its cytotoxic effects on pathogens, but also cause self-harm (Sadd & Siva-Jothy, 2006) that must be countered by antioxidant enzymes such as catalase (CAT) and peroxidase (POX).

Field surveys of naturally occurring coral disease outbreaks show marked variability in mortality among conspecifics, despite the fact that neighboring colonies are exposed to the same environmental stressors and, presumably, the same potential pathogens (Gochfeld, Olson, & Slattery, 2006; Vollmer & Kline, 2008). One possible explanation is that some corals resist disease by making greater contributions to constitutive or inducible immunity. Coral families that invest more in innate immunity (*e.g.*, production of cytotoxic defenses) are less likely to suffer infectious disease outbreaks (Palmer, McGinty, et al., 2011; Palmer, Bythell, & Willis, 2010). One of the hardiest coral species in the Caribbean – *Porites astreoides* – is characterized by elevated immunity compared to species from other coral families (Palmer et al., 2010). However, no laboratory experiments have yet addressed the role of immunity or other molecular characteristics in driving variation in disease outcomes among conspecifics within any coral species.

In this study, I comprehensively examine coral host immune activity, genome-wide gene expression, *Symbiodinium* profiles, and coral-associated microbial communities in a bacterial challenge experiment to understand the physiological and molecular features underpinning intraspecific variation in mortality rate. Fragments of

eight colonies of *Acropora millepora* from two locations on the Great Barrier Reef (GBR) were individually challenged in a full-factorial design with bacteria (*Vibrio owensii* and *V. diazotrophicus*) and mechanical abrasion (n = 3 per experimental group, Figure A11). These fragments were monitored over a week of lesion development and progression. Unchallenged control samples were used to identify baseline correlations of constitutive physiological parameters with survivorship. Post-challenge, yet asymptomatic, samples demonstrated genotype-specific gene expression responses to the bacterial challenges.

METHODS

Coral collection

Corals in the experiment were collected under the permit number G12/35236.1 by the Great Barrier Reef Marine Park Authority of Australia. *A. millepora* were sampled from 3–6 m depth at the lagoon at Lizard Island (14°41'13.64S:145°27.75E) and the sheltered side of Wilkie Island (13°46'43.33S:143°38.75E; n = 4 colonies per reef) in the Great Barrier Reef in October 2013. Each colony is hereafter referred to as an individual genotype, a classification that is confirmed by our transcriptomic results that clearly distinguish separate colonies (genotypes). Colonies were maintained in an outdoor raceway under flow through conditions and filtered natural light at the National Sea Simulator at the Australian Institute of Marine Science until fragmentation in November 2013. Colonies were further fragmented (Figure A11) into replicate nubbins (4–5 cm) and secured on wire hooks (n = 18 per genotype).

Experimental aquaria and abrasion procedure

Coral fragments were secured upright in individual jars containing 200 mL 0.04 μM-filtered seawater (FSW). Fluorescent lights provided light on a 12:12 h day/night

schedule and the temperature was maintained at 26–27°C. Half of the 18 coral fragments received two small (~1 cm2) abrasions with a high-pressure airgun. These small abrasions mimicked clean lesion-associated injuries that occur in nature (*e.g.*, corallivorous fish bites). The original purpose of the abrasion was to increase the probability of lesion development after bacterial challenge, in the event that inoculation with bacteria alone did not affect the corals. In reality both abraded and non-abraded corals developed lesions, thus all treatments were included in the analysis to maximize statistical power.

Bacterial culturing and challenge

Vibrio owensii strain DY05 and a diazotroph with high sequence similarity to *V. diazotrophicus* were used in this study. These bacteria were chosen based on their published pathologies (or lack thereof) and the availability of local isolates to minimize biocontainment risks. *V. owensii* has been implicated as the pathogenic agent of a tissue-loss disease in a Hawaiian coral, *Montipora capitata* (Ushijima et al., 2012). This isolate of *V. owensii* had been recently sampled during an infectious disease outbreak in cultured lobsters at the research facility. At the time of this study *V. diazotrophicus*, a nitrogen-fixing bacterium that had been isolated from healthy *A. millepora* juveniles (Lema et al., 2016), had not been implicated as a causative agent of any coral disease. Single isolates of each bacterial strain were recovered from glycerol stocks on Difco Marine Agar-2216 (BD, Franklin Lakes, NJ, USA) at 28°C. Cultures were incubated overnight at 28°C with shaking (150 rpm) in Difco Marine Broth-2216 (BD). Overnight cultures were triple-washed in FSW by centrifugation at 5000 *g* for ten minutes and resuspended in FSW. Washed cells were diluted to a final concentration of 1×10^6 colony forming units (CFUs) $\cdot$ mL^{-1} in FSW. Cell densities were determined by counting CFUs resulting from

plated serial dilutions and constructing a cell density calibration curve of absorbance (595 nm) versus CFU number. Of the nine abraded fragments per genotype, three were challenged with *V. owensii*, three were challenged with *V. diazotrophicus*, and three received daily "inoculations" of FSW (control). The nine non-abraded fragments received the same treatments. Aquarium water was changed daily preceding each bacterial challenge. Fragments were monitored for tissue loss and photographed twice daily throughout the experiment with a Nikon D300 digital camera (Nikon, Tokyo, Japan). Corals were photographed and removed from the experiment when tissue loss was visually estimated at 50% or more of the total surface area of the fragment (*e.g.*, Figure A12A: Genotypes 9 and 26). Symptomatic fragments (*i.e.*, those that developed a lesion) were not included in subsequent analyses. All remaining asymptomatic fragments were frozen in liquid nitrogen and stored at -80°C on the sixth day following the initial bacterial challenge for subsequent gene expression and protein analyses.

Survival analysis

All statistical analyses were performed in R version 3.3.1 (R Core Team, 2016). The time when fragments suffered ~50% tissue loss was recorded for each fragment as time of death. Survivorship analyses were performed for each genotype, reef, abrasion treatment, and bacterial challenge using the Kaplan-Meier estimate of the survival function as implemented by survfit in the R package survival (Therneau, 2014). Step-AIC analysis based on Cox proportional hazards model was performed using stepAIC function of the MASS package and coxph function of the survival package. The full model tested involved abrasion (abrasion/no abrasion), bacteria (control, V. owensii, V. diazotrophicus), genotype (eight categories) and the interaction between bacteria and genotype. The selected model with the lowest AIC score retained all these factors except

the bacteria:genotype interaction, which increases the AIC score by 3 points. Testing for conformity of these factors to the model assumptions using the cox.zph function of package survival revealed that abrasion was not suitable as a factor; it was therefore modeled as a data stratification variable using the strata function of the survival package.

Enzymatic assays

Coral proteins were extracted following a protocol adapted from established procedures (Mydlarz, Couch, Weil, Smith, & Harvell, 2009). Briefly, coral tissue was removed using an airbrush and cold extraction buffer (100 mM Tris-HCl, pH 7.8, with 0.05 mM dithiothreitol). Airbrushed tissue slurries were homogenized with 1 mm glass beads (BioSpec, Bartlesville, OK, USA) by vortexing for two minutes. The tissue slurry was centrifuged at 4°C for 10 minutes at 3200 *g* to separate coral and algal fractions. The coral protein supernatant (protein extraction) was removed and stored at -80°C until use. Surface area determinations of airbrushed skeletons were made following a modified wax dipping protocol (Stimson & Kinzie, 1991). A standard curve was prepared from a series cylinders of known surface area dipped in paraffin wax (Gulf Wax, Roswell, GA, USA) at 60°C. Coral skeletons were weighed and dipped twice in paraffin wax (59–60°C), weighing after each wax dip. For each fragment, the difference between initial weight and weight after second dip was compared to the standard curve to yield surface area in cm2.

Total protein was assessed in triplicate using the RED660 protein assay (G Biosciences, St. Louis, MO, USA) with a standard curve prepared from bovine serum albumin. Sample absorbance at 660 nm was compared to the curve and normalized to surface area and the tissue slurry volume.

Prophenoloxidase activity was assayed in triplicate by mixing 20 μL of sodium phosphate buffer (50 mM, pH 7.0), 25 μL of trypsin (0.1 mg · mL^{-1}), and 20 μL of protein extract. Dopamine (30 μL, 10 mM) was added as substrate and absorbance at 490 nm was measured every 30 seconds for 15 minutes. Change in absorbance was calculated during the linear range of the curve (1–3 minutes). Activity was expressed as the change in absorbance per mg of protein (ΔA_{490} · mg $protein^{-1}$ · min^{-1}). Phenoloxidase activity was assayed in triplicate by mixing 20 μL of sodium phosphate buffer (50 mM, pH 7.0), 25 μL of sterile water, and 20 μL of protein extract. Dopamine (30 μL, 10 mM) was added as substrate and absorbance at 490 nm was measured every 30 seconds for 15 minutes. Change in absorbance was calculated during the linear range of the curve (1–3 minutes). Activity was expressed as the change in absorbance per mg of protein (ΔA_{490} · mg $protein^{-1}$ · min^{-1}). Catalase activity was assayed in triplicate by mixing 45 μL of sodium phosphate buffer (50 mM, pH 7.0), 75 μL of 25 mM H_2O_2, and 5 μL of protein extract. Samples were loaded on ultraviolet transparent plates (UltraCruz, Santa Cruz Biotechnology, Dallas, TX, USA) and absorbance at 240 nm was measured every 30 seconds for 15 minutes. Change in absorbance was calculated during the linear range of the curve (1–3 minutes). Activity was expressed as the change in hydrogen peroxide concentration per mg of protein (ΔH_2O_2 · mg $protein^{-1}$ · min^{-1}). Peroxidase activity was assayed in triplicate by mixing 40 μL of sodium phosphate buffer (10 mM, pH 6.0), 25 μL of 10 mM guaiacol, and 10 μL of protein extract. Absorbance at 470 nm was measured every 30 seconds for 15 minutes. Change in absorbance was calculated during the linear range of the curve (1–3 minutes). Activity was expressed as the change in absorbance per mg of protein (ΔA_{470} · mg $protein^{-1}$ · min^{-1}).

Activities of CAT, POX, PO, and PPO were normalized to the total protein concentration, log-transformed, and compared among treatments using MCMCglmm

function (Hadfield, 2010). Log-transformation was chosen based on diagnostic plots of a linear model with abrasion, bacteria and genotype as factors. The MCMC model included abrasion and bacterial treatment as fixed factors and genotype-specific mean and reaction norm in response to bacteria as random effects. The reaction norm was calculated as the change in enzymatic activity for each genotype. I used the standard weakly informative inverse-Wishart priors for the random effects. The model was run for 55,000 iterations collecting parameter samples every 50 iterations; parameters collected during the first 5000 iterations were discarded.

Gene expression

All tissue samples for gene expression were collected from asymptomatic individuals within one hour on the sixth day following the initial bacterial challenge. RNA was extracted from whole preserved coral nubbins (including any mucus, holobiont tissue containing intracellular algal symbionts, and skeleton) using RNAqueous Total RNA Isolation kits (Ambion). Genome-wide gene expression was analyzed using tag-based RNA-seq (TagSeq) method (Meyer et al., 2011). The reads were trimmed, deduplicated, quality filtered, mapped to the *A. millepora* reference transcriptome (Moya et al., 2012) using bowtie2 (Langmead & Salzberg, 2012), and converted to UTCs representing the number of independent observations of a transcript of a specific gene, summed over all isoforms for each gene. Such read processing in TagSeq was recently shown to result in more accurate representation of transcript abundances than standard RNA-seq (Lohman, Weber, & Bolnick, 2016). Sample outliers were detected using R package the arrayQualityMetrics (Kauffmann et al., 2009) and differential gene expression analysis was performed using DESeq2 (Love et al., 2014). P-values for significance of contrasts between treatments, survival, and the survival by treatment

interaction were generated based on Wald statistics and adjusted for multiple testing using the Benjamini-Hochberg method (Benjamini & Hochberg, 1995) applied following an independent filtering procedure (integral to the DESeq2 pipeline) to maximize the number of detected differentially expressed genes. Gene expression heatmaps with hierarchical clustering of expression profiles were created with the pheatmap package in R (Kolde, 2013).

***Symbiodinium* analysis**

Trimmed and quality filtered RNAseq reads were mapped to *Symbiodinium* clade A, B, C, and D transcriptomes with bowtie2 (Langmead & Salzberg, 2012). A custom perl script generated counts from mapped reads and calculated clade fractions. The R package MCMC.OTU (Green, Davies, Matz, & Medina, 2014) was used to implement generalized linear mixed model analysis to test for significant differences in clade abundances.

Microbial community analysis

Microbial communities were profiled for one pre-treatment (separated from the colony before the experiment began), *V. diazotrophicus*-treated, *V. owensii*-treated, and untreated control fragment for each genotype. DNA was isolated using an RNAqueous kit together with the RNA for gene expression analysis. DNA samples were diluted to 10 ng · μL^{-1}. The bacterial 16S rRNA gene V4/V5 region was amplified using the Hyb515F (5'-TCGTCGGCAGCGTCAGATGTGTATAAGAGACAGGTGYCAGCMGCCGCGGTA-3') and Hyb806R (3'-TAATCTWTGGGVHCATCAGGGACAGAGAATATGTGTAGAGGCTCGGGTGCTCTG-5') primers and sequenced on the MiSeq V2 platform to generate 250 bp paired

reads. Sequences with homopolymer runs of six or more consecutive bases (12,128 sequences) or incorrect primer sequence (63,719 sequences) were discarded using split_libraries.py in QIIME (Quantitative Insights Into Microbial Ecology) (Caporaso et al., 2010). Sequences of 97% similarity were clustered into operational taxonomic units (OTUs). A phylogeny was generated by aligning representative sequences that were filtered to remove gaps and hypervariable regions. Principal coordinate analyses and PERMANOVA (adonis) were conducted based on UniFrac distances (Lozupone, Lladser, Knights, Stombaugh, & Knight, 2011) using the R package vegan (P. Dixon, 2003). Significant differences in abundances of OTU types between treatment and continuous survival were assessed using generalized linear mixed model implemented in the MCMC.OTU package in R (Green et al., 2014).

Validation experiment

The bacterial challenge was repeated in March 2013. *A. millepora* (N = 43 genotypes, five fragments per genotype) were challenged daily with 10^6 CFU · mL^{-1} *V. owensii* DY05 as described above. An equal number of control fragments for each genotype were maintained under ambient conditions (26°C). Survival was monitored for seven days of daily bacterial challenges. On the final day, ~1cm^2 tissue samples were preserved in 100% ethanol and stored at -20°C. These corals were collected under the permit number G12/35236.1 by the Great Barrier Reef Marine Park Authority of Australia. Nineteen genotypes spanning a range of survival rates were used in the qPCR validation.

Quantitative real-time PCR (qPCR) validation of putative biomarkers

Candidate diagnostic gene expression biomarkers were selected based on differential expression with regard to survival in the response gene expression dataset and

had putative functions that could be related to immune defense. Primers were designed using Primer3 (Untergasser et al., 2012). For *dmbt1*, the forward and reverse primers were 5'-TCATGTGACCTGTGTTGGGA-3' and 5'-GGTGACGCTCCGATCAAAC-3', respectively. For *mmp*, the forward and reverse primers were 5'-GTTCCAAAATCGGCCACACC-3' and 5'-CGTTATGCAGGGCTTCCAGA-3', respectively. Primer pair specificity was verified by gel electrophoresis and melt curve analysis of the amplification product obtained with template *A. millepora* cDNA. Primer efficiencies were determined by amplifying a series of two-fold dilutions of *A. millepora* cDNA and analyzing the results using function PrimEff of the MCMC.qpcr package in R (Matz, Wright, & Scott, 2013). Briefly, C_T (threshold cycle) results were plotted as C_T vs. $\log_2$[cDNA], and amplification efficiencies (amplification factor per cycle) of each primer pair were derived from the slope of the regression using formula: efficiency = $2^{-(1/\text{slope})}$ (Pfaffl, 2001). RNA isolation, cDNA preparation, and qPCR were carried out as previously described (Kenkel et al., 2011) with the exception that the RNAqueous Total Isolation Kit (Ambion) was used to isolate total RNA. Linear regression implemented in R was used to test for the relationship between survival fraction and the log-difference in expression between the two candidate genes, as in (Kenkel et al., 2011).

RESULTS

A. millepora genotypes show significant differences in mortality

No lesions formed under control conditions in any genotype, whereas some fragments died after abrasion (Figure 2.1A) and many more died under bacterial or combined treatment (Figure 2.1B). There was no significant difference in mortality among genotypes with respect to the abrasion treatment alone (Figure 2.1A); I only find evidence for differential mortality among genotypes to the biotic challenges (Figure

2.1B). I performed stepwise Akaike information criterion analysis of Cox proportional hazards models to determine which experimental factors and/or interactions affected mortality (Table A1).

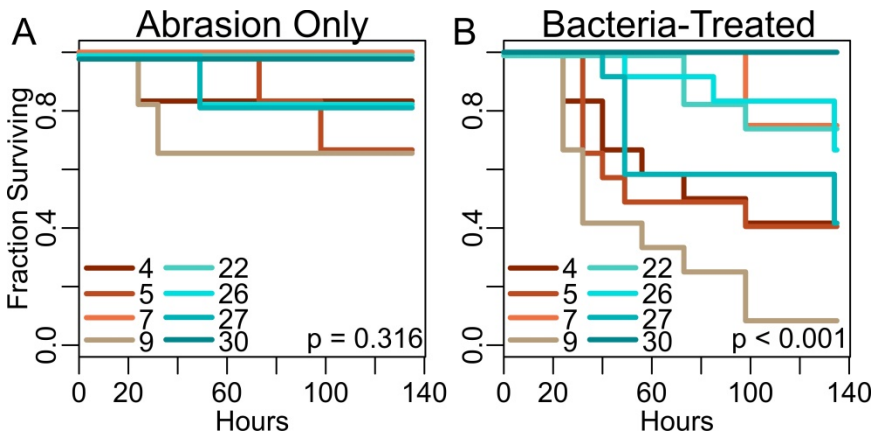

Figure 2.1: Differences in survival among *A. millepora* genotypes. (A) Survival of abraded fragments without bacterial challenge. (B) Survival of bacteria-treated fragments (abraded and non-abraded). Differential mortality among genotypes is only observed in response to the bacterial challenge. No mortality was observed among control fragments. P-values correspond to the effect of genotype in a Cox proportional hazards model. Genotypes 4, 5, 7, 9 are from Lizard Island, genotypes 22, 26, 27, 30 are from Wilkie Island.

Coral genotypes differed significantly in their mortality rates under bacterial challenge (Figure 2.1B; $p < 0.001$). Bacterial treatment significantly increased mortality ($p < 0.001$) regardless of the genotype (*i.e.*, mortality under bacterial challenge was modeled as mortality under abrasion amplified by the same factor in all genotypes). The increased mortality was similar between challenge agents (*V. diazotrophicus*: 5.7-fold; *V. owensii*: 3.7-fold), and there was no significant difference in time-dependent mortality between the two bacterial species (Figure A13; $p = 0.108$). Although abrasion clearly led to increased mortality (Figure A13), it did not conform to the assumptions of the Cox proportional hazards model ($p < 1e\text{-}6$ for model conformity) since it affected mortality only in the first several days, violating the assumption of risk invariance throughout the experiment. To nevertheless account for variation in mortality associated with abrasion, I ran our Cox proportional hazards model with abrasion included as a data stratification variable.

Based on the lack of difference between two *Vibrio* species I simplified our subsequent analyses by considering only two bacteria-related factor levels where corals were either exposed to bacteria ($n = 12$ per genotype, pooling *V. owensii* and *V. diazotrophicus* treatments) or not ($n = 6$ per genotype). Also, since bacterial challenge led to statistically indistinguishable multiplicative increases in mortality among genotypes (about 4–6 fold), I focused our study on variation in overall genotype robustness, expressed as the fraction of replicate fragments surviving until the end of experiment. As two extremes, >90% of all fragments of genotype 9 died in response to the experiment while genotype 30 experienced no mortality at all. The remaining six genotypes experienced intermediate mortality (42–75%). This distribution, with few individuals showing extreme values while the majority shows intermediate values, is expected of a natural quantitative trait following a beta distribution.

Higher constitutive immune activities and responses do not translate into lower mortality rates

Phenoloxidase (PO) and prophenoloxidase (PPO) measurements serve as proxies for cytotoxic defenses via the melanin-synthesis pathway, and catalase (CAT) and peroxidase (POX) activities indicate antioxidant capabilities. CAT, POX and PO were expected to increase as a result of infection, while PPO was expected to decrease due to conversion to PO. I measured these activities in asymptomatic bacteria-challenged and unchallenged fragments sampled at the conclusion of the experiment. The data were analyzed using Markov Chain Monte Carlo-based Bayesian linear mixed model with two fixed factors: abrasion (yes or no) and bacterial challenge (challenged or control). Genotype-specific means and genotype-specific changes in activity in response to bacteria (reaction norms) were modeled as random effects. The estimates of genotype-specific effects were sampled 1000 times from the posterior distribution of parameters and tested for the sign of correlation with survival. The proportion of sampled parameter series exhibiting a particular sign of correlation can be interpreted as a posterior probability of correlation with that sign.

All observed changes in immune activity were in the expected direction. Although pronounced changes in immunity-related enzyme activities were apparent as a result of bacterial challenge in some genotypes (Figure 2.2), only the 3.2-fold increase in CAT activity was significant overall (Figure 2.2A; $P_{MCMC} = 0.002$). POX and PO activities both increased ~1.5-fold under bacterial challenge (Figure 2.2B,C), while PPO decreased 2-fold (PMCMC = 0.06, Figure 2.2D). Notably, for all enzymes, low-mortality genotypes tended to have lower means and reaction norms (Figure 2.3). This negative correlation was significant (posterior probability >0.95) for POX and PO reaction norms (Figure 2.3F, G), implying weaker responses of these enzymes to bacterial treatment in more

robust genotypes. These correlations were largely driven by the most robust genotype (30, no mortality under any treatment). Significant genotype correlations disappeared after excluding this one genotype (Figure A14).

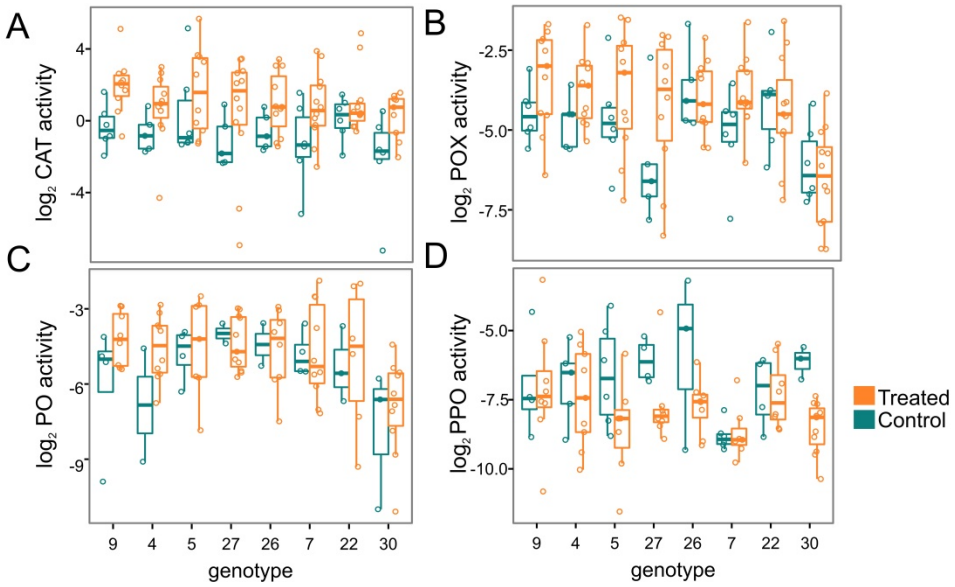

Figure 2.2: Immunity-related enzyme activities by genotype. Catalase (CAT), peroxidase (POX), phenoloxidase (PO), and prophenoloxidase (PPO) activities are represented as log2-transformed Δ absorbance mg protein^{-1} min^{-1}. Genotypes are sorted by increasing survival from left to right.

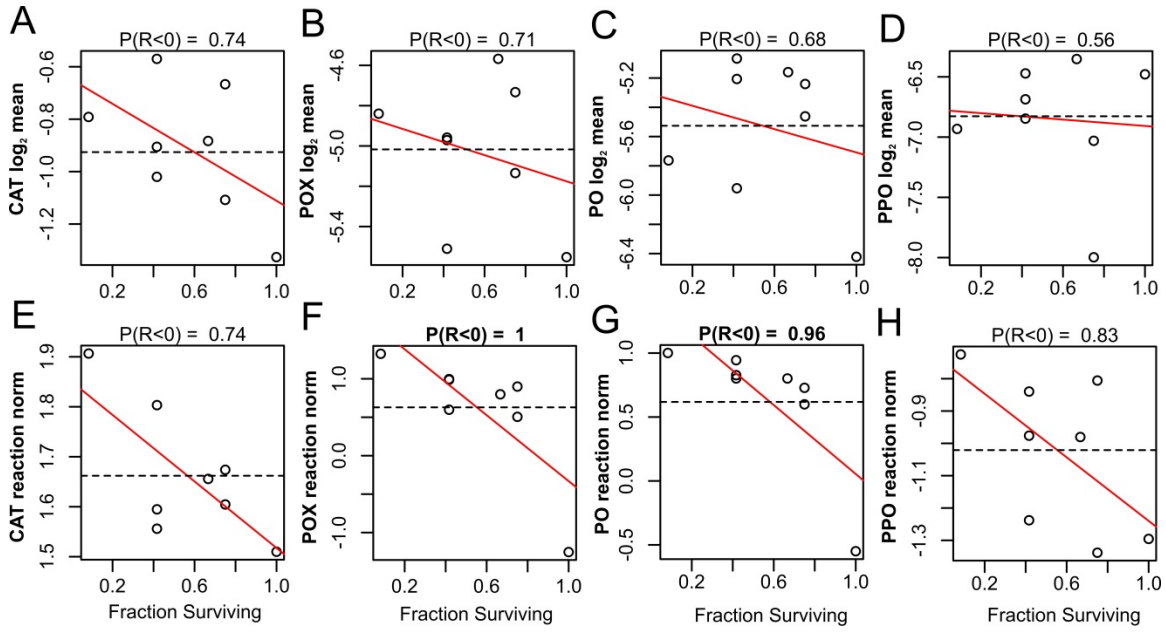

Figure 2.3: Correlations of mean immunity-related enzyme activities (A–D) and their reaction norms in response to bacterial challenge (E–H) with survival across genotypes. Mean catalase (CAT), peroxidase (POX), phenoloxidase (PO), and prophenoloxidase (PPO) activities are represented as $\log_2$-transformed Δ absorbance mg protein^{-1} min^{-1}. Each point represents a posterior mean of the parameter for a genotype; dotted lines represent means across genotypes, red line is the linear model fit with survival as predictor variable. Value above the graph indicates posterior probability that the correlation with survival is negative.

Sequencing results

Sequencing data have been deposited to the National Center for Biotechnology Information's Short Reads Archive under accession numbers SRP074065 and SRP073937. Genome-wide gene expression was analyzed using TagSeq, a cost-efficient highly accurate alternative of RNA-seq (Lohman et al., 2016; Meyer et al., 2011). Sequencing yielded an average of 2,042,678 reads per sample. Because only one readable fragment per transcript is generated in TagSeq, each read represents an observation of a unique transcript (a "unique transcript count", UTC) after removing PCR duplicates. A total of 44,687 genes were detected after mapping to the *A. millepora* transcriptome (A

Moya et al., 2012). UTCs for all isoforms of a given gene were summed. An average of 360,642 UTCs per sample was obtained. The expression dataset was restricted to genes with a mean UTC greater than three, retaining 14,633 genes. No outlier samples were detected.

Bacterial treatment triggered gene expression response in high-mortality corals

Only control and asymptomatic bacteria-challenged fragments sampled at the conclusion of the experiment were included in the gene expression analysis. Gene expression was analyzed using DESeq2 models including bacterial treatment (treated or control), percent survival (continuous variable), the interaction between the survival and bacterial treatment (*i.e.,* survival-dependent effect of bacteria) and abrasion (yes or no) as a covariate. In a separate set of models, I also performed pairwise comparisons among all three bacterial treatments (control, *V. diazotrophicus*, and *V. owensii*). Only one gene was differentially expressed between the *V. diazotrophicus* and *V. owensii* treatments, further justifying pooling of these treatments as a general bacterial challenge.

The contrast between control vs. bacteria challenge yielded 288 DEGs at FDR = 0.1. Testing for associations between gene expression and survival yielded 1412 DEGs at FDR = 0.1. To improve readability, I have only depicted the top 16 annotated DEGs for the effect of bacterial treatment (Figure 2.4A; FDR = 0.01) and the top 41 annotated DEGs for the effect of survival (Figure 2.4B; FDR = 1e-4). Bacterial challenge triggered up-regulation of phosphoenolpyruvate carboxykinase (PEPCK) and several matrix metalloproteinases (MMPs) (FDR < 0.001; Figure 2.4A). Interferon gamma (FDR = 0.07) and apoptosis regulator Bcl-W (FDR < 0.001) were upregulated in bacteria-challenged corals, whereas deleted in malignant brain tumors protein 1 (*dmbt1*; FDR = 0.002), cryptochrome (FDR = 0.004), carbonic anhydrase (only one out of 21 paralogous

genes in this *A. millepora* transcriptome; FDR = 0.07), and galaxin (FDR = 0.04) were downregulated. Notably, the gene expression response to bacterial challenge was driven by higher-mortality genotypes, as expression profiles of the more robust corals (*i.e.*, lower mortality) remained similar to the control condition (Figure 2.4A). Indeed, a DESeq2 model predicted lower fold-changes in more robust corals for essentially all the bacteria-responding DEGs, implying minimal if any effect of bacterial challenge on more robust genotypes (Figure A15). Relative to less robust corals, challenged and unchallenged resistant corals expressed elevated glucose-6-phosphate 1-dehydrogenase and fluorescent proteins (cyan and green) and diminished stress-related MAP kinase-interacting protein, ubiquitin ligase, hemicentin-1, complement factor B, and C-type lectin (FDR < 0.001; Figure 2.4B).

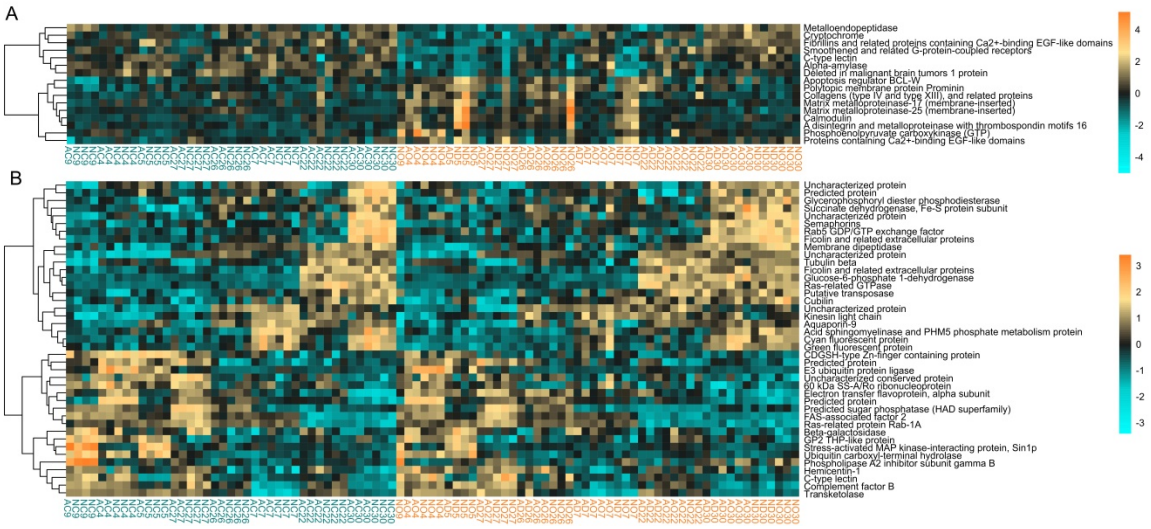

Figure 2.4: Gene expression differences in response to bacterial challenge (A, FDR = 0.01) and associated with survival rate among genotypes (B, FDR = 1e-4). In all panels, rows are genes and columns are samples. Samples are ordered by genotype survival, from lowest to highest, within each treatment group. The color scale is in $\log_2$-fold change relative to the gene's mean. Genes are hierarchically clustered based on Pearson's correlations of expression across samples. Bacteria-challenged samples are indicated in orange font below the heatmap; control samples are turquoise. Sample names correspond indicate abrasion (yes, "A", or no, "N"), bacterial treatment (control, "C", *V. diazotrophicus*, "D", *V. owensii*, "O"), and genotype (number).

Tests of the interaction between survival and treatment yielded two DEGs at FDR = 0.1. A rank-based gene ontology analysis revealed significant enrichment of terms including G-protein coupled receptor signaling pathway and protein ubiquitination, which were more upregulated in response to treatment in high mortality corals than in lower mortality corals. Ribosome biogenesis, small molecule metabolic process, protein folding, stress responses, and establishment of protein localization processes were less upregulated in response to treatment in high mortality corals compared to corals with lower mortality (Figure A16). No biological processes or molecular functions were significantly enriched with respect to the effect of treatment or survival.

Symbiodinium profiles differ only by reef

Symbiodinium communities were profiled using RNA-seq reads mapping uniquely to clade A, B, C, or D *Symbiodinium* transcriptomes. On average I obtained 25,480 reads mapping to these transcriptomes per sample (maximum = 156,098, minimum = 4644). As expected for *A. millepora* in the northern region of the GBR, clade C dominated most genotypes (Cooper et al., 2011) but two colonies from Wilkie were dominated by D (Figure A17). There was no association of *Symbiodinium* clade dominance with survival rate ($p = 0.33$).

Microbial community profiles differ between individuals and in response to bacterial challenge

The presence of *V. owensii* and *V. diazotrophicus* sequences was verified by NCBI BLAST queries (E-value cutoff 1e-100) using reference sequences for these strains (GenBank accession numbers GU018180 (Cano-Gómez, Goulden, Owens, & Høj, 2010) and KF691569 (Lema et al., 2016), respectively). Overall, more *V. owensii* sequences were found (59 in untreated, 1920 in VO-treated, and 1115 in VD-treated). Only one diazotroph read was found in a control sample, whereas 350 and 45 were found in VD- and VO-treated samples, respectively. Clustering at 97% similarity identified 1238 operational taxonomic units (OTUs) based on the 16S rRNA V4/V5 region. Two best-surviving genotypes (22 and 30) had significantly more cyanobacterial and chloroplast-derived OTUs than other genotypes (Figure A12B; FDR = 0.001). Chloroplast OTUs were homologous to the green marine algae, *Ulvophyceae*, a group that includes common endolithic photoautotrophs (Marcelino & Verbruggen, 2016). The skeletons of genotypes 22 and 30 were noticeably green (Figure A12A), supporting the hypothesis that elevated proportion of chloroplast OTUs in these corals is due to higher loads of endolithic algae. All chloroplast-derived OTUs were excluded from subsequent analysis of the bacterial

populations. One sample that did have a lesion (NO53) was accidentally included in the sequencing, but removed from subsequent analysis. The microbiome of this one sample is massively different from all other samples, yet *Vibrio spp*. are still noticeably absent.

Faith's phylogenetic diversity (PD_whole_tree) for each sample was calculated using the alpha_diversity.py script in QIIME. Generalized linear models tested the fixed effects of continuous survival (fraction) and treatment with reef, genotype, and number of sequences used to calculate the distances as random effects. Phylogenetic diversity of the microbial communities was greater in treated corals (effect = 2.35, $p < 0.001$) and in corals with lower mortality (effect = 2.51, $p = 0.04$) (Figure A18).

Principal coordinate analysis (PCoA) of weighted (quantitative) UniFrac distances separated samples by survival along PCo1 and by treatment along PCo2 (Figure 2.5A). Principal coordinates analysis based on unweighted UniFrac (qualitative) distances clustered samples only by treatment along the major axis (Figure 2.5B).

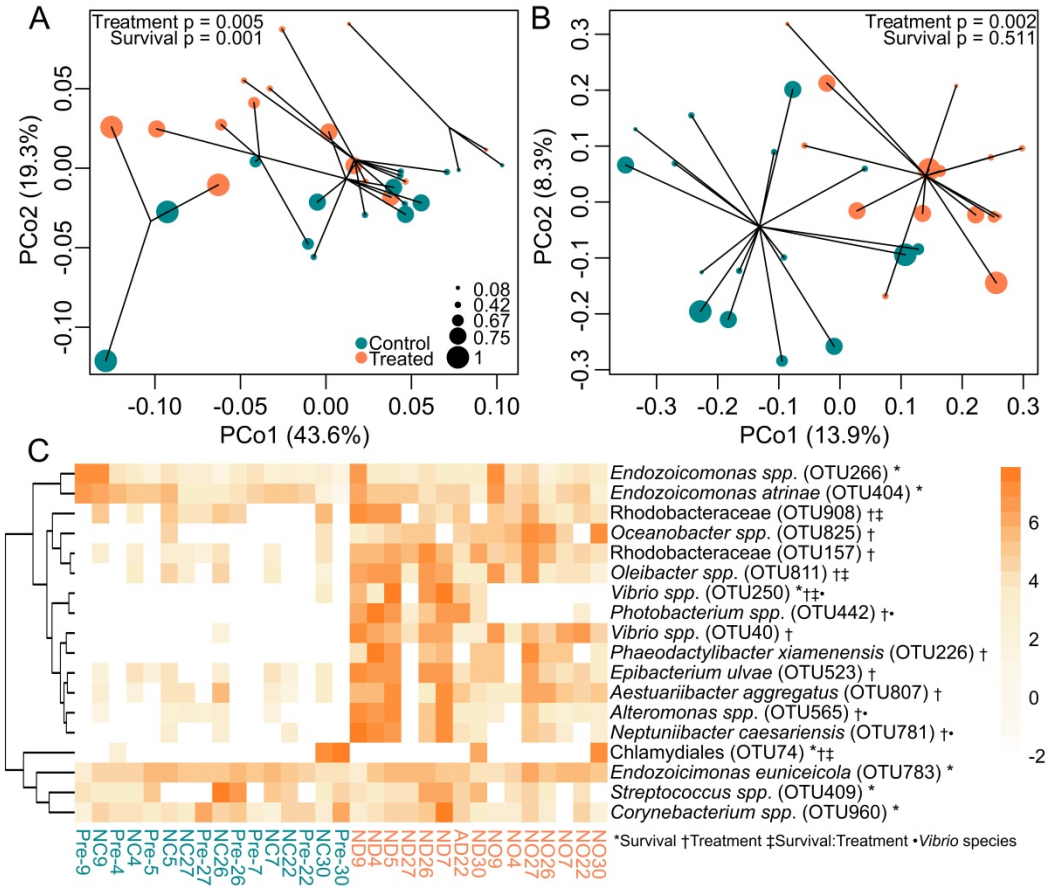

Figure 2.5: Microbial community composition by treatment and survival. Principal coordinate analysis of microbial community profiles using weighted (A) and unweighted (B) UniFrac distances. Samples are clustered according to the variable that separates along the major axis: survival fraction in (A) and by treatment in (B). P-values were generated by a PERMANOVA testing the effect of survival fraction and treatment. Sphere size represents survival fraction. (C) Heatmap of the most significantly ($P_{MCMC} < 0.1$) differentially abundant OTUs by treatment, survival, or their interaction. Symbols following OTU names indicate significance (see inset key). Color scale is in log_2-fold change relative to the OTU's mean. OTUs are hierarchically clustered based on Pearson's correlations of abundance across samples. Samples are ordered by genotype survival, from lowest to highest, within each treatment group. Bacteria-challenged samples are indicated in orange font below the heatmap; control samples are turquoise. Sample names correspond indicate abrasion (yes, "A", or no, "N"), bacterial treatment (control, "C", *V. diazotrophicus*, "D", *V. owensii*, "O"), and genotype (number). Samples labeled "pre-" were sampled before the experiment began.

To investigate the relationship between host gene expression and microbial composition, I subset the RNAseq dataset for individuals with 16S sequencing data (n = 31) and modeled gene expression correlated with the first principal coordinate axis based on weighted UniFrac scores (Figure 2.5A) after accounting for the effects of treatment and survival. A total of 123 genes were significantly differentially expressed with respect to the PCo1 axis (FDR = 0.1). GO enrichment analysis (Figure A19) suggested that elevated DNA repair and/or replication and macromolecule biosynthesis is associated with higher microbiome PCo1 values (samples that tended to have higher mortality) and elevated environmental sensing (GPCR signaling) is associated with lower PCo1 values (samples that tended to have lower mortality).

I used Poisson-lognormal generalized linear mixed models to test for significant differences in abundances in OTUs depending on treatment (bacteria-challenged vs. control), *Vibrio* species (control, *V. diazotrophicus*, and *V. owensii*), and survival (continuous variable), as well as the interaction between treatment and survival (Figure 2.5C) after rarefaction to 800 sequences per sample. Seven OTUs varied by survival fraction: *Vibrio spp.* (OTU250), *Streptococcus spp.* (OTU409), *Chlamydiales* (OTU74), *Endozoicomonas euniceicola* (OTU783), and *Corynebacterium spp.* (OTU960) were significantly more abundant in corals with higher survival over all treatments. Another two *Endozoicomonas* species (OTU266 and OTU404) were significantly positively associated with higher mortality. Thirteen OTUs were significantly differentially abundant by bacterial treatment: only one of these (*Chlamydiales* OTU74, which was only present in genotype 30) was less abundant in treated corals. Four of the OTUs that were significantly enriched by bacterial challenge differed by *Vibrio* species used: *Vibrio spp.* (OTU250), *Photobacterium spp.* (OTU442), *Alteromonas spp.* (OTU565), and

Neptuniibacter caesariensis (OTU781) were all significantly more abundant in *V. diazotrophicus*-treated corals than in *V. owensii*-treated corals. Tests for the interaction of bacterial treatment and survival revealed that *Vibrio spp.* (OTU250), *Oleibacter spp.* (OTU811), and *Rhodobacteraceae* (OTU908) were all less abundant in treated corals with high survivorship than in corals with low survivorship.

Diagnostic gene expression biomarker identification and validation

Two candidate survival-specific genes were selected based on their high and dynamic expression: deleted in malignant brain tumors protein 1 (*dmbt1*) and matrix metalloproteinase (*mmp*). *Dmbt1* expression was positively correlated with survival and *mmp* expression was negatively associated with survival in our gene expression analysis. Thus, a *Dmbt1:mmp* expression ratio greater than 1 indicates lower risk. This gene pair was used in a self-normalizing double-gene qPCR assay quantifying the log-ratio of expression of these two genes, sensu Kenkel et al. (Kenkel et al., 2011). I quantified expression of these two genes in 74 samples from 19 genotypes from the independent validation experiment using qPCR. I measured the predictive power of the double-gene assay using logistic regression models testing binary survival outcomes: "low risk" corals had survival fractions exceeding 0.5 and all other corals were classified as "high risk." The original (n = 50) and validation (n = 74) *Dmbt1:mmp* expression ratios and survival rates (n = 83 low risk; n = 41 high risk) were pooled and randomly split into training (80%) and testing (20%) subsets over 500 iterations. Risk values were predicted from the test dataset based on the logistic model fit to the training dataset using the predict function in R. Total accuracy was defined as the percent correct risk predictions using a cutoff of 0.5 on the predicted value. The area under the curve (AUC) of the receiver operating characteristic (ROC) curve was calculated using the R package ROCR (ref). An

AUC equal to 1 indicates a perfectly discriminatory test, whereas an AUC equal to 0.5 indicates that the test operates no better than chance alone. The average overall accuracy of the model was 73% (Figure 2.6A). The average AUC was 81%, indicating good discriminatory power (Figure 2.6B). Thus, using just the expression level of these two genes, a reef manager could distinguish asymptomatic corals that were likely to become sick from identical healthy corals with 73% accuracy using this model. Excluding any samples with 100% survival from the model only reduces the model accuracy to 72% and the AUC to 0.77 (Figure 2.6C–D).

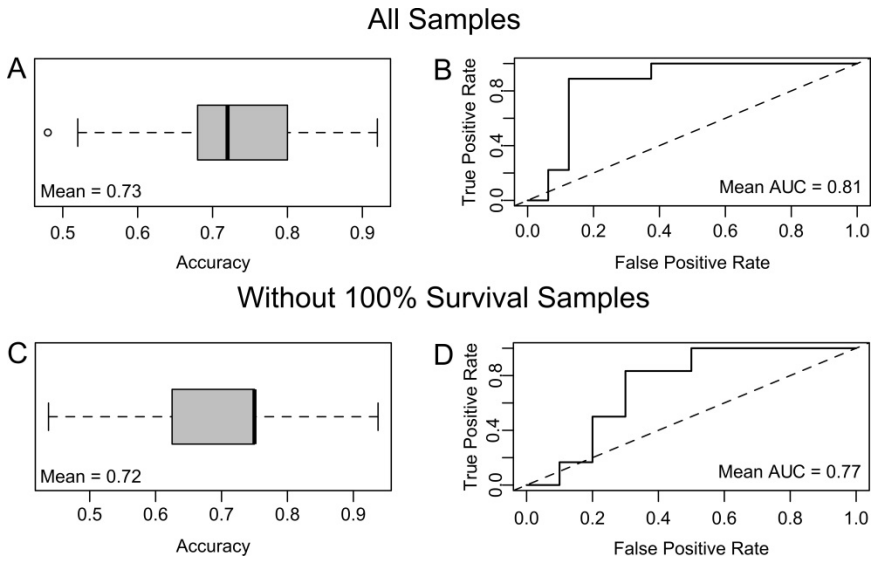

Figure 2.6: Double-gene biomarker predictive power. Average accuracy using a predicted value cutoff of 0.5 (A, C) and receiver operator characteristic (ROC) curves (B, D) for all data (top) and only corals with less than 100% survival (bottom) over 500 iterations. The mean area under the curve (AUC) indicates the sensitivity and specificity of the model. Common AUC score metrics are 0.90–1 = excellent, 0.80–0.90□ = □good, 0.70–0.80 = fair, 0.60–0.70 = poor, and 0.50–0.60□ = fail.

DISCUSSION

Documented differences in disease susceptibility across coral taxa have been attributed to baseline differences in constitutive immunity, where more resistant individuals invest in higher immune activity (Palmer, McGinty, et al., 2011; Palmer et al., 2010). Another study found that intraspecific differences in *Symbiodinium* composition correlated with coral disease susceptibility (Rouzé, Lecellier, Saulnier, & Berteaux-Lecellier, 2016). Here, I examined various aspects of holobiont physiology to investigate the physiological basis of colony-specific responses to a biotic challenge.

I find that individuals experiencing higher mortality also possessed higher antioxidant or cytotoxic activities, either as a baseline measure in the unchallenged fragments or in response to bacterial challenge (Figure 2.2). In contrast, low-mortality corals tended to respond less to the bacterial challenge (Figure 2.3), though this relationship was largely driven by a single genotype with 100% survival (Figure A14). The lack of positive correlation between immunity responses and survival suggests that mechanisms other than host immune activity contribute towards the observed variation in robustness to the bacterial challenge in our experiment. Alternatively, the immune response itself may lead to inflammation and tissue destruction (Lee et al., 2000).

Surprisingly few genes involved in stress responses or immunity were upregulated in low-mortality corals in response to bacterial challenge. Instead, these individuals exhibited a more "healthy" gene expression profile: they had elevated glucose-6-phosphate1-dehydrogenase expression that is important for cell growth (Tian et al., 1998), as well as increased levels of fluorescent proteins whose abundances have been linked to health status in corals (Roth & Deheyn, 2013; Wright, Aglyamova, Meyer, & Matz, 2015). Another signature of lower mortality was the diminished abundance of

ubiquitination-related transcripts, *e.g.*, ubiquitin ligases and ubiquitin carboxy-terminal hydrolases. Ubiquitination labels damaged proteins for removal and is a general hallmark of cellular stress (Kültz, 2005). Ubiquitin has been shown to be upregulated in heat-stressed corals with high levels of damaged proteins (Barshis et al., 2010; M. K. DeSalvo et al., 2008; Downs, Mueller, Phillips, Fauth, & Woodley, 2000). Differential expression of ubiquitination-related transcripts suggests that some genotypes may have been experiencing more baseline cellular stress than others throughout the experiment even though all genotypes were maintained in benign common conditions for over one month prior to and during the experimental procedure.

High-mortality corals exhibited abundant changes in gene expression in response to bacterial challenge, including upregulation of matrix metalloproteinases, which are also upregulated in naturally occurring coral disease and bleaching (M. K. DeSalvo et al., 2008; Wright et al., 2015), and an apoptosis regulator (Figure 2.4A). At the same time, gene expression in low-mortality corals responded to bacteria much less if at all (Figure 2.4A and Figure A15). Taken together with the lack of elevated immune activity in low-mortality corals (Figures 2.2–2.3), our conclusion is that these corals survived better because they were generally less sensitive to the adverse effects of bacterial challenge, not because they launched a more robust response. To explore why these coral hosts were less sensitive to the bacterial challenge, I investigated members of the coral holobiont. Previous research suggests that corals hosting clade D *Symbiodinium* can be more resistant to disease than those hosting clade A symbionts (Rouzé et al., 2016). The most robust genotype (30) was dominated by clade D, but so was a much weaker genotype (Figure A17). As only these two coral genotypes contained substantial proportions of clade D symbionts, our experiment cannot make firm conclusions concerning the effect

of *Symbiodinium* clade on ability to withstand biotic challenge, but this area of investigation deserves further attention.

Although the proportion of *Vibrio spp*. was higher in challenged corals than in controls (Figure 2.5C), these OTUs remained relatively rare, suggesting that the introduced *Vibrio spp*. were not the sole cause of lesion formation. This study is not the first instance wherein a simple "one pathogen = one disease" model fails to describe a coral lesion: microbiota of diseased corals often differ dramatically from the microbiota of healthy corals, suggesting that more than one bacterium is involved in deteriorating health (Roder et al., 2014). Likewise, healthy corals often harbor "pathogenic" microbes (Bourne & Munn, 2005). The "pathobiome" concept has been recently introduced to the field of coral disease biology to explain these apparent contradictions (M. J. Sweet & Bulling, 2017). The pathobiome describes interactions between pathogenic microbes and healthy microbiota that contribute towards disease processes (Vayssier-Taussat et al., 2014). Here, *Vibrio* treatment caused an increase in the abundance of taxa previously reported to be associated with disease and stress in marine organisms, including *Alteromonadaceae* (Sunagawa et al., 2009; Sweet & Bythell, 2015), *Pseudoalteromonadaceae* (Sunagawa et al., 2009), *Rhodobacteraceae* (Daniels et al., 2015; Fernandes, Steinberg, Rusch, Kjelleberg, & Thomas, 2012), and, expectably, *Vibrionaceae* (Cervino et al., 2008; Godwin, Bent, Borneman, & Pereg, 2012; Sunagawa et al., 2009; Vezzulli et al., 2010), suggesting that the introduced bacteria may have triggered a disturbance in the coral-associated microbiome that facilitated the proliferation of multiple bacterial species which contributed to the disease outcome (*i.e*., the pathobiome). To characterize the physiological consequences of harboring these distinct microbial communities in the host, I modeled gene expression by PCo1 value of the weighted UniFrac analysis (Figure 2.5A). This analysis revealed differences in host

gene expression that are associated with differences in microbial community membership, while controlling for the effects of survival and treatment. Major differences included stress responses, nucleic acid processing, and cell–cell signaling (Figure A19). These differentially expressed genes provide insight into the physiological consequences of harboring these distinct microbiomes and/or serve as targets for future investigations of genes that may modulate host–microbiome interactions.

The most striking difference in microbial composition is that the two best-surviving corals (genotypes 22 and 30) harbored high proportion of chloroplast-derived OTUs (Figure A12B). These OTUs are homologous to various cyanobacteria and *Ulvophyceae*, an abundant bioeroding marine algae (Sauvage, Schmidt, Suda, & Fredericq, 2016), suggesting the presence of endolithic algae or cyanobacteria that would also explain why the skeletons of these genotypes were noticeably green (Figure A12A). It is tempting to speculate that these microbes facilitate host defense by actively secreting antimicrobial compounds, an ability that has been well characterized in cyanobacteria (Gantar, Kaczmarsky, Stanić, Miller, & Richardson, 2011; Martins et al., 2008). Similarly, an OTU with similarity to *Chlamydiales* (Horn et al., 2002) was uniquely found in the coral with the highest survival rate. As obligate intracellular microbes, *Chlamydiales* can infect new host cells or segregate within dividing host cells to be vertically transmitted to daughter cells. Thus, these microbes can establish lasting relationships with hosts and contribute towards host health (Horn, 2008). I cannot be certain what the role of this microbe is in coral health, but the association between this intracellular microbe and disease resistance merits further investigation.

This study developed and validated a double-gene assay (Kenkel et al., 2011) predicting whether an asymptomatic coral will develop disease lesions in the near future (Figure 2.6), which can be used to assess mortality risks during coral disease outbreaks.

The putative roles of the genes forming the assay provide important insights into potential mechanisms underlying coral disease susceptibility. Deleted in malignant brain tumors 1 (*dmbt1*) is found in the gut mucosa of humans where it acts as a pattern recognition receptor that maintains mucosal homeostasis by inhibiting bacterial invasion and suppressing inflammation (Kang & Reid, 2003; Rosenstiel et al., 2007). Other transcriptomic studies have found that *dmbt1* was downregulated in oysters upon bacterial challenge (McDowell et al., 2014), upregulated in the *Symbiodinium*-hosting coral *Orbicella faveolata* after lipopolysaccharide challenge (Fuess, Pinzón, Weil, & Mydlarz, 2014), and upregulated in aposymbiotic sponges compared to sponges infected with clade G *Symbiodinium*, suggesting that *dmbt1* may play a role in mediating various marine symbioses (Riesgo et al., 2014). Elevated *dmbt1* in all control fragments and in the low-mortality corals relative to high-mortality, bacterial-challenged corals may signify the role of this protein in maintaining healthy stable symbiotic associations with commensal microbes. The diagnostic gene that was regulated in the opposite direction, a matrix metalloproteinase (*mmp*), belongs to a family of enzymes with a wide range of functions. The upregulation of MMPs in response to parasitic protists in a gorgonian coral (Burge et al., 2013) and in *A. hyacinthus* affected with White Syndrome-like symptoms (Wright et al., 2015) suggests an active role of these proteins in the immune response of cnidarians. Changes in *dmbt1* and *mmp* may represent some of the earliest coral responses to immune challenge, as they are detectable even in asymptomatic corals.

I found that neither introduced *Vibrio* species proliferated within the coral host in sampled asymptomatic fragments, but both bacterial treatments triggered the rise of putative opportunistic pathogens in the coral microbiome and subsequent development of disease lesions in corals that exhibited less healthy gene expression profiles. I would not be the first to argue that a coral disease can be caused by opportunistic infection

exploiting a compromised host (Lesser et al., 2007), and many coral diseases are associated with broad shifts in microbial community composition beyond the rise of a single "pathogen" (Gignoux-Wolfsohn & Vollmer, 2015; Roder et al., 2014; Sunagawa et al., 2009). If coral diseases in nature similarly arise because of weaknesses in holobiont physiology, instead of the virulence of any single etiological agent, environmental stressors compromising coral condition might play a larger role in disease outbreaks than is currently thought.

Chapter 3: Fitness trait evolvability in a reef-building coral under multiple climate change-related stressors

ABSTRACT

Climate change threatens organisms in a variety of synergistic ways that require simultaneous adaptation of multiple traits. In multivariate trait space, the actual response to selection might deviate from the direction of selection if genetically correlated traits are under opposing selective forces. Thus far, only a handful of studies have tackled this problem in the context of climate change, and none of them in an organism of high ecological importance. This project investigates the capacity for a reef-building coral, *Acropora millepora*, to adapt to multiple environmental stressors: rising sea surface temperature, ocean acidification, and increased prevalence of infectious diseases. I measured growth rates, coral color (a proxy for *Symbiodinium* densities), survival, and a number of physiological estimates of coral and algal health in response to these three stressors, as well as a combined treatment of all three stressors. Whereas treatments resulted in the predicted responses (*i.e.*, corals developed lesions after bacterial challenge and bleached under thermal stress), I found no synergistic activity between stressors (*i.e.*, corals did not suffer increased mortality under simultaneous bacterial challenge, elevated temperatures, and increased pCO_2). In some circumstances, the presence of one stressor counteracted the effects of another (*e.g.*, reduced bleaching under all stressors relative to thermal stress alone). The responses to these three stressors were all positively correlated across coral genotypes, indicating that being tolerant to one stressor does not incur a tradeoff in terms of tolerance to other stressors. The genetic variance–covariance matrix (G matrix) constructed using four fitness phenotypes (growth, carbohydrate, *Symbiodinium* density, and chlorophyll content) across all treatments showed extensive within-trait variance and all positive genetic covariances. Estimates for changes in trait

means using the multivariate breeder's equation show that co-variances between these fitness traits reinforce, rather than constrain, adaptation to environmental threats. These findings emphasize the importance of acknowledging adaptive capacity when predicting reef cover under future climate scenarios. Future studies should investigate the genetic architecture of tolerance traits and estimate the extent of their heritable variation across coral populations and species, without which natural selection could not result in rapid ecosystem-wide adaptation.

INTRODUCTION

Reef-building corals are experiencing unprecedented declines due to worsening environmental conditions, such as rising sea surface temperatures that lead to coral bleaching and ocean acidification that threatens to undermine coral growth (Andersson & Gledhill, 2011; Hoegh-Guldberg et al., 2007). Climate change has also indirectly lead to increasingly prevalent coral diseases, which are often attributed to bacterial pathogens (Ben-Haim, 2003; Maynard et al., 2015; Vezzulli et al., 2010). In the face of these stressors, corals are left with tragically few options: move, adapt, or die. A number of studies have documented corals' capacities to expand their ranges to more suitable habitats (Greenstein & Pandolfi, 2008; Makino et al., 2014; Yamano, Sugihara, & Nomura, 2011), but the capacity for corals to adapt remains unclear and underreported in climatic modeling scenarios to predict future coral cover (Bozec & Mumby, 2015; Logan, Dunne, Eakin, & Donner, 2014; Okazaki et al., 2016).

Adaptation to rapidly changing conditions requires standing phenotypic variation upon which selection can act, provided that this heterogeneity has a heritable genetic basis. Although a large and ever-growing number of studies examine mean responses of coral species to individual effects of climate change (Marubini, Ferrier-Pages, & Cuif,

2003; Okazaki et al., 2016), few have measured standing genetic variation and heritability of these responses (Nikolaus B M Császár, Ralph, Frankham, Berkelmans, & van Oppen, 2010; Dixon et al., 2015; Vollmer & Kline, 2008) and even fewer have assessed variation in multiple stress tolerance phenotypes (Shaw, Carpenter, Lantz, & Edmunds, 2016). Whereas corals have demonstrated remarkable variation in stress tolerance traits upon which selection could theoretically act, univariate analyses assessing a single stress-response phenotype, such as mortality under bacterial challenge or bleaching under thermal stress, fail to fully account for the genetic basis of the phenotypes under selection. Selection is an inherently multivariate process that acts simultaneously on sets of functionally related traits. Indeed, centuries of animal and plant breeding have demonstrated that selection on one trait will often result in changes in another correlated trait (Rauw, Kanis, Noordhuizen-Stassen, & Grommers, 1998; Zhao, Atlin, Bastiaans, & Spiertz, 2006). The prospects for future reef-building corals are exceedingly poor if success under one stress is impossible without developing susceptibility to a co-occurring environmental challenge.

I quantified the capacity to adapt to multiple stressors in a reef-building coral, *Acropora millepora*, a model representative of the keystone group of marine organisms that are among the most vulnerable to climate change (Reusch, 2014). Multiple genotypes (n = 40) were separated into replicate clonal fragments (n= 5 per treatment) that were exposed to elevated temperature (30°C), increased pCO2 (pH = 8.0, 700 ppm), bacterial challenge (10^6 CFU mL^{-1} *V. owensii*), a combination of these three stressors, or a control condition (27°C, pH = 7.8, 400 ppm, no bacteria). I measured multiple coral and algal traits to assess success in each condition, and constructed a genetic variance–covariance matrix to identify potential genetic trade-offs or reinforcements between phenotypes.

METHODS

Study organism and aquarium conditions

Forty-one colonies of *Acropora millepora* were sampled between October–December 2014 from Davies Reef lagoon (78 km offshore; 18°50’11’’S, 147°38’41’’E), Rib Reef (56 km offshore; 18°28’55’’S, 146°52’15’’E), Pandora Reef (16 km offshore; 18°48’44’’S, 146°25’59’’E), and Esk Island (24 km offshore; 18°46’04’’S, 146°30’57’’E). These colonies were transferred to holding tanks at the National Sea Simulator system at the Australian Institute of Marine Science (Townsville, Australia). After approximately two weeks acclimatization, each colony was fragmented into 25 replicate fragments (“nubbins”), which were mounted on aragonite plugs and placed in sequential order on trays. Trays were maintained in six indoor holding tanks which were supplied with 0.2 μM filtered seawater (FSW) at 27°C. Three lights (AI Aqua Illumination, USA) were suspended above each tank providing an average underwater light intensity of 80 μmol photons m^{-2} s^{-1} on a 10-/14-hour light–dark cycle. Corals were fed freshly hatched *Artemia nauplii* twice daily and cleaned three times a week to prevent algal growth. Coral nubbins were acclimated to these conditions for 3–5 months, depending on the date of collection. Unique genotypes were later confirmed via 2b-RAD (Wang, Meyer, McKay, & Matz, 2012) and identified clones were corrected. The final total genotypes for each sampling location are as follows: Davies (n = 10), Rib (n = 11), Pandora (n = 14), and Esk (n = 6).

Experimental treatments and sample preparation

On 2 March 2015, coral nubbins (25 per genotype) were placed into 25 50-L treatment tanks fitted with 3.5-W Turnbelle nanostream 6015 pumps (Tunze, Germany) with flowthrough seawater (˜25-L hour-1) at the same temperature and light conditions as

in the previous holding tanks. Initial weights for each nubbin were measured following the method described by Davies (1989). Tanks (n = 5 per treatment) were allocated to the following treatments: elevated temperature (30°C), increased pCO_2 (700 ppm, pH = 7.8), bacterial challenge (10^6 CFU mL^{-1} *Vibrio owensii*), a combined treatment (30°C, 700 ppm, 10^6 CFU mL^{-1} *V. owensii*), and control (27°C, 400 ppm, pH = 8.0, no bacteria). Temperature and pCO_2were gradually increased in their respective tanks to 30°C and 400 ppm (pH = 8.0). To minimize exposure risks, the bacterial challenge was conducted in separate isolated tanks (no flowthrough) for six hours. *Vibrio owensii* was added at a final concentration of 10^6 CFU mL^{-1} to every bacterial challenge tank, including the combined treatment (which was also maintained at 30°C and 700 ppm pCO_2 for these six hours). Corals were returned to their respective treatment tanks until the next day's bacterial challenge. Coral fragments were photographed daily to quantify bleaching via the Coral Health Chart (Siebeck, Marshall, Klüter, & Hoegh-Guldberg, 2006) and lesion progression. Net oxygen production and total alkalinity change under light were measured for randomly selected genotypes following methods described in (Strahl et al., 2015). Fragments exhibiting any tissue loss were removed from treatment tanks, buoyant weighed, and preserved in liquid nitrogen. The time of death (day post initial exposure) was recorded at each instance. The experiment continued for 11 days, until approximately 21% mortality was recorded over all treatments. At this time, all surviving corals were photographed, buoyant weighed, preserved in liquid nitrogen, and stored at -80°C until sample processing.

Tissue was removed from coral skeletons using an air gun, and homogenized for 60 seconds using a Pro250 homogenizer (Perth Scientific Equipment, Australia). A 1 mL aliquot of the tissue homogenate was centrifuged for 3 minutes at 1500 ×g at 4°C and the pellet was stored at -80°C for chlorophyll analyses. The remaining homogenate was

centrifuged for 3 minutes at 1500 ×*g* at 4°C to separate host and symbiont fractions. The fractions were frozen in 96-well tissue culture plates and stored at -80°C. Coral skeletons were rinsed with 10% bleach then dried at room temperature (~24°C). Skeletal surface area was quantified using the single paraffin wax dipping method (Stimson and Kinzie 1991) and skeletal volume was determined by calculating water displacement in a graduated cylinder.

Physiological trait assays

Assays were conducted to detect cellular and metabolic activity changes within the *Symbiodinium* or coral host tissue in response to the treatment. All standards and samples were loaded as duplicates, and absorbance was recorded with a Cytation 3 multi-mode microplate reader (BioTek, Winooski, USA) and analyzed using Gen5 software (BioTek, Winooski, USA).

To quantify chlorophyll concentrations, tissue homogenate algal pellets were resuspended in 1 mL chilled 90% acetone. The homogenate was sonicated on ice for 10 seconds at 40% amplitude, left in the dark for 20 minutes, and centrifuged for 5 minutes at 10,000 ×*g* at 4°C. A 200 μL aliquot of sample extract was loaded to a 96-well plate, and absorbance was recorded at 630 and 663 nm. Chlorophyll a and c2 concentrations were calculated with the equations in Jeffrey and Haxo (1966) and were normalized to surface area:

$$\text{Chlorophyll a } (\mu\text{g ml}^{-1}) = 13.31 \times A663 - 0.27 \times A630$$

$$\text{Chlorophyll c2 } (\mu\text{g ml}^{-1}) = 51.72 \times A630 - 8.37 \times A663$$

A commercial colorimetric protein assay kit (DCTM Protein Assay Kit, Bio-Rad, Hercules, USA) was used to quantify total protein content of the coral host tissue. A 100 μL aliquot of *Symbiodinium*-free coral tissue sample was digested using 100 μL sodium

hydroxide in a 96-well plate for 1 hour at 90°C. The plate was centrifuged for 3 minutes at 1500 ×g. Following manufacturer's instructions, 5 μL digested tissue was mixed with 25 μL alkaline copper tartrate solution and 200 μL dilute Folin reagent in a fresh 96-well plate. Absorbance at 750 nm was recorded after a 15 minute incubation. Sample protein concentrations were calculated using a standard curve of bovine serum albumin ranging from 0 and 1000 μg mL-1.

Carbohydrate content of the *Symbiodinium*-free coral tissue was estimated following the method by Masuko et al. (2005) that measures monosaccharides, including glucose, which is the major photosynthate translocated between symbionts and host corals (Burriesci, Raab, & Pringle, 2012). A 50 μL aliquot of coral tissue was mixed with 150 μL concentrated sulfuric acid and 30 μL 5% phenol in a 96-well plate for 5 minutes at 90°C. After another 5 minute incubation at room temperature, absorbance at 485 nm was recorded. The total carbohydrate concentrations of samples were calculated using a standard curve of D-glucose solutions ranging from 0 to 2000 μg ml^{-1}.

To analyze non-fluorescent chromoprotein content, a 30 μL aliquot of coral tissue was loaded to a black/clear 384-well plate and absorbance was recorded at 588 nm. Mean absorbance was standardized to sample protein content.

The activity of catalase (CA), a reactive oxygen species scavenging enzyme (Lesser 2006), was measured by estimating the change in hydrogen peroxide (H_2O_2) substrate concentration. A 20 μL aliquot of coral tissue was mixed with 30 μL 50 mM phosphate-buffered saline solution (PBS; pH 7.0) and 50 μL 50 mM H_2O_2 in a 96-well plate. CA activity was calculated as the change in absorbance at 240 nm every 30 seconds over the linear portion of the reaction curve for 15 minutes and was standardized to sample protein content:

$$\text{CA (mg protein-1)} = \text{Initial } A_{240} - \text{Final } A_{240}$$

The activity of phenoloxidase (PO), the enzyme that catalyzes the first reaction of the melanin synthesis pathway triggered by pathogens and thermal stress (Palmer and Traylor-Knowles 2012), was measured as the change in absorbance at 490 nm every 30 seconds over the linear portion of the reaction curve for 15 minutes after mixing 20 μL coral tissue, 20 μL 50 mM PBS (pH 7.0), and 30 μL 10 mM dopamine hydrochloride (Sigma-Aldrich H8502). PO activity was standardized to sample protein content:

$$\text{PO (mg protein}^{-1}) = \text{Final } A_{490} - \text{Initial } A_{490}$$

The change in coral color was estimated using photographs taken during the experiment with a Nikon D300 digital camera. Brightness values were measured over the entire front and back sections of each nubbin using image analysis software (ImageJ, NIH). Corals become brighter (whiter) when they lose darkly colored algal symbionts, so changes in brightness reflect changes in *Symbiodinium* densities (Winters, Holzman, Blekhman, Beer, & Loya, 2009). A standard curve of brightness values was constructed using standard coral color cards that were present in each image. Brightness values were standardized to color cards to normalize for differences across photo sessions.

Statistical analyses

The time of death was noted for each individual nubbin. Survival was modeled as time of death ~ treat + reef + (1|tank) using coxme package in R 3.3.1 (R Core Team, 2016; Therneau, 2012), where treatment was specified as the presence of absence of elevated heat, bacteria, or increased pCO_2 (*i.e.*, bac = 1 for "bacteria" and "all" treatments; heat = 1 for "heat" and "all" treatments). After adding a constant to ensure positive values (if necessary), all trait data were log-transformed using powers determined by Box-Cox transformations performed using the powerTransform function in the R package car (Fox & Weisberg, 2001). Linear mixed-effects models implemented

using the R package nlme (Pinheiro, Bates, DebRoy, & Sarkar, 2017) tested the effects of treatments, treatment interactions, and reef-of-origin on trait values. The stepAIC function in the R package MASS (Venables & Ripley, 2002) determined which terms to include in the best-fit model. Principal components analysis on mean-centered and variance-scaled values was performed using the prcomp function in base R. Pearson correlations between trait values were calculated using the cor function in base R, and correlation heatmaps were constructed using the corrplot function. The genetic variance–covariance matrix was constructed using the R package MCMCglmm (Hadfield, 2010). Trait data were mean-centered and variance scaled. The multivariate model was fit for four traits (growth, color, chlorophyll c2, and carbohydrate) with treatment as a fixed effect and reef and nested genotype as random effects, using the idh variance structure. The model was run for 20000 iterations after a 5000 iteration burn-in, storing the Markov chain after 20 iteration intervals. Partial regression coefficients for each trait on binomial survival outcome were modeled using a categorical MCMCglmm model with genotype as a random effect. The selection gradient was composed of these partial regression coefficients, scaled to unit variance. Predicted changes in trait values ($\Delta\bar{z}$) were calculated using the multivariate breeder's equation (Lande & Arnold, 1983):

$$\Delta\bar{z} = G\beta$$

G is the genetic variance–covariance matrix and $\beta$is the selection gradient.

RESULTS

Mean treatment responses

Corals in the control tank experienced the least mortality (13.5%), with increased mortality under elevated temperature (21.5%), combined treatment (23.7%), bacteria challenge (26.4%), and elevated pCO2 (27.4%). Bacteria challenge significantly

increased mortality risks (HR = 3.32, p = 0.018), and a weak interaction between bacteria challenge and increased temperature showed a trend towards improving survival odds compared to bacterial challenge alone (HR = 0.17; p = 0.09). Though elevated pCO_2 caused the most mortality, most events occurred after the first week; thus, corals in elevated pCO_2 tanks were indistinguishable from control corals throughout most of the experiment (Figure 3.1A). Interestingly, the combined treatment did not appear to impose additional harm on these corals, indicating that, in this experiment, treatments did not act synergistically to harm coral health. Sampling location impacted survival outcomes in these corals across all treatments. Corals from Rib had the lowest mortality (16.5%), and corals from Pandora were statistically indistinguishable from Rib corals. Corals from Davies and Esk had higher mortality rates (HR = 0.54, p = 0.007 and HR = 0.58, p = 0.01, respectively) than corals from Rib (Figure 3.1B).

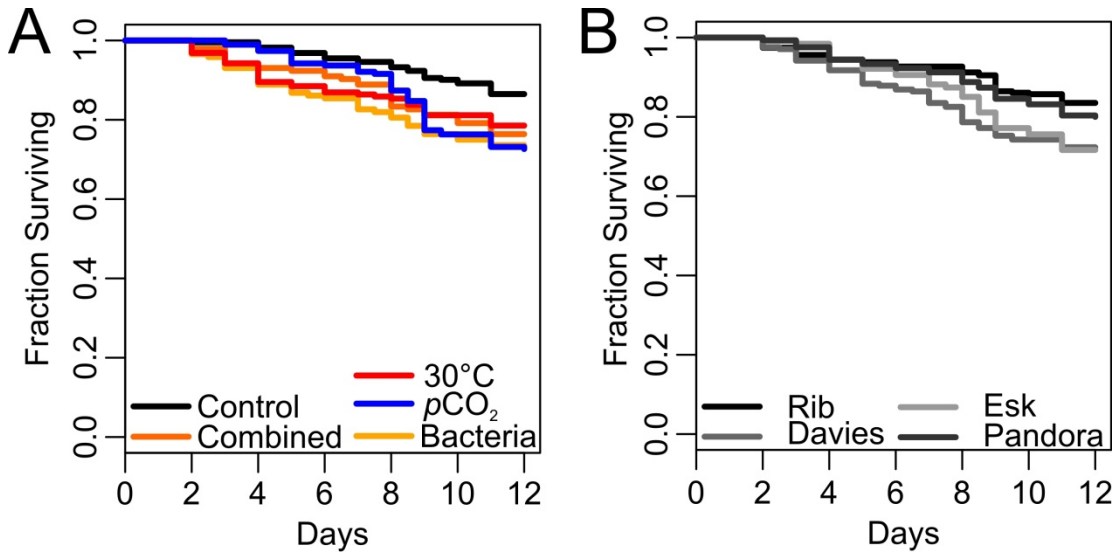

Figure 3.1: Treatment and reef-of-origin affect survival rates. (A) Elevated pCO_2 caused the most mortality, but many of the events occurred late in the experiment. Only the bacteria challenge significantly increased mortality rates relative to the control condition (HR = 3.32, p = 0.18). (B) Mortality rates were highest in corals from Esk and Davies.

A suite of algal and host-associated traits indicates how corals responded to each treatment. Coral color (an indicator of *Symbiodinium* densities), chlorophyll content, and carbohydrate measurements represent the ability of the coral to maintain healthy algal symbionts that grow, photosynthesize, and provide the coral host with photosynthetically fixed carbon. Bacteria treatment made corals significantly darker ($\beta = 0.71$, $p < 0.001$; Figure 3.2A), whereas corals became lighter ("bleached") in the elevated temperature treatment ($\beta = -0.52$, $p < 0.001$). These findings are echoed in algal pigment measurements: bacterial treatment increased chlorophyll A ($\beta = 2.1$; $p < 0.001$; Figure 3.2C) and chlorophyll c2 ($\beta = 0.90$, $p = 0.001$; Figure 2D) content in the algal fraction of the coral tissue. Carbohydrate byproducts of photosynthesis are translocated from the algal symbiont to the coral host (Davy, Allemand, & Weis, 2012). Accordingly, I also saw increased carbohydrate content in the coral tissues of fragments exposed to the bacterial challenge ($\beta = 0.72$, $p < 0.001$; Figure 3.2B). These results suggest that while the elevated temperature treatment induced the expected bleaching response, bacteria treatment improved algal productivity, leading to increased photosynthetically fixed carbon available for the coral host.

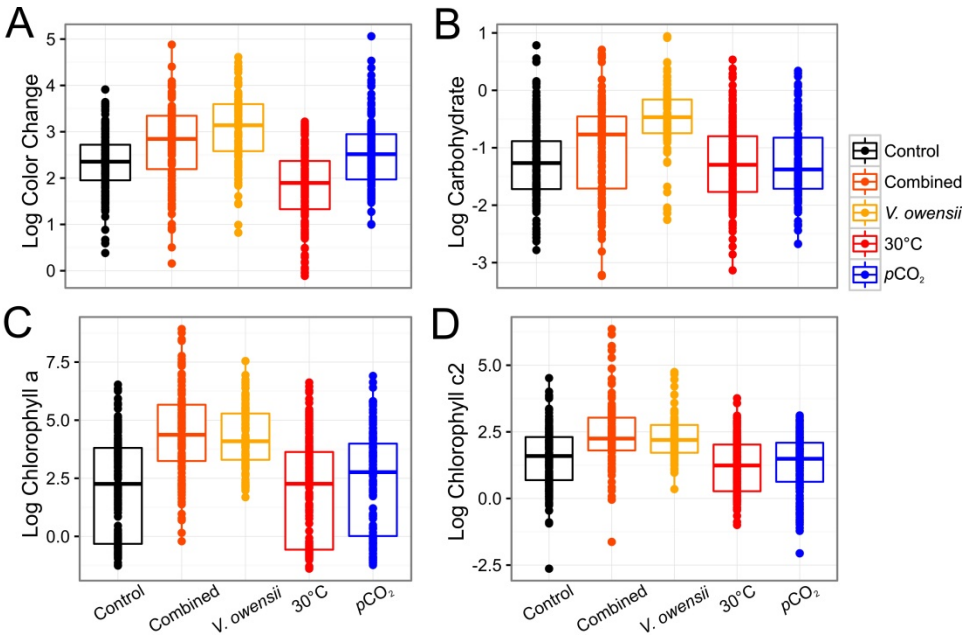

Figure 3.2: Thermal stress and bacterial challenge differentially impact algal traits. The addition of bacteria in the combined and bacteria-only treatments improved coral color, an indicator for *Symbiodinium* densities (A), coral carbohydrate content (B), chlorophyll a (C) and chlorophyll c2 content (D). Each data point represents an individual coral fragment.

Buoyant weights indicate coral skeletal growth (Figure 3.3A). Corals in the elevated temperature treatment experienced unexpected miniscule increases in growth rates (β = 2.3e-3, p = 0.008), but there was also a weak negative interaction between the pCO2 and elevated temperature treatments (β = -2.4e-3, p = 0.07).

Catalase, phenoloxidase, and chromoprotein measurements indicate the level of host stress, as each of these proteins has been linked to coral stress responses (Fuess et al., 2014; Vidal-Dupiol et al., 2014). I found no significant effect of treatment on any of these measurements. However, there was a weak interaction between the effects of elevated temperature and bacterial treatment on catalase activity (β = 0.3, p = 0.10; Figure 3.3B).

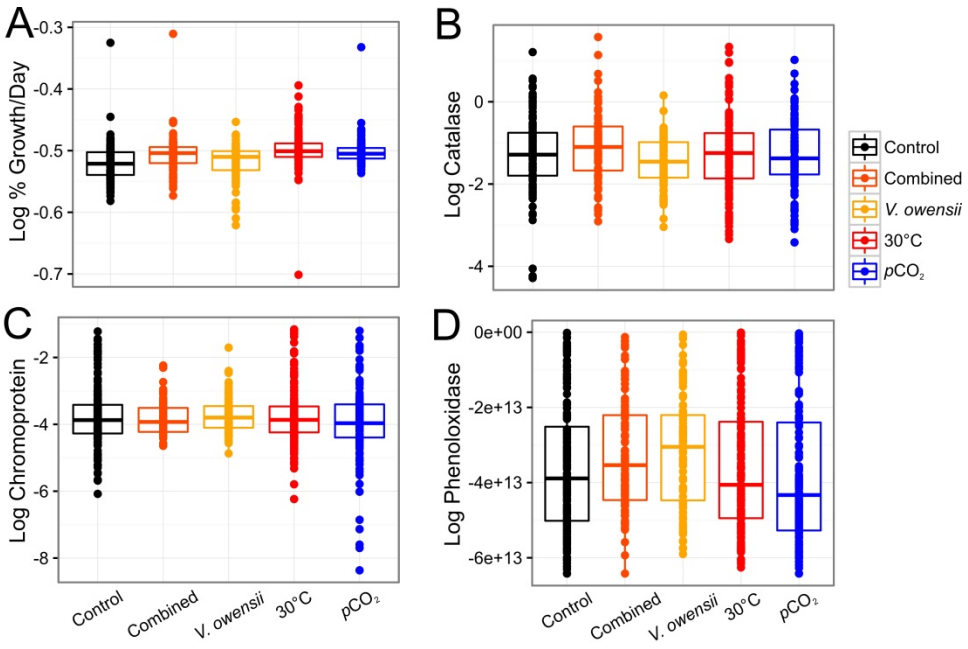

Figure 3.3: Growth, catalase and phenoloxidase activities, and chromoprotein content were largely unaffected by the treatments. (A) Corals exposed to elevated temperatures displayed improved growth rates as measured by buoyant weights ($p = 0.008$). No treatment significantly affected catalase activity (B), chromoprotein content (C), or phenoloxidase activity (D). Each data point represents an individual coral fragment.

Photosynthetic and instant calcification rates were measured for a subset of the coral genotypes. Elevated temperatures reduced photosynthetic rates ($\beta = -0.58$, $p < 0.001$), potentially as a consequence of lower *Symbiodinium* densities in heat-treated corals (Figure 3.2A). Coincident with findings of improved algal traits under bacterial challenge (Figure 3.2), the bacterial treatment apparently rescued photosynthetic rates under elevated temperatures, resulting in a positive effect of the interaction between these two stressors ($\beta = 0.40$, $p = 0.04$; Figure 3.4A). Only the elevated pCO_2 treatment affected instant calcification rates ($\beta = -0.52$, $p = 0.008$; Figure 3.4B).

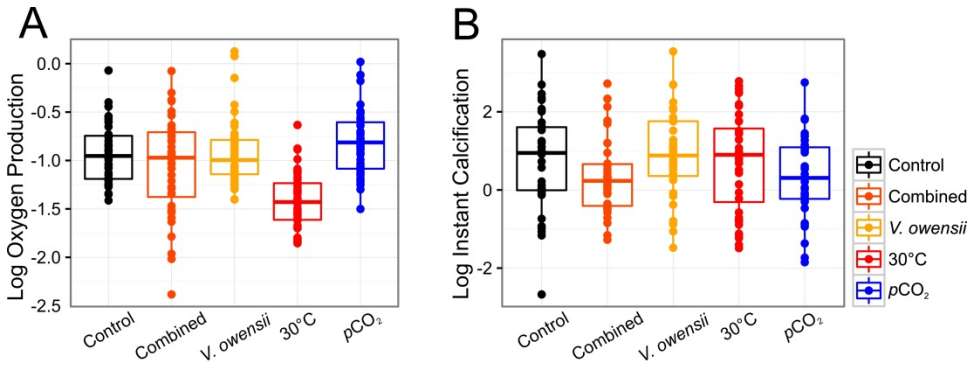

Figure 3.4: Photosynthesis and calcification rates were reduced by thermal stress and acidification, respectively. (A) Oxygen production, a proxy for photosynthetic rate, was reduced in corals exposed to elevated temperatures alone, but not in corals exposed to combined stressors. (B) Elevated pCO_2 reduced calcification rates ($p = 0.008$). Each data point represents an individual coral fragment.

Phenotypic space, correlations, and evolvability calculations

The lack of synergistic treatment effects on coral fitness proxies provides encouraging evidence for an individual coral's capacity to resist multiple stressors. To address whether a population of corals can respond to simultaneous threats, I explored correlations between treatment effects for each genotype.

Principal components analysis was used to explore patterns in phenotypic space of 449 individual fragments (Figure 3.5A) with complete phenotypic datasets for growth, color change, chlorophyll A, chlorophyll c2, chromoprotein, catalase, phenoloxidase, and survival fraction (the proportion of fragments surviving for the genotype in each respective treatment). The first principal component (PC, the projection that includes the greatest variance) separates samples by differential algal responses to treatment (Figure 3.5B). The second PC separates samples by host stress responses (chromoprotein, catalase and phenoloxidase activity), suggesting that algal maintenance and stress responses are unrelated in these corals. Coral fitness metrics (growth and survival

fraction) are projected in the third PC, which represents 12% of the total variance (Figure 3.5C).

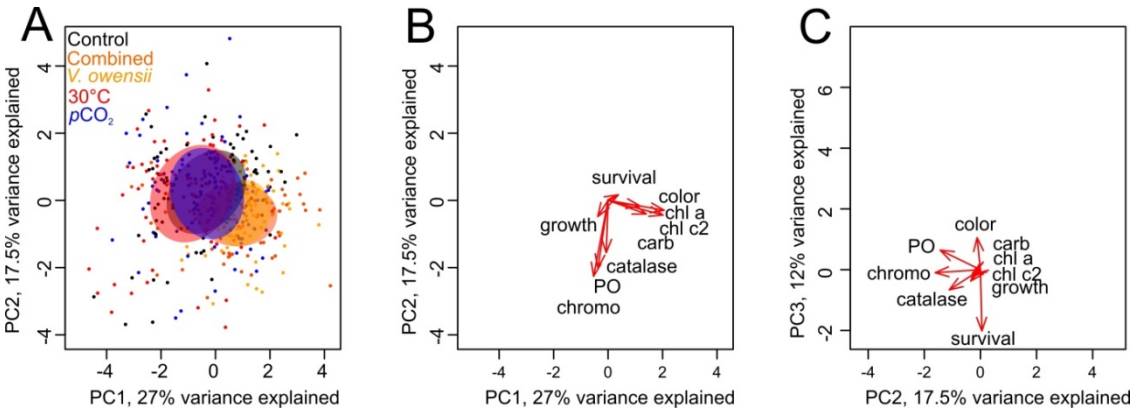

Figure 3.5: Phenotypic measurements exhibit extensive variation. (A) Principal components analysis based on complete trait data for 438 fragments. (B) The first two axes separate treatments according to algal effects (color, chl a, chlc2, carb) mediated by the bacteria and combined treatments and coral stress responses (catalase, PO, chromo). (C) Coral survival is projected along the third PC axis. Colors correspond to treatments: black = control, yellow = bacteria only, orange = combined treatment, red = elevated heat, blue = elevated pCO_2.

Pearson correlations measured the relationship between all pairwise combinations of traits to identify reinforcements (positive correlations) and tradeoffs (negative correlations). The correlation heatmap shows mostly positive correlations between trait pairs, or no significant correlation, but very few negative correlations (Figure 3.6). Most importantly, survival rates are highly correlated among treatments. In other words, corals that survive one stressor are likely to survive other stressors. Algal responses to the bacterial treatments were also generally positively correlated, but some of these showed negative associations with survival and growth. For example, surviving individuals that experienced increases in *Symbiodinium* densities after the bacteria challenge originated

from colonies where the majority of replicate fragments died in the *V. owensii* and elevated temperature treatments.

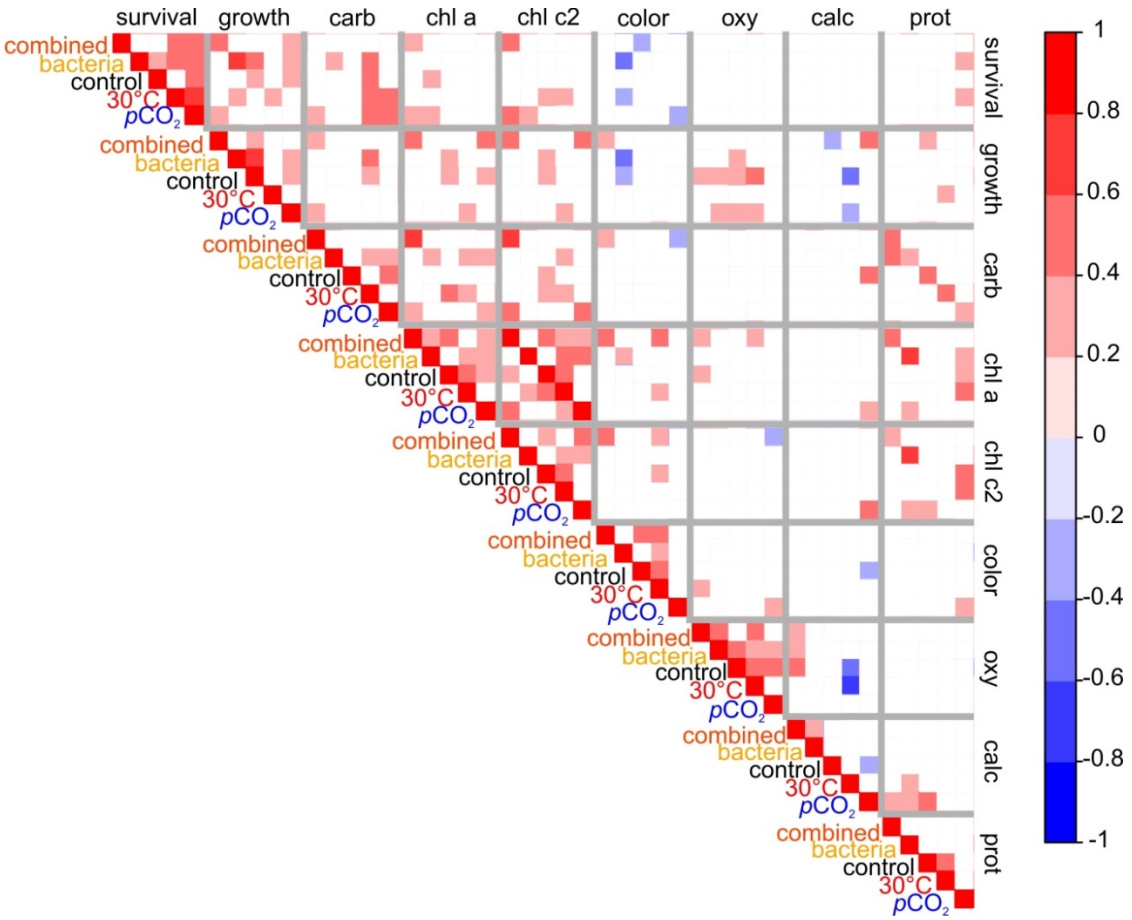

Figure 3.6: Tolerances to different stressors are predominantly positively correlated across coral genotypes. Pearson correlation heatmap based on scaled average phenotypic values for 38 genotypes. Label colors correspond to treatments: black = control, yellow = bacteria only, orange = combined treatment, red = elevated heat, blue = elevated pCO_2. Colors within the heatmap squares represent the magnitude and direction of the Pearson correlation according to the color scale provided. Only significant ($p < 0.05$) correlations are shown.

Principal components analysis and pairwise trait correlations show an overall lack of trait relationship, with few negative associations between treatment response

measurements and fitness proxies (growth and survival). However, pairwise comparisons fail to capture overall genetic structure of the population. To explore the evolvability of these traits while accounting genetic covariance among traits, I analyzed broad-sense genetic variation (*i.e.*, attributable to differences between coral individuals) by examining the genetic variance–covariance G matrix using four traits with the least missing data that best describe various aspects of host and symbiont physiology: *Symbiodinium* density (color change), growth, chlorophyll c2 content, and total host carbohydrate. Overall, I found only positive genetic correlations between traits; however, only positive covariances between growth and carbohydrate, growth and chlorophyll c2, and chlorophyll c2 and color are significant at the 95% confidence level (Figure 3.7).

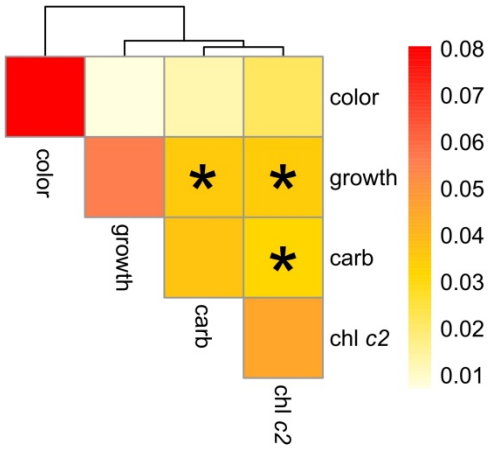

Figure 3.7: Fitness-related traits are positively genetically associated. Genetic variance–covariance metric for four traits across five treatments in 39 genotypes. The diagonal elements represent trait variance, and off-diagonal elements show covariances between paired traits. Significant co-variances at the 95% credible interval are indicated with asterisks.

In multivariate analyses, the response to selection may deviate from the direction of selection due to influences of genetically associated traits. I generated a selection gradient (a vector of partial regression coefficients standardized to unit length) by regressing the four traits against binomial survival (1 = fragment survived; 0 = fragment died). All selection coefficients were positive, but only growth was significantly associated with survival (posterior mean = 0.61, $p < 0.001$). I applied the multivariate breeder's equation to estimate how trait values would be expected to change given our G matrix and selection gradient (Figure 3.8). Because all selection coefficients and covariances were positive, the change in every trait mean over one generation was also positive. In other words, corals with high survival rates would tend to produce offspring with increased growth rates, carbohydrate content, *Symbiodinium* densities, and chlorophyll content, assuming that the differences that I measured between coral individuals are attributable to genetics.

I isolated individual associations between traits and survival by generating selection gradients where only one trait was under directional selection (all other trait selection coefficients = 0). I calculated changes in trait means using these modified selection gradients to evaluate the contribution of selection on each trait (Figure 3.8). These analyses emphasize that increases in trait means estimated using the full selection gradient were not due to equal selective forces on all traits, but result from stronger selection on few traits that co-vary with more weakly favored traits. The most striking example is the case of growth rate. A strong association between growth rate and survival results in large increases in carbohydrate and chlorophyll c2 content (Figure 3.8, grey bars), because these traits are significantly associated with growth (Figure 3.7). Color (algal density), which has a near-zero covariance with growth rate, is weakly improved when selection acts only on growth rate. Selection acting only on carbohydrate or

chlorophyll c2 content improves trait values by very modest amounts due to the smaller selection coefficients associated with these traits (Figure 3.8, blue and red bars). Selection acting on color (algal density) was weakest of all, and this trait was relatively unassociated with any other trait (Figure 3.7).

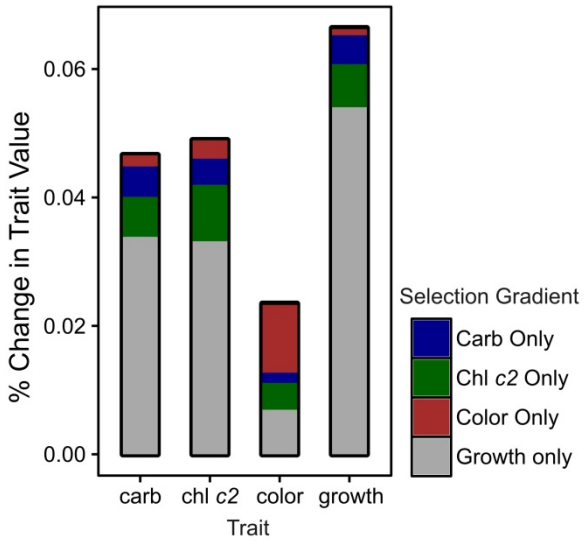

Figure 3.8: All trait values are predicted to increase in the next generation of corals. Estimated changes in trait means using different selection gradients. The height of each whole bar represents the total expected change in each trait mean expressed as a percent of the variation measured in the population using a selection gradient composed of partial regression coefficients for each trait on survival (fitness). Stacked partial bars isolate the contribution of selection on a single trait (indicated by the color in the inset key) towards the trait change for all traits.

In summary, positive genetic covariances and positive associations between all traits and survival (fitness) resulted in overall increases in all trait values modeled for the next generation of coral. Algal density and carbohydrate and chlorophyll c2 content increased more under the full model as a result of positive genetic covariance with a more strongly selected fitness trait: growth. However, these results were generated using

broad-sense heritability estimates (total genetic variance) rather than narrow-sense heritability (additive genetic variance) and thus may overestimate the amount of change that could actually be inherited by the next generation.

DISCUSSION

Overall, the experimental treatments resulted in the expected mean responses. Elevated temperatures reduced algal parameters (*Symbiodinium* densities, chlorophyll A and c2 content). The treatments that included a bacterial challenge caused an unexpected increase in these same algal traits, potentially because corals that could withstand the bacterial challenge engaged in heterotrophic feeding. This hypothesis can unfortunately not be supported with these data, but reef-building corals do feed on bacteria (Houlbreque & Ferrier-Pages, 2009) and added nutrients do encourage algal productivity (Radecker, Pogoreutz, Voolstra, Wiedenmann, & Wild, 2015; Sawall, Al-Sofyani, Banguera-Hinestroza, & Voolstra, 2014). Though a meta-analysis of coral stress responses suggests that most stressors act synergistically (Ban, Graham, & Connolly, 2014), I failed to observe many interactive effects of the combined challenge. In this experiment, the combination of treatments tended to improve holobiont health relative to a single stress. For example, bacterial challenge alone caused more mortality than the combined treatment (Figure 3.1A). A tempting hypothesis to explain this phenomenon is that elevated temperatures primed the coral's stress response system to balance oxidative stress associated with launching an innate immune response (Lu, Wang, & Liu, 2015). Indeed, multiple gene expression studies have shown that thermal stress upregulates antioxidant genes that could mitigate redox damage associated with an innate immune response to bacterial invasion (Császár, Seneca, & Van Oppen, 2009; M. K. DeSalvo et al., 2008). I also saw that coral bleaching was minimized in the combined treatment

relative to thermal stress alone (Figure 3.2A), possibly as a result of heterotrophic feeding: both coral host and algal symbiont had access to extra nutrients (bacteria) in the combined treatment. Heterotrophic compensation has been investigated as a method by which corals withstand extended bleaching events (Baumann, Grottoli, Hughes, & Matsui, 2014; Grottoli, Rodrigues, & Palardy, 2006; Hughes & Grottoli, 2013), but the capacity for heterotrophic feeding to prevent bleaching deserves more attention.

Pairwise correlations of trait values in each treatment revealed mostly positive associations. Importantly, survival under most treatments was significantly positively correlated (Figure 3.6). Corals that could survive one stress tended to be able to survive withstand other stressors as well. Coral color (algal density) in the bacterial challenge was negatively correlated with survival under *Vibrio* challenge and thermal stress, and with growth in the control condition and *Vibrio* challenge. Algal density measurements in corals exposed to *Vibrio* in this experiment reflect the ability of a coral to experience the bacteria-mediated benefit to algal traits. Negative correlations with survival and growth seem to suggest that only the weakest corals were able to receive this increase in algal density.

While the aforementioned univariate analyses were useful for examining treatment effects and identifying pairwise correlations between genotypes, multivariate analyses based on genetic associations between traits are necessary to describe how these traits might change under directional selection. The variance–covariance structure estimated in this study indicates that our focal species possesses the genetic heterogeneity and flexibility to respond to multiple selective pressures in a number of ways. The G matrix for four key traits (growth, color, chlorophyll c2 content, and total carbohydrate) contained no negative covariances. Using the multivariate breeder's equation, I found that positive genetic covariance between fitness-associated traits reinforced evolution of

all traits. Most strikingly, I found that growth rate was most associated with survival outcome. In other words, corals that survived the treatments tended to have higher growth rates as well. Although directional selection was weaker for other traits, genetic association with growth resulted in increases in algal density and carbohydrate and chlorophyll c2 content. In summary, stress responses and fitness-related traits are positively genetically associated in *Acropora millepora*. Selection acting to improve one character (*e.g.*, growth rate) reinforces associated improvements in other coral health parameters (*e.g.*, nutrient stores). However, these findings should be taken with extreme caution and require further investigation. Evolutionary rates in sexually reproducing organisms are affected not only by the extent of between-individual variation, but the heritability of this variation. However, the G matrix in this experiment specifies total between-genotype variance, only a fraction of which might be heritable. Furthermore, that unknown fraction of genetic variance would include additive and non-additive (*e.g.*, dominance, epistasis) variance and thus may overestimate the ability of the population to evolve in response to directional selection. Future experiments should include individuals with known pedigrees or multiple generations of corals to more accurately characterize heritable variation in tolerance traits existing in natural coral populations.

Despite these limitations, these findings still offer critical implications for reef management. Importantly, adaptive processes should not be ignored in ecological climate modeling. Dire estimates for future coral cover are derived from experiments wherein a coral from today's environment is placed in conditions representative of a reef that is nearly 100 years older (Okazaki et al., 2016). *A. millepora* have been shown to reach reproductive maturity as early as three-years after fertilization (Baria, dela Cruz, Villanueva, & Guest, 2012); thus, current modeling strategies based on end-of-the-century climate scenarios ignore dozens of generations of adaptive evolution that might

be sufficiently rapid based on standing genetic variation (Dixon et al., 2015). Thankfully, in our case, co-varying traits tended to reinforce each other such that selection would result in simultaneous increases in multiple fitness metrics, such as growth and algal density. Thus, natural selection will continue to experiment on the reef, selecting for corals that thrive despite multiple harassments brought about by climate change. This finding that *A. millepora* appear to possess the phenotypic heterogeneity and genetic flexibility to respond to moderate, slow changes in environmental variables should not undermine the critical urgency to protect reef environments from anthropogenic stressors that outpace these corals' capacities to adapt.

Appendix

	coefficient	exp(coefficient)	SE(coefficient)	z	p
L5	-0.03	0.97	0.50	-0.07	0.945
L7	-1.61	0.20	0.69	-2.35	0.0188
L9	1.08	2.96	0.47	2.32	0.0206
W22	-1.58	0.21	0.68	-2.31	0.021
W26	-1.03	0.36	0.58	-1.78	0.075
W27	-0.25	0.78	0.50	-0.49	0.6212
W30	-19.40	0.00	4120.00	0	0.9962
V. diazotrophicus	1.74	5.67	0.43	4	6.20E-05
V. owensii	1.30	3.66	0.46	2.81	0.005
Abrasion	0.87	2.39	0.31	2.81	0.0049

Table A1: Stepwise Akaike information criterion analysis of Cox proportional hazards models to determine which factors in the experimental design affected mortality. The exponent of the coefficient is the ratio of the hazard rates of two levels of the explanatory variable. The hazard ratio for each genotype is expressed relative to L4. The hazard ratios for bacteria treatments (*V. diazotrophicus* and *V. owensii*) are expressed relative to the control condition. The abrasion effect is expressed relative to the non-abraded treatment.

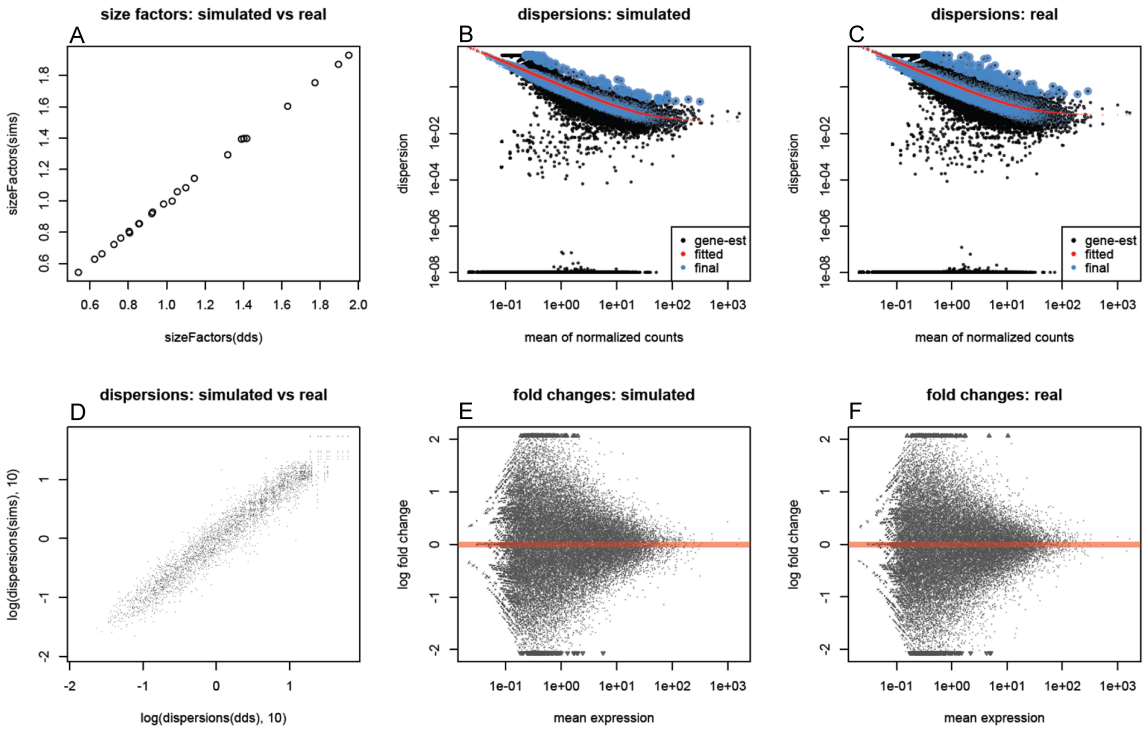

Figure A1: Simulation quality plots compare real and simulated DESeq2 datasets. (A) Size factors are nearly identical between real (dds) and simulated (sims) data sets. (B-C) Dispersion estimates of the real data set strongly agree with simulated dispersion estimates. (D) Dispersions are nearly identical between real (dds) and simulated (sims) data sets. (E-F) MA plots of log-fold change by mean expression value of real and simulated datasets are nearly identical.

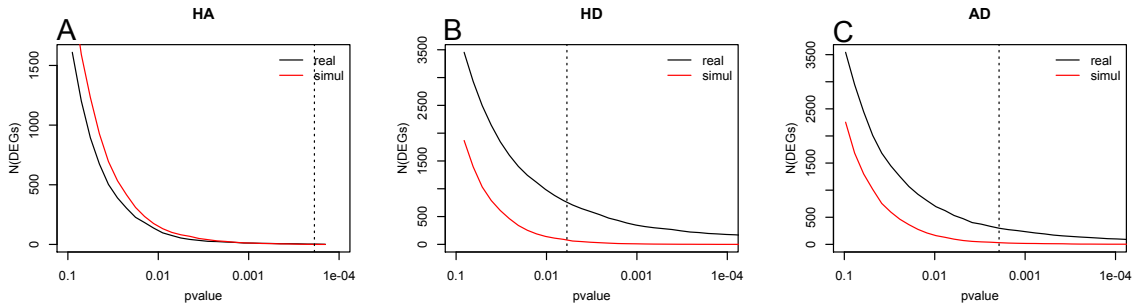

Figure A2: Calculating empirical false discovery rates using simulated data. The x-axis is the Wald test p-value and the y-axis is the number of differentially expressed genes (DEGs) passing this p-value cutoff. The black line corresponds to DEGs discovered in the real dataset and red line corresponds to DEGs discovered in the simulated dataset (false positives). The vertical dashed line indicates the empirical 10% false discovery rate (FDR) cutoff. (A) Healthy-AL comparison. (B) Healthy-Disease. (C) AL-Disease comparison.

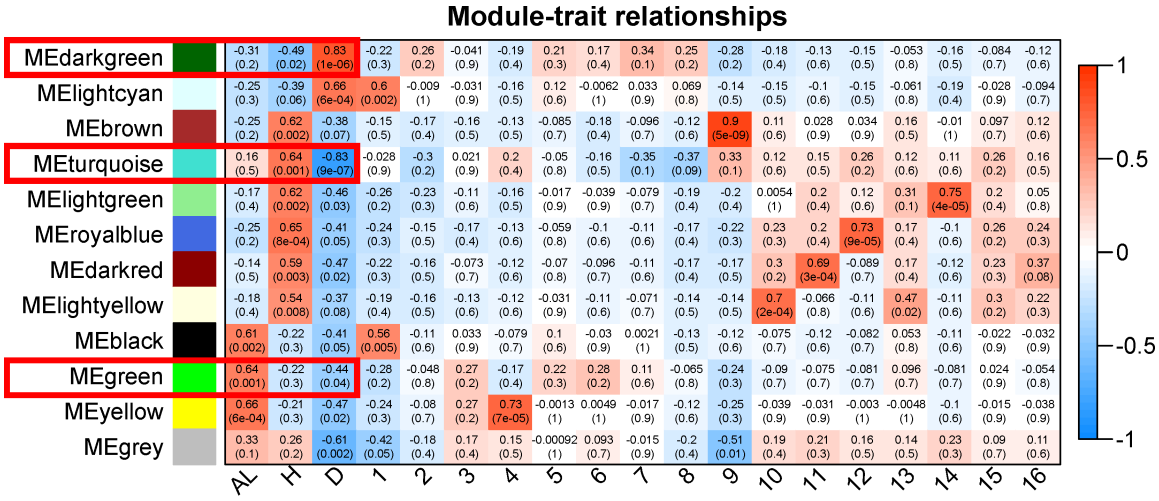

Figure A3: Heatmap of module-trait correlations. The strength of the correlations between traits (health states or individual corals) and gene coexpression modules are indicated by the intensity of color. The numbers in the cells give Pearson's correlation between the module eigengene and the trait and the p-value according to the correlation test. Red boxes mark the three modules that are highly and specifically correlated to each of the health states.

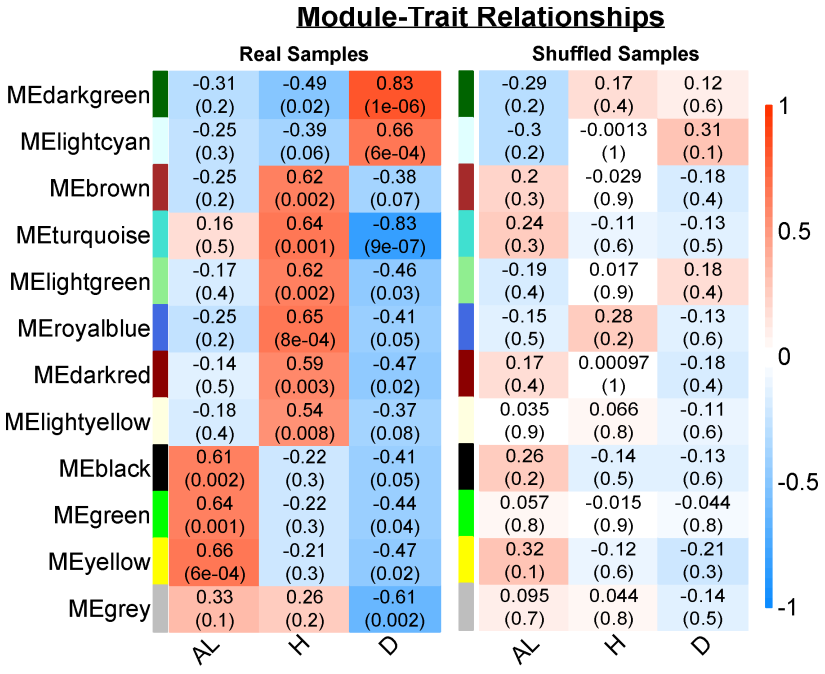

Figure A4: Shuffling sample-condition assignments dissolves module-trait relationships in WGCNA. On both panels, rows are module eigengenes (MEs) and the columns are traits (AL – ahead of lesion, H – healthy, and D –diseased). The color scale reflects the correlation of the module's eigengene with the trait. The numbers in the cells are the Pearson r and the p-value of the correlation test (in parentheses). Strong correlations between modules of gene co-expression and health states were identified when the samples were assigned to correct conditions (left). These correlations disappeared when condition designations were shuffled among samples (right), providing evidence of a true biological relationship between the identified gene coexpression modules and health states.

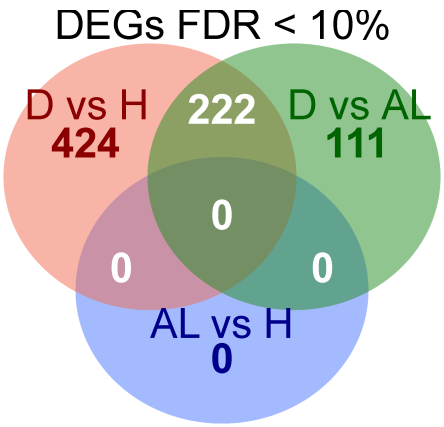

Figure A5: Venn diagram of DEGs passing the FDR threshold of 10% for each of the contrasts. The largest number of DEGs resulted from the contrast of diseased (D) tissue to healthy (H) tissues, followed by the contrast of diseased to tissues ahead of the lesion (AL). No isogroups passed the FDR cutoff for the AL-healthy contrast.

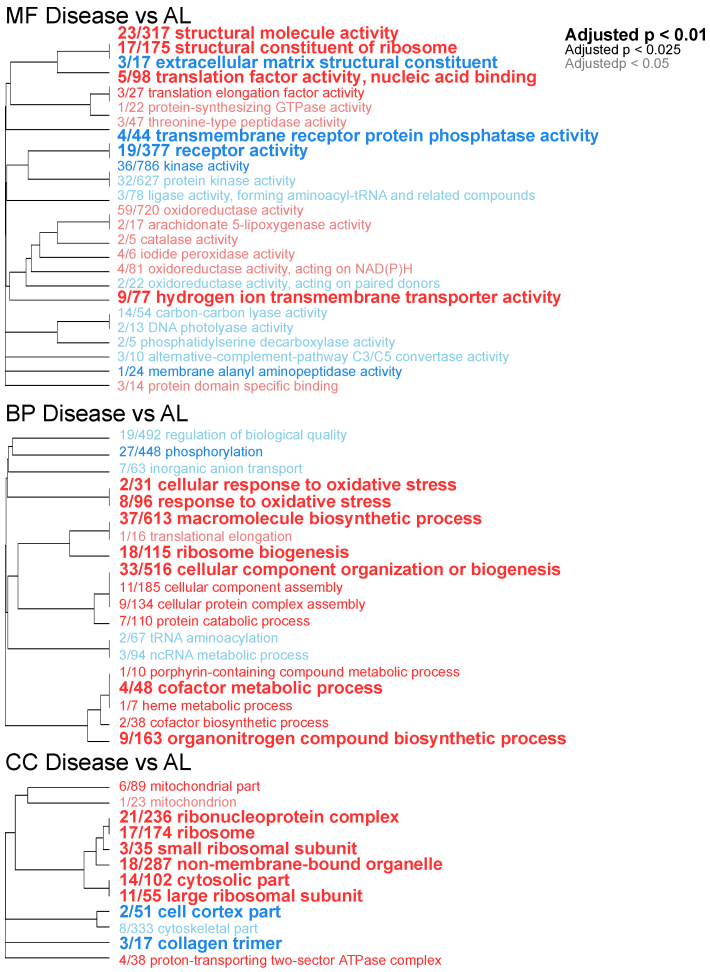

Figure A6: Gene ontology categories enriched by genes up-regulated (red) or down-regulated (blue) in diseased compared to AL samples, summarized by molecular function (MF), biological process (BP), and cellular component (CC). The size of the font indicates the significance of the term as indicated by the inset key. The fraction preceding the GO term indicates the number of genes annotated with the term that pass an unadjusted p-value threshold of 0.05. The trees indicate sharing of genes among GO categories (the categories with no branch length between them are subsets of each other).

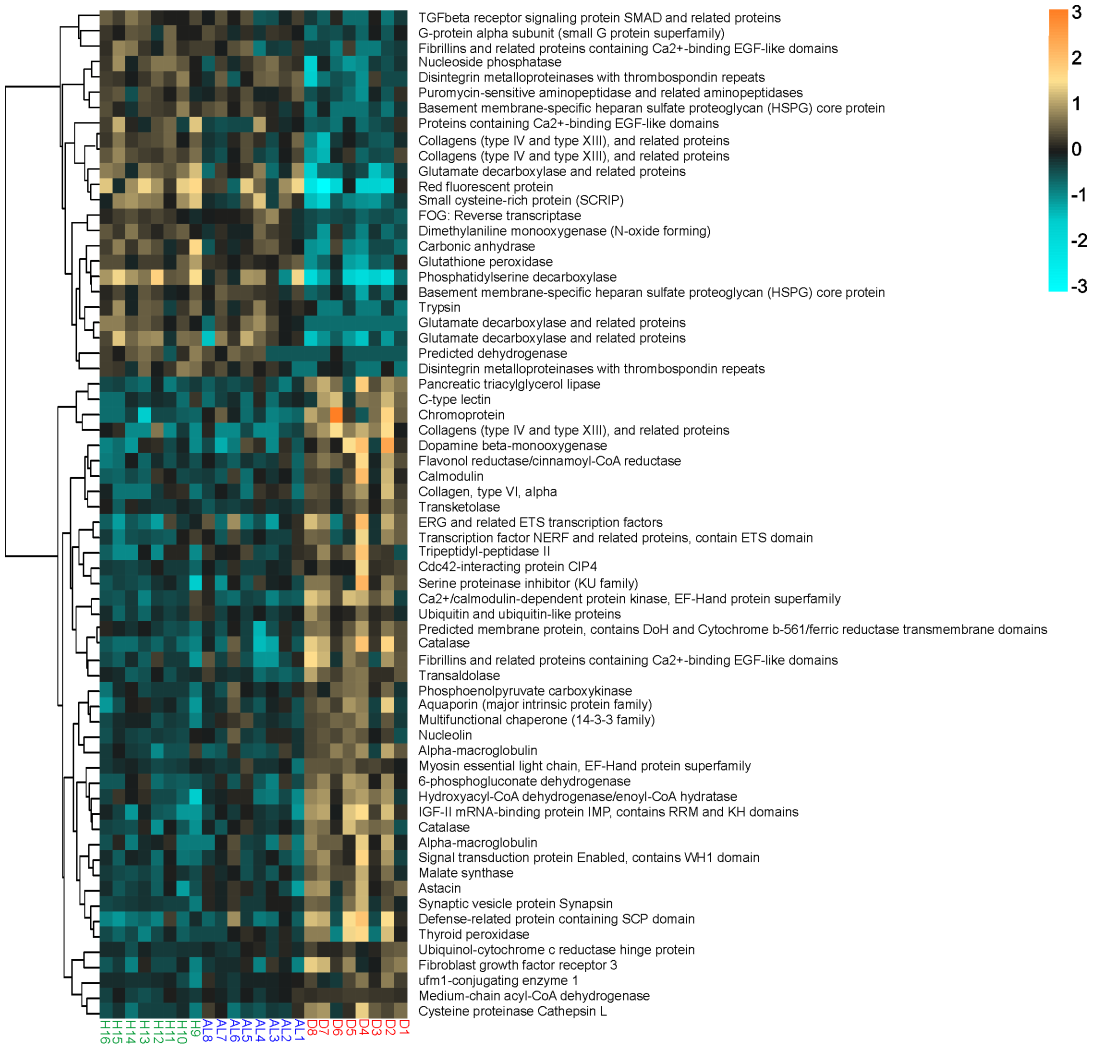

Figure A7: Gene expression heatmaps for annotated DEGs (adjusted p-value < 0.01) for the disease-healthy contrast. Rows are genes, columns are samples ordered as in the bottom panel: ahead-of-lesion (AL), healthy (H), and diseased (D). The color scale is in log2 (fold change relative to the gene's mean). The trees are a hierarchical clustering of genes based on Pearson's correlation of their expression across samples.

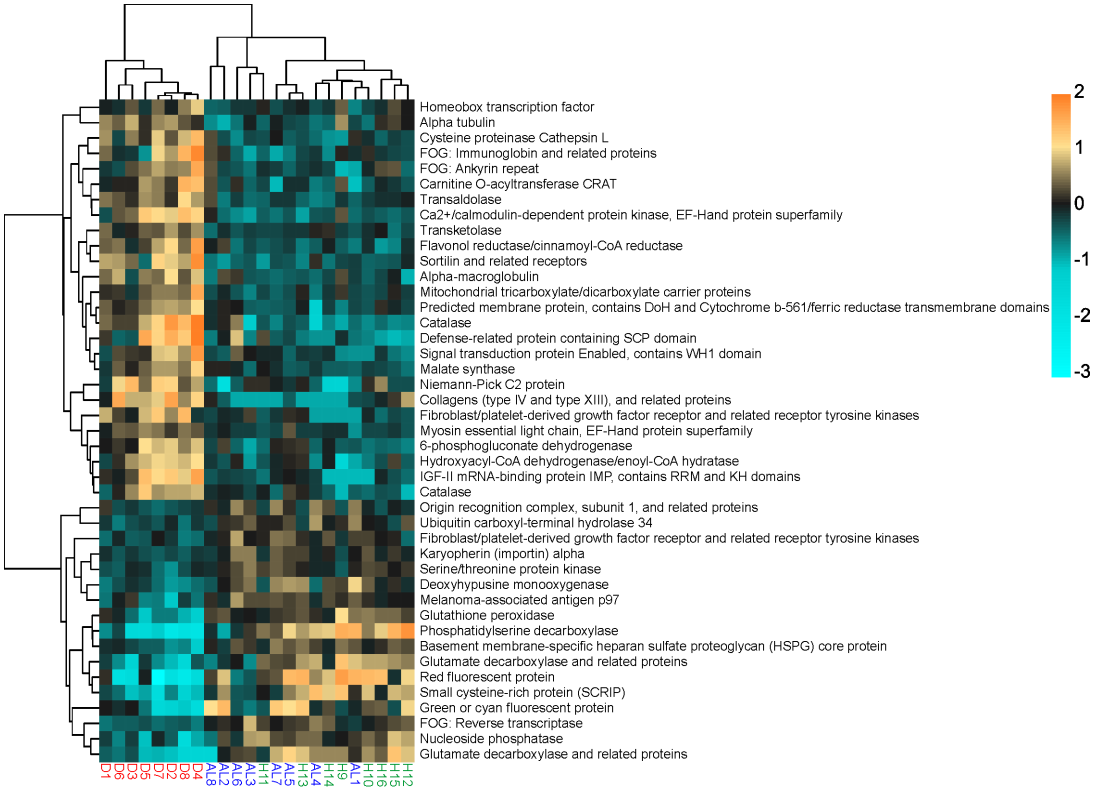

Figure A8: Gene expression heatmaps for annotated DEGs (unadjusted p-value < 0.01) for the disease-AL contrast. Rows are genes, columns are samples ordered as in the bottom panel: ahead-of-lesion (AL), healthy (H), and diseased (D). The color scale is in log2 (fold change relative to the gene's mean). The trees are hierarchical clustering of genes based on Pearson's correlation of their expression across samples.

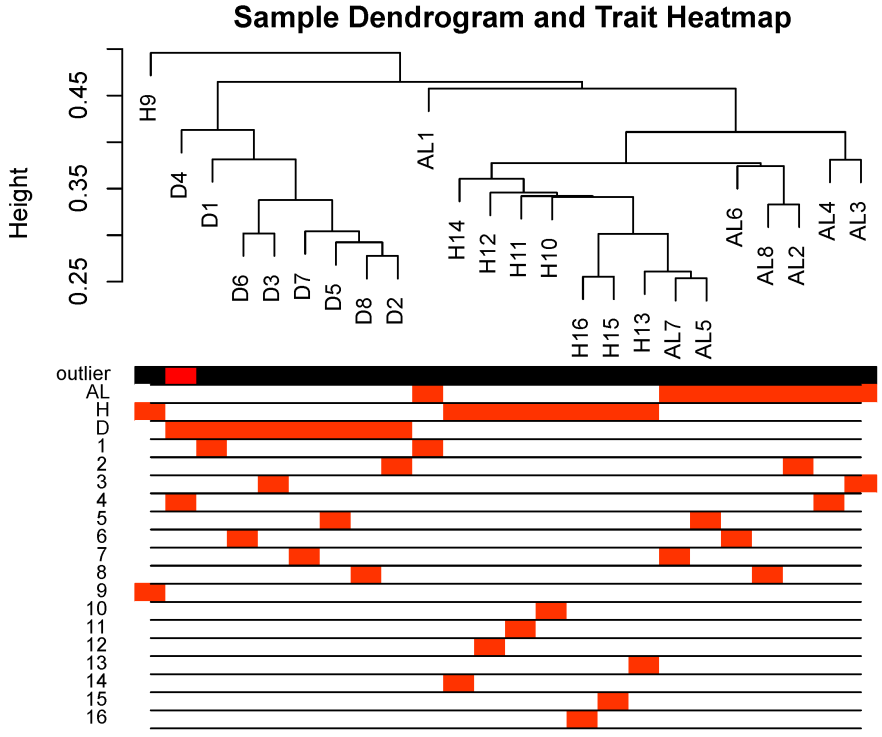

Figure A9: Sample dendrogram and outlier heatmap for WGCNA. Sample clustering allows the visualization of how traits (health states and individual genotypes in this case) relate to samples. The dendrogram does not present any obvious outliers, but individual "D4" is called as an outlier based on a standardized connectivity test.

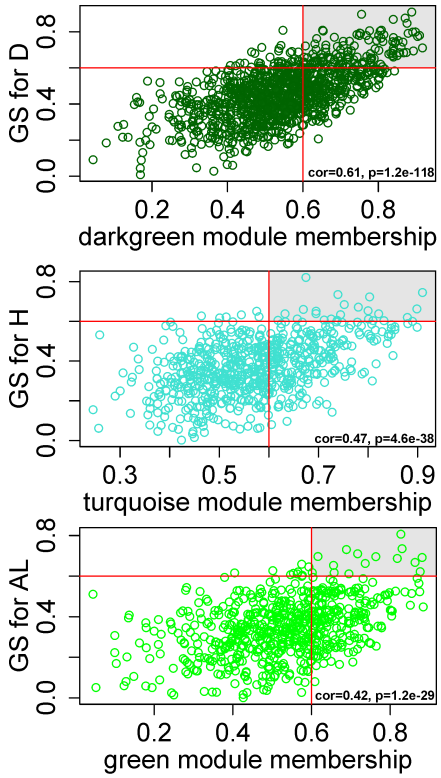

Figure A10: Dependency between individual genes' module membership (correlation with module's eigengene) and significance for the disease state (correlation of the gene with the disease state). The grey region encompasses genes with both module membership and gene significance scores higher than 0.6. Pearson correlation values and the p-value of the correlation test are indicated in the lower-right hand of each scatterplot.

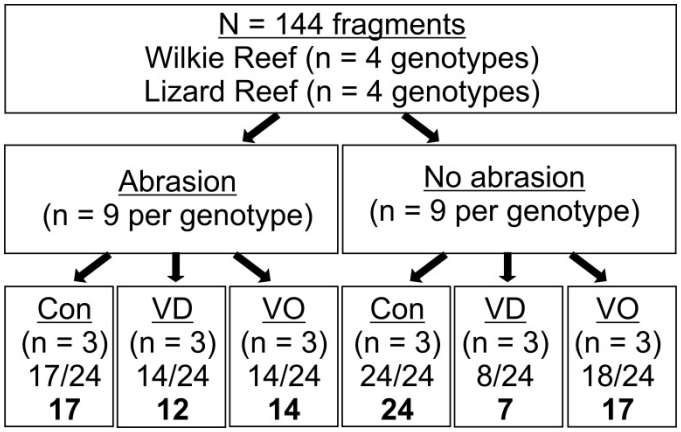

Figure A11: Experimental design. Eight genotypes (four from Lizard Island, four from Wilkie Island) were separated into 18 fragments, half of which were abraded. Three fragments from each abrasion treatment received filtered seawater as a control (Con), *Vibrio diazotrophicus* (VD), or *V. owensii* (VO). Fractions indicate the number of corals alive at the end of the experiment in each treatment (n = 24 per treatment). Bolded numbers indicate the number of samples included in the gene expression analysis after expression outliers were removed.

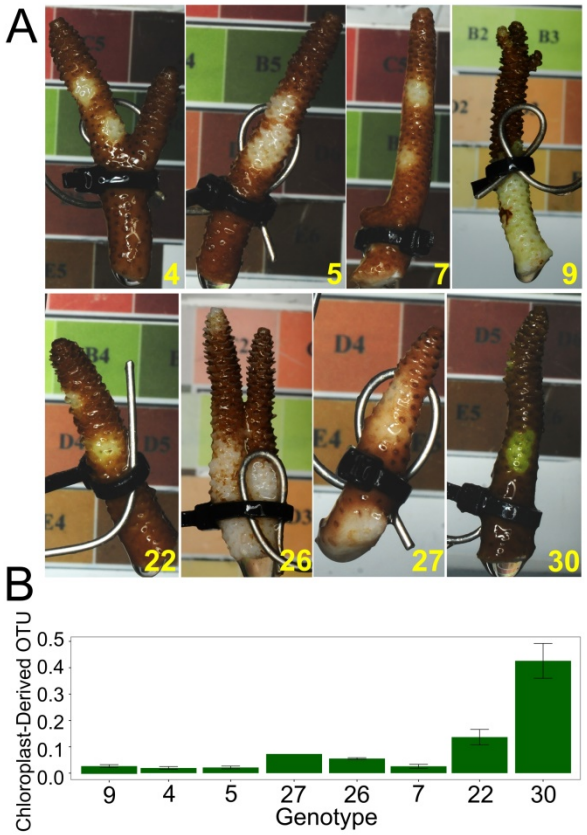

Figure A12: Example photos of each genotype and chloroplast-derived OTU counts. (A) Genotypes are indicated in yellow text. Genotypes 4, 5, 7, 22, 27, and 30 were abraded with an airgun. Genotypes 9 and 26 demonstrate lesion development at ~50% tissue loss (time of death in this experiment). (B) Mean chloroplast-derived OTU counts (±SE) for each genotype normalized to total counts.

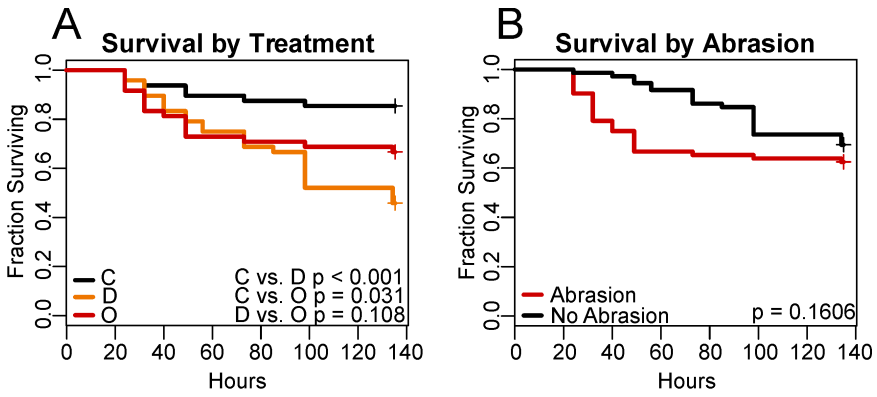

Figure A13: *A. millepora* survival by treatment during bacterial challenge. (A) Black, orange, and red lines represent the survival of control, *V. diazotrophicus*-challenged, and *V. owensii*-challenged corals, respectively. (B) Black and red lines represent the survival of corals that abraded and non-abraded corals, respectively. P-values were generated by Cox proportional hazards models testing the effect of each treatment.

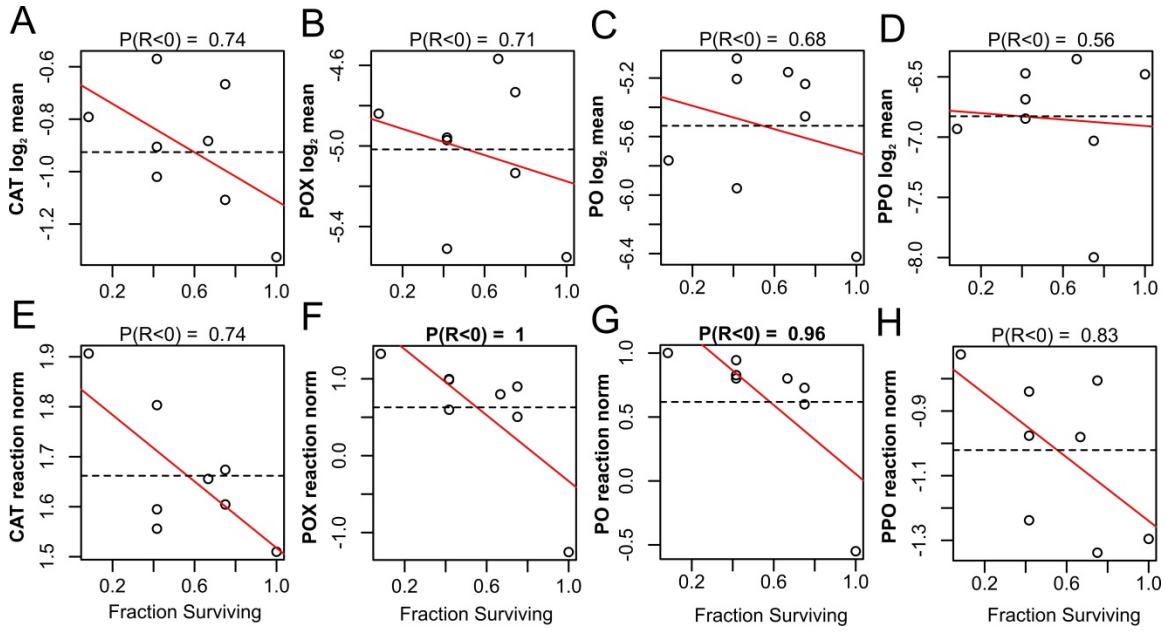

Figure A14: Correlations of mean immunity-related enzyme activities (A–D) and their reaction norms in response to bacterial challenge (E–H) with survival across genotypes, with genotype 30 excluded. Mean catalase (CAT), peroxidase (POX), phenoloxidase (PO), and prophenoloxidase (PPO) activities are represented as $\log_2$-transformed Δ absorbance mg protein^{-1} min^{-1}. Each point represents a posterior mean of the parameter for a genotype; dotted lines represent means across genotypes, red line is the linear model fit with survival as predictor variable. Value above the graph indicates posterior probability that the correlation with survival is negative.

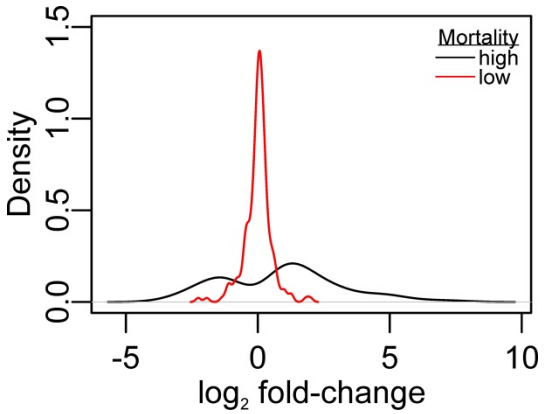

Figure A15: Density plots of predicted gene expression changes in response to bacteria treatment in the worst-surviving corals (survival = 0, black line) and best-surviving corals (survival = 1, red line). Expression changes are extrapolated from the DESeq2 model incorporating bacterial challenge as a categorical predictor (yes or no), survival as a continuous predictor, and their interaction. The plots are based on 388 bacteria-responding DEGs identified at FDR = 0.1.

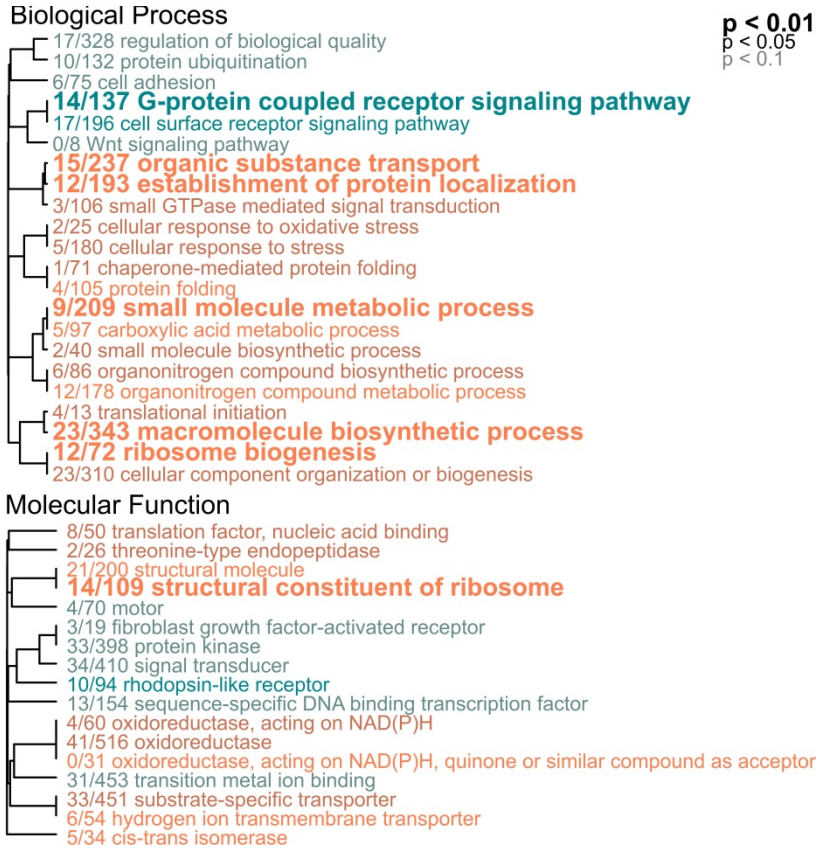

Figure A16: Gene ontology enrichment by interaction between treatment and survival. Biological processes enriched according to the Wald statistic ($\log_2$ fold change divided by standard error) generated by testing the interaction between bacterial treatment (control and treated) and survival fraction (continuous). The text color indicates the direction of expression difference between corals with high and low survival (turquoise = more upregulated in lower survival corals, orange = more downregulated in lower survival corals). The text size indicates the significance of the term as indicated by the inset key. The fraction preceding the term indicates the number of genes within the term that had an absolute Wald statistic greater than 2. Trees indicate gene sharing among gene ontology categories (categories with no branch length between them are subsets of each other).

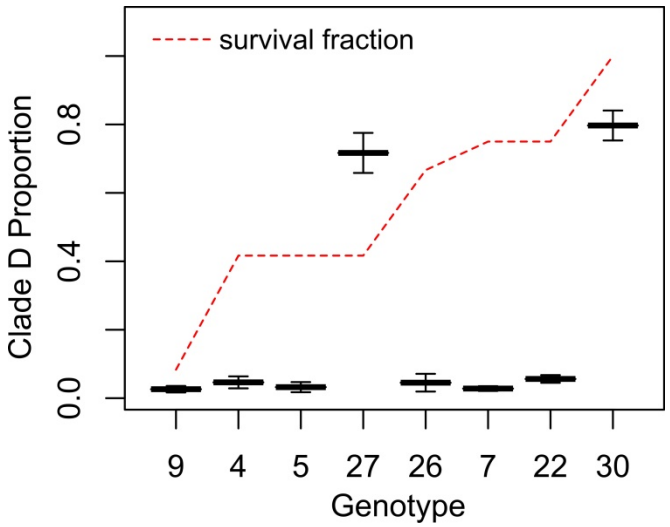

Figure A17: Proportions of clade D *Symbiodinium* in *A. millepora* based on RNA-seq reads mapping to clade D transcriptomes. Genotypes 30 and 27 were dominated by clade D. All other genotypes were dominated by clade C. Genotypes are ordered by survival fraction increasing from left to right, which is indicated by the red dashed line. This is a boxplot of clade proportions in all TagSeq-analyzed fragments for a given genotype; the box (interquartile range) is not visible since the values are very similar for all fragments of the same genotype. The whiskers show 2.5X interquartile distance away from the median.

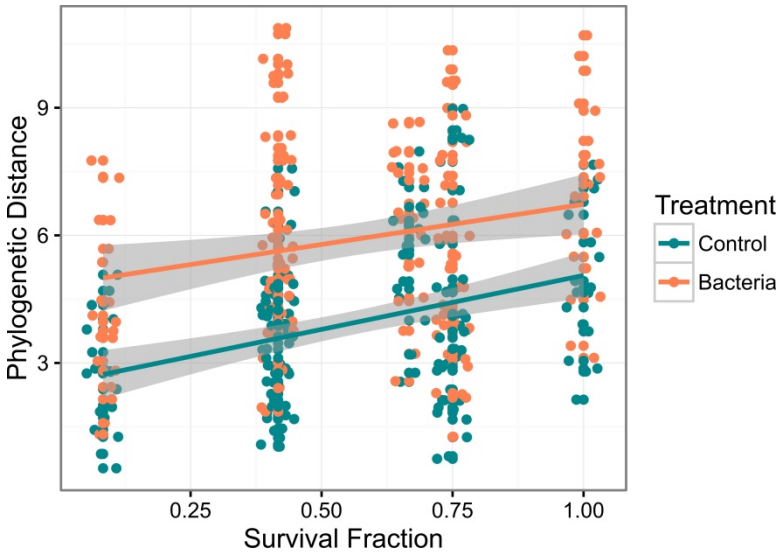

Figure A18: Phylogenetic diversity between treatments and mortality rates. Faith's phylogenetic diversity was calculated for each sample (n = 31) at ten sequencing depths ranging from 100 to 1000 reads. Each point represents a sample at a single sampling depth. Lines represent linear functions with 95% confidence regions shaded gray. Bacteria-challenged samples are orange, and controls are turquoise. Phylogenetic diversity of the microbial communities is higher in treated corals than controls ($p < 0.001$) and in corals with lower mortality ($p = 0.04$).

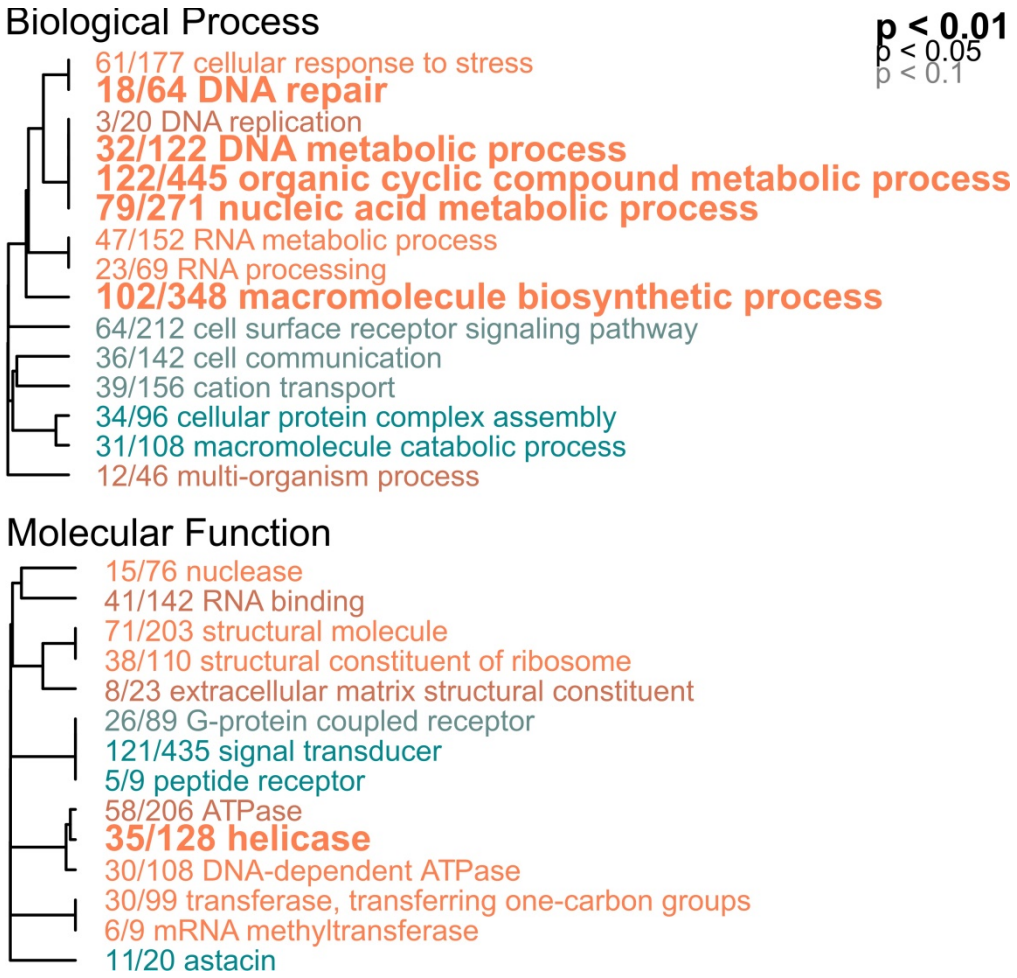

Figure A19: Gene ontology enrichment of genes differentially expressed by PCo1 value calculated using weighted UniFrac analysis. Biological processes enriched according to the Wald statistic (log2 fold change divided by standard error) generated by modeling gene expression (n = 31) by PCo1 coordinate value (Fig. 5A). The text color indicates the direction of expression difference between corals with higher or lower PCo1 values (orange = upregulated in samples with higher PCo1 values; turquoise = upregulated in samples with lower PCo1 values). The text size indicates the significance of the term as indicated by the inset key. The fraction preceding the term indicates the number of genes within the term that had an absolute Wald statistic greater than 2. Trees indicate gene sharing among gene ontology categories (categories with no branch length between them are subsets of each other).

References

Ainsworth, T. D., Krause, L., Bridge, T., Torda, G., Raina, J.-B., Zakrzewski, M., … Leggat, W. (2015). The coral core microbiome identifies rare bacterial taxa as ubiquitous endosymbionts. The ISME Journal, 9, 2261–2274.

Ainsworth, T. D., Kvennefors, E. C., Blackall, L. L., Fine, M., & Hoegh-Guldberg, O. (2007). Disease and cell death in white syndrome of Acroporid corals on the Great Barrier Reef. Marine Biology, 151, 19–29.

Allemand, D., Ferrier-pagès, C., Furla, P., Houlbrèque, F., Darwin, C., Fitz, C., … Eds, J. M. (2004). Biomineralisation in reef-building corals□: from molecular mechanisms to environmental control. General Paleontology (Paleobiochemistry), 3, 453–467.

Altschul, S. F., Madden, T. L., Schaffer, A. A., Zhang, J. H., Zhang, Z., Miller, W., & Lipman, D. J. (1997). Gapped BLAST and PSI-BLAST: a new generation of protein database search programs. Nucleic Acids Research, 25, 3389–3402.

Andersson, A. J., & Gledhill, D. (2011). Ocean Acidification and Coral Reefs: Effects on Breakdown, Dissolution, and Net Ecosystem Calcification. Annual Review of Marine Science, 5, 321–348.

Armstrong, P. B., & Quigley, J. P. (1999). a 2 -macroglobulin□: an evolutionarily conserved arm of the innate immune system. Developmental and Comparative Immunology, 23, 375–390.

Baird, A. H., Guest, J. R., & Willis, B. L. (2009). Systematic and Biogeographical Patterns in the Reproductive Biology of Scleractinian Corals. Annual Review of Ecology Evolution and Systematics, 40, 551–571.

Ban, S. S., Graham, N. a J., & Connolly, S. R. (2014). Evidence for Multiple Stressor Interactions and Effects on Coral Reefs. Global Change Biology, 20, 681–697.

Baria, M. V. B., dela Cruz, D. W., Villanueva, R. D., & Guest, J. . (2012). Spawning of Three-Year-Old Acropora Millepora Corals Reared From Larvae In Northwestern Philippines. Bulletin of Marine Science, 88, 61–62.

Barshis, D. J., Stillman, J. H., Gates, R. D., Toonen, R. J., Smith, L. W., & Birkeland, C. (2010). Protein expression and genetic structure of the coral Porites lobata in an environmentally extreme Samoan back reef: Does host genotype limit phenotypic plasticity? Molecular Ecology, 19, 1705–1720.

Baumann, J., Grottoli, A. G., Hughes, A. D., & Matsui, Y. (2014). Photoautotrophic and heterotrophic carbon in bleached and non-bleached coral lipid acquisition and storage. Journal of Experimental Marine Biology and Ecology, 461, 469–478.

Bay, L. K., Ulstrup, K. E., Nielsen, H. B., Jarmer, H., Goffard, N., Willis, B. L., … Van Oppen, M. J. H. (2009). Microarray analysis reveals transcriptional plasticity in the reef building coral Acropora millepora. Molecular Ecology, 18, 3062–3075.

Beeden, R., Willis, B. L., Raymundo, L. J., Page, C. A., & Weil, E. (2008). Underwater Cards for Assessing Coral Health on Indo-Pacific Reefs. Global Environment Facility Coral Reef Targeted Research Program, St. Lucia.

Ben-Haim, Y. (2003). Vibrio coralliilyticus sp. nov., a temperature-dependent pathogen of the coral Pocillopora damicornis. International Journal of Systematic and Evolutionary Microbiology, 53, 309–315.

Benavides, M., Bednarz, V. N., & Ferrier-Pagès, C. (2017). Diazotrophs: Overlooked key players within the coral symbiosis and tropical reef ecosystems? Frontiers in Marine Science, 4. doi:10.3389/fmars.2017.00010

Benjamini, Y., & Hochberg, Y. (1995). Controlling the False Discovery Rate: A Practical and Powerful Approach to Multiple Testing. Journal of the Royal Statistical Society. Series B (Methodological), 57, 289–300.

Bosch, T. C. G. (2007). Why polyps regenerate and we don't: towards a cellular and molecular framework for Hydra regeneration. Developmental Biology, 303, 421–433.

Bourne, D. G., & Munn, C. B. (2005). Diversity of bacteria associated with the coral Pocillopora damicornis from the Great Barrier Reef. Environmental Microbiology, 7, 1162–1174.

Bozec, Y. M., & Mumby, P. J. (2015). Synergistic impacts of global warming on the resilience of coral reefs. Philosophical Transactions of the Royal Society of London B: Biological Sciences, 370, 20130267.

Brown, B., & Bythell, J. (2005). Perspectives on mucus secretion in reef corals. Marine Ecology Progress Series, 296, 291–309.

Brown, B. E. (1997). Coral bleaching: causes and consequences. Coral Reefs, 16, 129–138.

Brown, T., Bourne, D., & Rodriguez-Lanetty, M. (2013). Transcriptional Activation of c3 and hsp70 as Part of the Immune Response of Acropora millepora to Bacterial Challenges. PLoS ONE, 8, e67246.

Burge, C. a, Mouchka, M. E., Harvell, C. D., & Roberts, S. (2013). Immune response of the Caribbean sea fan, Gorgonia ventalina, exposed to an Aplanochytrium parasite as revealed by transcriptome sequencing. Frontiers in Physiology, 4, 1–9.

Burriesci, M. S., Raab, T. K., & Pringle, J. R. (2012). Evidence that glucose is the major transferred metabolite in dinoflagellate-cnidarian symbiosis. The Journal of Experimental Biology, 215, 3467–77.

Bythell, J. C., Bythell, M., & Gladfelter, E. H. (1993). Initial results of a long-term coral reef monitoring program□: Impact of Hurricane Hugo at Buck Island Reef National Monument, St. Croix, U.S. Virgin Islands. Journal of Experimental Marine Biology and Ecology, 172, 171–183.

Bythell, J. C., Hillis-Starr, Z. M., & Rogers, C. S. (2000). Local variability but landscape stability in coral reef communities following repeated hurricane impacts. Marine Ecology Progress Series, 204, 93–100.

Cano-Gómez, A., Goulden, E. F., Owens, L., & Høj, L. (2010). Vibrio owensii sp. nov., isolated from cultured crustaceans in Australia. FEMS Microbiology Letters, 302, 175–81.

Caporaso, J. G., Kuczynski, J., Stombaugh, J., Bittinger, K., Bushman, F. D., Costello, E. K., … Knight, R. (2010). QIIME allows analysis of high-throughput community sequencing data. Nature Methods, 7, 335–336.

Casey, J. M., Connolly, S. R., & Ainsworth, T. D. (2015). Coral transplantation triggers shift in microbiome and promotion of coral disease associated potential pathogens. Scientific Reports, 5, 1–11.

Cervino, J. M., Thompson, F. L., Gomez-Gil, B., Lorence, E. a, Goreau, T. J., Hayes, R. L., … Bartels, E. (2008). The Vibrio core group induces yellow band disease in Caribbean and Indo-Pacific reef-building corals. Journal of Applied Microbiology, 105, 1658–1671.

Clausen, C. D., & Roth, A. A. (1975). Effect of Temperature and Temperature Adaptation on Calcification Rate in the Hermatypic Coral Pocillopora damicomis. Marine Biology, 33, 93–100.

Closek, C. J., Sunagawa, S., DeSalvo, M. K., Piceno, Y. M., DeSantis, T. Z., Brodie, E. L., … Medina, M. (2014). Coral transcriptome and bacterial community profiles reveal distinct Yellow Band Disease states in Orbicella faveolata. The ISME Journal, 8, 2411–2422.

Cooper, T. F., Berkelmans, R., Ulstrup, K. E., Weeks, S., Radford, B., Jones, A. M., … van Oppen, M. J. H. (2011). Environmental factors controlling the distribution of *symbiodinium* harboured by the coral acropora millepora on the great barrier reef. PLoS ONE, 6. doi:10.1371/journal.pone.0025536

Császár, N. B. ., Seneca, F. O., & Van Oppen, M. J. H. (2009). Variation in antioxidant gene expression in the scleractinian coral Acropora millepora under laboratory thermal stress. Marine Ecology Progress Series, 392, 93–102.

Császár, N. B. M., Ralph, P. J., Frankham, R., Berkelmans, R., & van Oppen, M. J. H. (2010). Estimating the Potential for Adaptation of Corals to Climate Warming. PLoS ONE, 5. doi:10.1371/journal.pone.0009751

Cummins, E. P., Berra, E., Comerford, K. M., Ginouves, A., Fitzgerald, K. T., Seeballuck, F., … Taylor, C. T. (2006). Prolyl hydroxylase-1 negatively regulates IkappaB kinase-beta, giving insight into hypoxia-induced NFkappaB activity. Proceedings of the National Academy of Sciences of the United States of America, 103, 18154–18159.

D'Angelo, G., Duplan, E., Boyer, N., Vigne, P., & Frelin, C. (2003). Hypoxia up-regulates prolyl hydroxylase activity: a feedback mechanism that limits HIF-1 responses during reoxygenation. The Journal of Biological Chemistry, 278, 38183–38187.

Daniels, C. a., Baumgarten, S., Yum, L. K., Michell, C. T., Bayer, T., Arif, C., … Voolstra, C. R. (2015). Metatranscriptome analysis of the reef-building coral Orbicella faveolata indicates holobiont response to coral disease. Frontiers in Marine Science, 2, 1–13.

Davy, S. K., Allemand, D., & Weis, V. M. (2012). Cell biology of cnidarian-dinoflagellate symbiosis. Microbiology and Molecular Biology Reviews, 76, 229–261.

DeSalvo, M. K., Voolstra, C. R., Sunagawa, S., Schwarz, J. a, Stillman, J. H., Coffroth, M. a, … Medina, M. (2008). Differential gene expression during thermal stress and bleaching in the Caribbean coral Montastraea faveolata. Molecular Ecology, 17, 3952–3971.

DeSalvo, M., Sunagawa, S., Voolstra, C., & Medina, M. (2010). Transcriptomic responses to heat stress and bleaching in the elkhorn coral Acropora palmata. Marine Ecology Progress Series, 402, 97–113.

Dixon, G. B., Davies, S. W., Aglyamova, G. A., Meyer, E., Bay, L. K., & Matz, M. V. (2015). Genomic determinants of coral heat tolerance across latitudes. Science, 348, 1460–1462.

Dixon, P. (2003). VEGAN, a package of R functions for community ecology. Journal of Vegetation Science, 14, 927–930.

Downs, C. A., Mueller, E., Phillips, S., Fauth, J. E., & Woodley, C. M. (2000). A molecular biomarker system for assessing the health of coral (Montastraea faveolata) during heat stress. Marine Biotechnology, 2, 533–544.

Dunlap, W. C., Starcevic, A., Baranasic, D., Diminic, J., Zucko, J., Gacesa, R., … Long, P. F. (2013). KEGG orthology-based annotation of the predicted proteome of Acropora digitifera: ZoophyteBase - an open access and searchable database of a coral genome. BMC Genomics, 14, 509.

Fang, L. S., Chen, Y. W. J., & Chen, C. S. (1989). Why does the white tip of stony coral grow so fast without zooxanthellae? Marine Biology, 103, 359–363.

Fang, L. S., & Shen, P. (1988). A living mechanical file: the burrowing mechanism of the coral-boring bivalve Lithophaga nigra. Marine Biology, 97, 349–354.

Fernandes, N., Steinberg, P., Rusch, D., Kjelleberg, S., & Thomas, T. (2012). Community Structure and Functional Gene Profile of Bacteria on Healthy and Diseased Thalli of the Red Seaweed Delisea pulchra. PLoS ONE, 7, 1–8.

Fox, J., & Weisberg, S. (2001). An R Companion to Applied Regression, Second Edition.

Fuess, L. E., Pinzón, J. H., Weil, E., & Mydlarz, L. D. (2014). Associations between transcriptional changes and protein phenotypes provide insights into immune regulation in corals. Developmental and Comparative Immunology, 62, 17–28.

Fujita, T. (2002). Evolution of the lectin-complement pathway and its role in innate immunity. Nature Reviews Immunology, 2, 346–353.

Furla, P., Galgani, I., Durand, I., & Allemand, D. (2000). Sources and mechanisms of inorganic carbon transport for coral calcification and photosynthesis. The Journal of Experimental Biology, 203, 3445–3457.

Gantar, M., Kaczmarsky, L. T., Stanić, D., Miller, A. W., & Richardson, L. L. (2011). Antibacterial Activity of Marine and Black Band Disease Cyanobacteria against Coral-Associated Bacteria. Marine Drugs, 9, 2089–2105.

Gignoux-Wolfsohn, S. A., & Vollmer, S. V. (2015). Identification of Candidate Coral Pathogens on White Band Disease-Infected Staghorn Coral. PLoS ONE, 10, e0134416.

Gladfelter, E. H. (1983). Circulation of Fluids in the Gastrovascular System of the Reef Coral Acropora cervicornis. Biological Bulletin, 165, 619–636.

Gochfeld, D. J., Olson, J. B., & Slattery, M. (2006). Colony versus population variation in susceptibility and resistance to dark spot syndrome in the Caribbean coral Siderastrea siderea. Diseases of Aquatic Organisms, 69, 53–65.

Godwin, S., Bent, E., Borneman, J., & Pereg, L. (2012). The Role of Coral-Associated Bacterial Communities in Australian Subtropical White Syndrome of Turbinaria mesenterina. PLoS ONE, 7. doi:10.1371/journal.pone.0044243

Goffredo, S., Vergni, P., Reggi, M., Caroselli, E., Sparla, F., Levy, O., … Falini, G. (2011). The skeletal organic matrix from Mediterranean coral Balanophyllia europaea influences calcium carbonate precipitation. PloS ONE, 6, e22338.

Green, E. A., Davies, S. W., Matz, M. V., & Medina, M. (2014). Quantifying cryptic *Symbiodinium* diversity within Orbicella faveolata and Orbicella franksi at the Flower Garden Banks, Gulf of Mexico. PeerJ, 2, e386.

Greenstein, B. J., & Pandolfi, J. M. (2008). Escaping the heat: Range shifts of reef coral taxa in coastal Western Australia. Global Change Biology, 14, 513–528.
Grottoli, A. G., Rodrigues, L. J., & Palardy, J. E. (2006). Heterotrophic plasticity and resilience in bleached corals. Nature, 440, 1186–1189.
Hadfield, J. D. (2010). MCMC methods for multi-response generalized linear mixed models: the MCMCglmm R package. Journal of Statistical Software, 33, 1–22.
Harvell, C. D., Kim, K., Burkholder, J. M., Colwell, R. ., Epstein, P. ., Grimes, D. ., … Vasta, G. . (1999). Emerging Marine Diseases-Climate Links and Anthropogenic Factors. Science, 285, 1505–1510.
Hoegh-Gulberg, O. (1999). Climate change, coral bleaching and the future of the world's coral reefs. Marine Freshwater Resources, 839–866.
Hoegh-Guldberg, O., Mumby, P. J., Hooten, A. J., Steneck, R. S., Greenfield, P., Gomez, E., … Hatziolos, M. E. (2007). Coral Reefs Under Rapid Climate Change and Ocean Acidification. Science, 318, 1737–1742.
Horn, M. (2008). Chlamydiae as Symbionts in Eukaryotes. Annual Review of Microbiology, 62, 113–131.
Horn, M., Fritsche, T. R., Linner, T., Gautom, R. K., Harzenetter, M. D., & Wagner, M. (2002). Obligate bacterial endosymbionts of Acanthamoeba spp. related to the beta-Proteobacteria: Proposal of "Candidatus Procabacter acanthamoebae" gen. nov., sp. nov. International Journal of Systematic and Evolutionary Microbiology, 52, 599–605.
Horvath, S. (2011). Weighted Network Analysis. Applications in Genomics and Systems Biology. Springer.
Houlbreque, F., & Ferrier-Pages, C. (2009). Heterotrophy in tropical scleractinian corals. Biological Reviews, 84, 1–17.
Hughes, A. D., & Grottoli, A. G. (2013). Heterotrophic compensation: A possible mechanism for resilience of coral reefs to global warming or a sign of prolonged stress? PLoS ONE, 8, 1–10.
Hwang, J. S., Takaku, Y., Momose, T., Adamczyk, P., Özbek, S., Ikeo, K., … Gojobori, T. (2010). Nematogalectin, a nematocyst protein with GlyXY and galectin domains, demonstrates nematocyte-specific alternative splicing in Hydra. Proceedings of the National Academy of Sciences of the United States of America, 107, 18539–18544.
Jombart, T. (2008). adegenet: an R package for the multivariate analysis of genetic markers. Bioinformatics, doi:10.1093/bioinformatics/btr521.
Kang, W., & Reid, K. B. M. (2003). DMBT1, a regulator of mucosal homeostasis through the linking of mucosal defense and regeneration? FEBS Letters, 540, 21–25.
Kauffmann, A., Gentleman, R., & Wolfgang Huber. (2009). arrayQualityMetrics--a bioconductor package for quality assessment of microarray data. Bioinformatics, 25, 415–416.
Kenkel, C. D., Aglyamova, G., Alamaru, A., Bhagooli, R., Capper, R., Cunning, R., … Matz, M. V. (2011). Development of gene expression markers of acute heat-light stress in reef-building Corals of the genus porites. PLoS ONE, 6. doi:10.1371/journal.pone.0026914
Kleypas, J. A. (1999). Geochemical Consequences of Increased Atmospheric Carbon Dioxide on Coral Reefs. Science, 284, 118–120.

Kolde, R. (2013). pheatmap: Pretty Heatmaps.
Kondrashov, F. A., Koonin, E. V, Morgunov, I. G., Finogenova, T. V, & Kondrashova, M. N. (2006). Evolution of glyoxylate cycle enzymes in Metazoa: evidence of multiple horizontal transfer events and pseudogene formation. Biology Direct, 1, 31.
Kornberg, H. L., & Krebs, H. A. (1957). Synthesis of Cell Constituents from C2-Units by a Modified Tricarboxylic Acid Cycle. Nature, 179, 988–991.
Kültz, D. (2005). Molecular and Evolutionary Basis of the Cellular Stress Response. Annual Review of Physiology, 67, 225–257.
Kushmaro, A., Banin, E., Loya, Y., Stackebrandt, E., & Rosenberg, E. (2001). Vibrio shiloi sp. nov., the causative agent of bleaching of the coral Oculina patagonica. International Journal of Systematic and Evolutionary Microbiology, 51, 1383–1388.
Kvennefors, E. C. E., Leggat, W., Hoegh-Guldberg, O., Degnan, B. M., & Barnes, A. C. (2008). An ancient and variable mannose-binding lectin from the coral Acropora millepora binds both pathogens and symbionts. Developmental and Comparative Immunology, 32, 1582–1592.
Kvennefors, E. C. E., Leggat, W., Kerr, C. C., Ainsworth, T. D., Hoegh-Guldberg, O., & Barnes, A. C. (2010). Analysis of evolutionarily conserved innate immune components in coral links immunity and symbiosis. Developmental and Comparative Immunology, 34, 1219–1229.
Lande, R., & Arnold, S. (1983). The measurement of selection on correlated characters. Evolution.
Langfelder, P., & Horvath, S. (2008). WGCNA: an R package for weighted correlation network analysis. BMC Bioinformatics, 9, 559.
Langmead, B., & Salzberg, S. L. (2012). Fast gapped-read alignment with Bowtie 2. Nat Methods, 9, 357–359.
Lee, E. G., Boone, D. L., Chai, S., Libby, S. L., Chien, M., Lodolce, J. P., & Ma, A. (2000). Failure to Regulate TNF-Induced NF-kappa B and Cell Death Responses in A20-Deficient Mice. Science, 289, 2350–2354.
Lema, K. A., Clode, P. L., Kilburn, M. R., Thornton, R., Willis, B. L., & Bourne, D. G. (2016). Imaging the uptake of nitrogen-fixing bacteria into larvae of the coral Acropora millepora. The ISME Journal, 10, 1804–1808.
Lesser, M. P., Bythell, J. C., Gates, R. D., Johnstone, R. W., & Hoegh-Guldberg, O. (2007). Are infectious diseases really killing corals? Alternative interpretations of the experimental and ecological data. Journal of Experimental Marine Biology and Ecology, 346, 36–44.
Libro, S., Kaluziak, S. T., & Vollmer, S. V. (2013). RNA-seq profiles of immune related genes in the staghorn coral Acropora cervicornis infected with white band disease. PloS ONE, 8, e81821.
Logan, C. A., Dunne, J. P., Eakin, C. M., & Donner, S. D. (2014). Incorporating adaptive responses into future projections of coral bleaching. Global Change Biology, 20, 125–139.
Lõhelaid, H., Teder, T., Tõldsepp, K., Ekins, M., & Samel, N. (2014). Up-Regulated Expression of AOS-LOXa and Increased Eicosanoid Synthesis in Response to Coral Wounding. PLoS ONE, 9, e89215.

Lohman, B. K., Weber, J. N., & Bolnick, D. I. (2016). Evaluation of TagSeq, a reliable low-cost alternative for RNAseq. Molecular Ecology Resources, 16, 1315–1321.

Love, M. I., Huber, W., & Anders, S. (2014). Moderated estimation of fold change and dispersion for RNA-Seq data with DESeq2. bioRxiv, doi: 10.11.

Lozupone, C., Lladser, M. E., Knights, D., Stombaugh, J., & Knight, R. (2011). UniFrac: An effective distance metric for microbial community comparison. The ISME Journal, 5, 169–172.

Lu, X., Wang, C., & Liu, B. (2015). The role of Cu/Zn-SOD and Mn-SOD in the immune response to oxidative stress and pathogen challenge in the clam Meretrix meretrix. Fish and Shellfish Immunology, 42, 58–65.

Makino, A., Yamano, H., Beger, M., Klein, C. J., Yara, Y., & Possingham, H. P. (2014). Spatio-temporal marine conservation planning to support high-latitude coral range expansion under climate change. Diversity and Distributions, 20, 859–871.

Marcelino, V. R., & Verbruggen, H. (2016). Multi-marker metabarcoding of coral skeletons reveals a rich microbiome and diverse evolutionary origins of endolithic algae. Scientific Reports, 31508.

Martins, R. F., Ramos, M. F., Herfindal, L., Sousa, J. A., Skærven, K., & Vasconcelos, V. M. (2008). Antimicrobial and cytotoxic assessment of marine cyanobacteria - Synechocystis and Synechococcus. Marine Drugs, 6, 1–11.

Marubini, F., Ferrier-Pages, C., & Cuif, J.-P. (2003). Suppression of skeletal growth in scleractinian corals by decreasing ambient carbonate-ion concentration: a cross-family comparison. Proceedings of the Royal Society B: Biological Sciences, 270, 179–184.

Matsushita, M., & Fujita, T. (1992). Activation of the Classical Complement Pathway by Marmose-binding Protein in Association with a Novel Cls-like Serine Protease. Journal of Experimental Medicine, 176, 1497–1502.

Matz, M. V, Wright, R. M., & Scott, J. G. (2013). No Control Genes Required: Bayesian Analysis of qRT-PCR Data. PloS ONE, 8, e71448.

Maynard, J., van Hooidonk, R., Eakin, C. M., Puotinen, M., Garren, M., Williams, G., … Harvell, C. D. (2015). Projections of climate conditions that increase coral disease susceptibility and pathogen abundance and virulence. Nature Climate Change, 5, 688–695.

McDowell, I. C., Nikapitiya, C., Aguiar, D., Lane, C. E., Istrail, S., & Gomez-Chiarri, M. (2014). Transcriptome of American Oysters, Crassostrea virginica, in Response to Bacterial Challenge: Insights into Potential Mechanisms of Disease Resistance. PloS ONE, 9, e105097.

Meyer, E., Aglyamova, G. V, & Matz, M. V. (2011). Profiling gene expression responses of coral larvae (Acropora millepora) to elevated temperature and settlement inducers using a novel RNA-Seq procedure. Molecular Ecology, 20, 3599–3616.

Meyer, E., Aglyamova, G. V, Wang, S., Buchanan-Carter, J., Abrego, D., Colbourne, J. K., … Matz, M. V. (2009). Sequencing and de novo analysis of a coral larval transcriptome using 454 GSFlx. BMC Genomics, 10, 219.

Miller, A. W., & Richardson, L. L. (2015). Emerging coral diseases: a temperature-driven process? Marine Ecology, 36, 278–291.

Miller, D. J., Hemmrich, G., Ball, E. E., Hayward, D. C., Khalturin, K., Funayama, N., … Bosch, T. C. G. (2007). The innate immune repertoire in cnidaria--ancestral complexity and stochastic gene loss. Genome Biology, 8, R59.

Moya, A., Huisman, L., Ball, E. E., Hayward, D. C., Grasso, L. C., Chua, C. M., … Miller, D. J. (2012). Whole transcriptome analysis of the coral Acropora millepora reveals complex responses to CO2-driven acidification during the initiation of calcification. Molecular Ecology, 21, 2440–2454.

Moya, A., Tambutté, S., Bertucci, A., Tambutté, E., Lotto, S., Vullo, D., … Zoccola, D. (2008). Carbonic anhydrase in the scleractinian coral Stylophora pistillata: characterization, localization, and role in biomineralization. The Journal of Biological Chemistry, 283, 25475–25484.

Muller, E. M., & van Woesik, R. (2012). Caribbean coral diseases: primary transmission or secondary infection? Global Change Biology, 18, 3529–3535.

Muscatine, L., & Porter, J. W. (1977). Reef corals: mutualistic symbioses adapted to nutrient-poor environments. BioScience, 27, 454–460.

Mydlarz, L. D., Couch, C. S., Weil, E., Smith, G., & Harvell, C. D. (2009). Immune defenses of healthy, bleached and diseased Montastraea faveolata during a natural bleaching event. Diseases of Aquatic Organisms, 87, 67–78.

Mydlarz, L. D., & Harvell, C. D. (2007). Peroxidase activity and inducibility in the sea fan coral exposed to a fungal pathogen. Comparative Biochemistry and Physiology, Part A, 146, 54–62.

Mydlarz, L. D., Holthouse, S. F., Peters, E. C., & Harvell, C. D. (2008). Cellular responses in sea fan corals: granular amoebocytes react to pathogen and climate stressors. PloS ONE, 3, e1811.

Mydlarz, L. D., Jones, L. E., & Harvell, C. D. (2006). Innate Immunity, Environmental Drivers, and Disease Ecology of Marine and Freshwater Invertebrates. Annual Review of Ecology, Evolution, and Systematics, 37, 251–288.

Okazaki, R. R., Towle, E. K., van Hooidonk, R., Mor, C., Winter, R. N., Piggot, A. M., … Langdon, C. (2016). Species-specific responses to climate change and community composition determine future calcification rates of Florida Keys reefs. Global Change Biology, 1023–1035.

Olano, C. T., & Bigger, C. H. (2000). Phagocytic activities of the gorgonian coral Swiftia exserta. Journal of Invertebrate Pathology, 76, 176–184.

Oren, U., Benayahu, Y., Lubinevsky, H., & Loya, Y. (2001). Colony integration during regeneration in the stony coral Favia favus. Ecology, 82, 802–813.

Oren, U., Rinkevich, B., & Loya, Y. (1997). Oriented intra-colonial transport of 14C labeled materials during coral regeneration. Marine Ecology Progress Series, 161, 117–122.

Palmer, C. V, Bythell, J. C., & Willis, B. L. (2010). Levels of immunity parameters underpin bleaching and disease susceptibility of reef corals. Federation of American Societies for Experimental Biology, 24, 1935–1946.

Palmer, C. V, McGinty, E. S., Cummings, D. J., Smith, S. M., Bartels, E., & Mydlarz, L. D. (2011). Patterns of coral ecological immunology: variation in the responses of Caribbean

corals to elevated temperature and a pathogen elicitor. The Journal of Experimental Biology, 214, 4240–4249.

Palmer, C. V, Traylor-Knowles, N. G., Willis, B. L., & Bythell, J. C. (2011). Corals use similar immune cells and wound-healing processes as those of higher organisms. PloS One, 6, e23992.

Parks, W. C., Wilson, C. L., & López-Boado, Y. S. (2004). Matrix metalloproteinases as modulators of inflammation and innate immunity. Nature Reviews Immunology, 4, 617–629.

Pearse, V. B., & Muscatine, L. (1971). Role of Symbiotic Algae (Zooxanthellae) in Coral Calcification. Biological Bulletin, 141, 350–363.

Petes, L., Harvell, C., Peters, E., Webb, M., & Mullen, K. (2003). Pathogens compromise reproduction and induce melanization in Caribbean sea fans. Marine Ecology Progress Series, 264, 167–171.

Pfaffl, M. W. (2001). A new mathematical model for relative quantification in real-time RT–PCR. Nucleic Acids Research, 29, e45.

Pinheiro, J., Bates, D., DebRoy, S., & Sarkar, D. (2017). nlme: Linear and Nonlinear Mixed Effects Models.

Polato, N. R., Altman, N. S., & Baums, I. B. (2013). Variation in the transcriptional response of threatened coral larvae to elevated temperatures. Molecular Ecology, 22, 1366–1382.

Pollock, F. J., Morris, P. J., Willis, B. L., & Bourne, D. G. (2011). The urgent need for robust coral disease diagnostics. PLoS Pathogens, 7, 1–10.

Porter, J. W., Dustan, P., Jaap, W. C., Patterson, K. L., Kosmynin, V., Meier, O. W., … Parsons, M. (2001). Patterns of spread of coral disease in the Florida Keys. Hydrobiologia, 460, 1–24.

Precht, W. F., Gintert, B. E., Robbart, M. L., Fura, R., & van Woesik, R. (2016). Unprecedented Disease-Related Coral Mortality in Southeastern Florida. Scientific Reports, 6, 31374.

Puill-Stephan, E., Seneca, F. O., Miller, D. J., van Oppen, M. J. H., & Willis, B. L. (2012). Expression of putative immune response genes during early ontogeny in the coral Acropora millepora. PloS ONE, 7, e39099.

Putnam, N. H., Srivastava, M., Hellsten, U., Dirks, B., Chapman, J., Salamov, A., … Rokhsar, D. S. (2007). Sea anemone genome reveals ancestral eumetazoan gene repertoire and genomic organization. Science, 317, 86–94.

R Core Team. (2014). R: A Language and Environment for Statistical Computing. Vienna: R Foundation for Statistical Computing, ISBN 3-900.

R Core Team. (2016). R: A language and environment for statistical computing. R Foundation for Statistical Computing, Vienna, Austria. Retrieved from https://www.r-project.org/

Radecker, N., Pogoreutz, C., Voolstra, C. R., Wiedenmann, J., & Wild, C. (2015). Nitrogen cycling in corals: The key to understanding holobiont functioning? Trends in Microbiology, 23, 490–497.

Rauw, W. ., Kanis, E., Noordhuizen-Stassen, E. ., & Grommers, F. . (1998). Undesirable side effects of selection for high production efficiency in farm animals: a review. Livestock Production Science, 56, 15–33.

Reusch, T. B. H. (2014). Climate change in the oceans: Evolutionary versus phenotypically plastic responses of marine animals and plants. Evolutionary Applications, 7, 104–122.

Riesgo, A., Peterson, K., Richardson, C., Heist, T., Strehlow, B., McCauley, M., … Hill, A. (2014). Transcriptomic analysis of differential host gene expression upon uptake of symbionts: a case study with *Symbiodinium* and the major bioeroding sponge Cliona varians. BMC Genomics, 15, 376.

Roder, C., Arif, C., Daniels, C., Weil, E., & Voolstra, C. R. (2014). Bacterial profiling of White Plague Disease across corals and oceans indicates a conserved and distinct disease microbiome. Molecular Ecology, 23, 965–974.

Rodriguez-Lanetty, M., Harii, S., & Hoegh-Guldberg, O. (2009). Early molecular responses of coral larvae to hyperthermal stress. Molecular Ecology, 18, 5101–5114.

Roff, G., Hoegh-Guldberg, O., & Fine, M. (2006). Intra-colonial response to Acroporid "white syndrome" lesions in tabular Acropora spp. (Scleractinia). Coral Reefs, 25, 255–264.

Roff, G., Kvennefors, E. C. E., Fine, M., Ortiz, J., Davy, J. E., & Hoegh-Guldberg, O. (2011). The ecology of "Acroporid white syndrome", a coral disease from the southern Great Barrier Reef. PloS ONE, 6, e26829.

Rosenberg, E., Koren, O., Reshef, L., Efrony, R., & Zilber-Rosenberg, I. (2007). The role of microorganisms in coral health, disease and evolution. Nature Reviews. Microbiology, 5, 355–62.

Rosenstiel, P., Sina, C., End, C., Renner, M., Lyer, S., Till, A., … Schreiber, S. (2007). Regulation of DMBT1 via NOD2 and TLR4 in intestinal epithelial cells modulates bacterial recognition and invasion. Journal of Immunology, 178, 8203–8211.

Roth, M. S., & Deheyn, D. D. (2013). Effects of cold stress and heat stress on coral fluorescence in reef-building corals. Scientific Reports, 3, 1421.

Rotjan, R., & Lewis, S. (2008). Impact of coral predators on tropical reefs. Marine Ecology Progress Series, 367, 73–91.

Rouzé, H., Lecellier, G., Saulnier, D., & Berteaux-Lecellier, V. (2016). *Symbiodinium* clades A and D differentially predispose *Acropora cytherea* to disease and Vibrio spp. colonization. Ecology and Evolution, 6. doi:10.1002/ece3.1895

Sadd, B. M., & Siva-Jothy, M. T. (2006). Self-harm caused by an insect's innate immunity. Proceedings of the Royal Society B, 273, 2571–2574.

Sauvage, T., Schmidt, W. E., Suda, S., & Fredericq, S. (2016). A metabarcoding framework for facilitated survey of endolithic phototrophs with tufA. BMC Ecology, 16, 8.

Sawall, Y., Al-Sofyani, A., Banguera-Hinestroza, E., & Voolstra, C. R. (2014). Spatio-temporal analyses of *Symbiodinium* physiology of the coral *Pocillopora verrucosa* along large-scale nutrient and temperature gradients in the Red Sea. PLoS ONE, 9, 1–12.

Shaw, E. C., Carpenter, R. C., Lantz, C. A., & Edmunds, P. J. (2016). Intraspecific variability in the response to ocean warming and acidification in the scleractinian coral *Acropora pulchra*. Marine Biology, 163, 210.

Shinzato, C., Shoguchi, E., Kawashima, T., Hamada, M., Hisata, K., Tanaka, M., & Fujie, M. (2011). Using the *Acropora digitifera* genome to understand coral responses to environmental change. Nature, 476, 320–323.

Siebeck, U. E., Marshall, N. J., Klüter, A., & Hoegh-Guldberg, O. (2006). Monitoring coral bleaching using a colour reference card. Coral Reefs, 25, 453–460.

Smith-Keune, C., & Dove, S. (2007). Gene expression of a green fluorescent protein homolog as a host-specific biomarker of heat stress within a reef-building coral. Marine Biotechnology, 10, 166–180.

Stimson, J., & Kinzie, R. A. (1991). The temporal pattern and rate of release of zooxanthellae from the reef coral Pocillopira damicornis (Linnaeus) under nitrogen-enrichment and control conditions. J Exp Mar Biol Ecol, 153, 63–74.

Strahl, J., Stolz, I., Uthicke, S., Vogel, N., Noonan, S. H. C., & Fabricius, K. E. (2015). Physiological and ecological performance differs in four coral taxa at a volcanic carbon dioxide seep. Comparative Biochemistry and Physiology -Part A□: Molecular and Integrative Physiology, 184, 179–186.

Sunagawa, S., DeSantis, T. Z., Piceno, Y. M., Brodie, E. L., DeSalvo, M. K., Voolstra, C. R., … Medina, M. (2009). Bacterial diversity and White Plague Disease-associated community changes in the Caribbean coral Montastraea faveolata. The ISME Journal, 3, 512–521.

Sussman, M., Willis, B. L., Victor, S., & Bourne, D. G. (2008). Coral pathogens identified for White Syndrome (WS) epizootics in the Indo-Pacific. PloS ONE, 3, e2393.

Sweet, M., & Bythell, J. (2015). White Syndrome in Acropora muricata: Non-specific bacterial infection and ciliate histophagy. Molecular Ecology, 1150–1159.

Sweet, M. J., & Bulling, M. T. (2017). On the Importance of the Microbiome and Pathobiome in Coral Health and Disease. Frontiers in Marine Science, 4, 9.

Sweet, M. J., Bythell, J. C., & Nugues, M. M. (2013). Algae as reservoirs for coral pathogens. PloS ONE, 8, e69717.

Tatusov, R. L., Fedorova, N. D., Jackson, J. D., Jacobs, A. R., Kiryutin, B., Koonin, E. V, … Natale, D. A. (2003). The COG database: an updated version includes eukaryotes. BMC Bioinformatics, 4, 41.

Taylor, D. L. (1977). Intra-colonial transport of organic compounds and calcium in some Atlantic reef corals. In Proceedings, 3rd International Coral Reef Symposium (pp. 431–436).

Tentori, E., & Allemand, D. (2006). Light-enhanced calcification and dark decalcification in isolates of the soft coral Cladiella sp. during tissue recovery. The Biological Bulletin, 211, 193–202.

Teplitski, M., & Ritchie, K. (2009). How feasible is the biological control of coral diseases? Trends in Ecology and Evolution, 24, 378–385.

Therneau, T. M. (2012). coxme: mixed effects models for Cox models.

Therneau, T. M. (2014). A Package for Survival Analysis in S.

Thurber, R. V., Willner-Hall, D., Rodriguez-Mueller, B., Desnues, C., Edwards, R. A., Angly, F., … Rohwer, F. (2009). Metagenomic analysis of stressed coral holobionts. Environmental Microbiology, 11, 2148–2163.

Tian, W., Braunstein, L. D., Pang, J., Stuhlmeier, K. M., Xi, Q., Tian, X., & Stanton, R. C. (1998). Importance of Glucose-6-phosphate Dehydrogenase Activity for Cell Growth. The Journal of Biological Chemistry, 273, 10609–10617.

Untergasser, A., Cutcutache, I., Koressaar, T., Ye, J., Faircloth, B. C., Remm, M., & Rozen, S. G. (2012). Primer3-new capabilities and interfaces. Nucleic Acids Research, 40, e115.

Ushijima, B., Smith, A., Aeby, G. S., & Callahan, S. M. (2012). Vibrio owensii Induces the Tissue Loss Disease Montipora White Syndrome in the Hawaiian Reef Coral Montipora capitata. PLoS ONE, 7, e46717.

Ushijima, B., Videau, P., Burger, A., Shore-Maggio, A., Runyon, C. M., Sudek, M., … Callahan, S. M. (2014). Vibrio coralliilyticus strain OCN008 is an etiological agent of acute Montipora white syndrome. Applied and Environmental Microbiology, 80, 2102–2109.

Vayssier-Taussat, M., Albina, E., Citti, C., & Cosson, J. (2014). Shifting the paradigm from pathogens to pathobiome□: new concepts in the light of meta-omics. Frontiers in Cellular and Infection Microbiology, 4, 1–7.

Venables, W. N., & Ripley, B. D. (2002). Modern Applied Statistics with S. Fourth Edition.

Vezzulli, L., Previati, M., Pruzzo, C., Marchese, A., Bourne, D. G., & Cerrano, C. (2010). Vibrio infections triggering mass mortality events in a warming Mediterranean Sea. Environmental Microbiology, 12, 2007–2019.

Vidal-Dupiol, J., Dheilly, N. M., Rondon, R., Grunau, C., Cosseau, C., Smith, K. M., … Mitta, G. (2014). Thermal Stress Triggers Broad Pocillopora damicornis Transcriptomic Remodeling, while Vibrio coralliilyticus Infection Induces a More Targeted Immuno-Suppression Response. PloS One, 9, e107672.

Vidal-Dupiol, J., Ladrière, O., Destoumieux-Garzón, D., Sautière, P.-E., Meistertzheim, A.-L., Tambutté, E., … Mitta, G. (2011). Innate immune responses of a scleractinian coral to vibriosis. The Journal of Biological Chemistry, 286, 22688–22698.

Vidal-Dupiol, J., Ladrière, O., Meistertzheim, A.-L., Fouré, L., Adjeroud, M., & Mitta, G. (2011). Physiological responses of the scleractinian coral Pocillopora damicornis to bacterial stress from Vibrio coralliilyticus. The Journal of Experimental Biology, 214, 1533–1545.

Vollmer, S. V, & Kline, D. I. (2008). Natural disease resistance in threatened staghorn corals. PloS ONE, 3, e3718.

Wang, G. L., & Semenza, G. L. (1993). General involvement of hypoxia-inducible factor 1 in transcriptional response to hypoxia. Proceedings of the National Academy of Sciences of the United States of America, 90, 4304–4308.

Wang, S., Meyer, E., McKay, J. K., & Matz, M. V. (2012). 2b-RAD: a simple and flexible method for genome-wide genotyping. Nature Methods, 9, 808–810.

Wanner, L., Keller, F., & Matile, P. (1991). Metabolism of radiolabelled galactolipids in senescent barley leaves. Plant Science, 78, 199–206.

Weil, E., & Rogers, C. S. (2011). Coral Reef Diseases in the Atlantic-Caribbean. In Z. Dubinsky & N. Stambler (Eds.), Coral Reefs: An Ecosystem in Transition (pp. 465–491). Dordrecht: Springer Netherlands.

Weiner, S., & Addadi, L. (1991). Acidic macromolecules of mineralized tissues: the controllers of crystal formation. Trends in Biological Sciences, 16, 252–256.

Weiss, Y., Forêt, S., Hayward, D. C., Ainsworth, T., King, R., Ball, E. E., & Miller, D. J. (2013). The acute transcriptional response of the coral Acropora millepora to immune challenge:

expression of GiMAP/IAN genes links the innate immune responses of corals with those of mammals and plants. BMC Genomics, 14, 400.

Winters, G., Holzman, R., Blekhman, a., Beer, S., & Loya, Y. (2009). Photographic assessment of coral chlorophyll contents: Implications for ecophysiological studies and coral monitoring. Journal of Experimental Marine Biology and Ecology, 380, 25–35.

Wright, R. M., Aglyamova, G. V, Meyer, E., & Matz, M. V. (2015). Gene expression associated with white syndromes in a reef building coral, Acropora hyacinthus. BMC Genomics, 16, 1–12.

Yamano, H., Sugihara, K., & Nomura, K. (2011). Rapid poleward range expansion of tropical reef corals in response to rising sea surface temperatures. Geophysical Research Letters, 38, 1–6.

Zhao, D. L., Atlin, G. N., Bastiaans, L., & Spiertz, J. H. J. (2006). Cultivar weed-competitiveness in aerobic rice: Heritability, correlated traits, and the potential for indirect selection in weed-free environments. Crop Science, 46, 372–380.